Program and Abstract Volume

LPI Contribution No. 1677

LUNAR AND PLANETARY INSTITUTE

USRA

Second Conference on the Lunar Highlands Crust

July 13–15, 2012 • Bozeman, Montana

SPONSORS

National Aeronautics and Space Administration
Universities Space Research Association
Lunar and Planetary Institute
NASA Lunar Science Institute
The Meteoritical Society

CONVENERS

Allan Treiman, *Lunar and Planetary Institute*
Charles Shearer (LEAG), *University of New Mexico*
Meenakshi Wadhwa (CAPTEM), *Arizona State University*

SCIENCE ORGANIZING COMMITTEE

Lars Borg, *Lawrence Livermore National Laboratory*
Jennifer Edmunson, *Marshall Space Flight Center*
Brad Jolliff, *Washington University*
Walter Kiefer, *Lunar and Planetary Institute*
Randy Korotev, *Washington University*
Georgiana Kramer, *Lunar and Planetary Institute*
David Kring, *Lunar and Planetary Institute*
Clive Neal, *Notre Dame University*
Marc Norman, *Australian National University*
Paul Spudis, *Lunar and Planetary Institute*

TECHNICAL ORGANIZATION

David Mogk, *Montana State University*
Stuart McCallum, *University of Washington*

Lunar and Planetary Institute 3600 Bay Area Boulevard Houston TX 77058-1113

LPI Contribution No. 1677

Compiled in 2012 by

Meeting and Publication Services
Lunar and Planetary Institute
USRA Houston
3600 Bay Area Boulevard, Houston TX 77058-1113

Abstracts in this volume may be cited as

Author A. B. (2012) Title of abstract. In *Second Conference on the Lunar Highlands Crust*, p. XX. LPI Contribution No. 1677, Lunar and Planetary Institute, Houston.

ISSN No. 0161-5297

Preface

This volume contains abstracts that have been accepted for presentation at the Second Conference on the Lunar Highlands Crust, July 13–15, 2012, Bozeman, Montana.

Administration and publications support for this meeting were provided by the staff of the Meeting and Publication Services Department at the Lunar and Planetary Institute.

Contents

Program

Friday, July 13, 2012
THE BIG PICTURES
8:30 a.m. Rooms 233/235

Chairs: **Walter Kiefer**
David Kring

8:30 a m. Treiman A. H. *
Introduction and Background

8:50 a m. Kring D. A. *
Impact Modification of the Lunar Highlands Crust During the Basin-Forming Epoch **[#9028]**
Basin-forming impact events modified the topography, internal structure, and composition of the lunar highlands crust.

9:30 a m. Hartmann W. K. *
Megaregoliths, Cataclysms, and Highlands: A Synopsis **[#9009]**
Highland samples are controlled by regolith evolution. We examine various models of highland evolution, focusing on the many inconsistent models of "cataclysm."

9:50 a m. Zuber M. T. * Smith D. E. Asmar S. W. Konopliv A. S. Lemoine F. G. Melosh H. J. Neumann G. A. Phillips R. J. Solomon S. C. Watkins M. M. Wieczorek M. A. Williams J. G. Head J. W. III Mazarico E. Torrence M. H.
Preliminary Results on the Structure of Lunar Highland Crust from GRAIL Gravity and LOLA Altimetry **[#9015]**
Substantial advances in our geophysical understanding of the lunar crust are now possible due to recent and ongoing acquisition of high resolution topography and gravity data sets from the LOLA and GRAIL missions.

10:30 a m. BREAK

10:50 a m. Balcerski J. A. * Hauck S. A. II Dombard A. J.
The Effect of Initial Compensation State on Retention of Superisostasy in Lunar Impact Basins **[#9020]**
Using numerical viscoelastic models, we find that there is a zone of parameters of initial thermal and superisostatic static states which allow for the preservation of superisostasy in some lunar impact basins, consistent with gravity observations.

11:10 a m. Kiefer W. S. * Macke R. J. Britt D. T. Irving A. J. Consolmagno G. J.
Density and Porosity of Lunar Feldspathic Rocks and Implications for Lunar Gravity Modeling **[#9006]**
We present new measurements of the density and porosity of lunar feldspathic rocks, which can be used to improve assumptions used in gravity model parameters.

Friday, July 13, 2012
OPTICAL REMOTE SENSING
1:30 p.m. Rooms 233/235

Chairs: **Paul Lucey**
Carle Pieters

1:30 p.m. Pieters C. M. * Dhingra D. Cheek L. Donaldson Hanna K. Moriarty D.
Character and Stratigraphy of the Lunar Highland Crust: The Evolving Story **[#9027]**
Global data acquired over the last decade allow a more detailed evaluation of the composition of the highland crust. Key mineral components of highland rocks include anorthite, olivine/troctolite, Mg-spinel, low-Ca pyroxene (Mg-rich).

2:10 p.m. Ohtake M. * Takeda H. Morota T. Ishihara Y. Matsunaga T. Yokota Y. Yamamoto S. Haruyama J. Ogawa Y. Hiroi T. Karouji Y. Saiki K.
Compositional Variation of the Lunar Highland Crust **[#9002]**
This study investigated spatial and vertical composition (modal abundance) of highland anorthosite rock over the entire lunar surface. Our result indicates decreased mafic mineral abundance with depth in both the upper and lower crusts.

2:30 p.m. Lucey P. G. * Greenhagen B. T.
Lunar Highland Mineral Maps Integrating Thermal and Near Infrared Multispectral Imaging **[#9014]**
Diviner Lunar Radiometer multispectral thermal emission imaging is combined with near-IR datasets to produce mineral and Mg-number data with improved fidelity. Mg-number estimates are similar to those derived from Lunar Prospector and SELENE.

2:50 p.m. Donaldson Hanna K. L. * Pieters C. M. Greenhagen B. T. Cheeks L. C.
Compositional Diversity of Crystalline Plagioclase in the Lunar Highlands **[#9024]**
Recent near infrared observations have uniquely identified Fe-bearing crystalline plagioclase across the lunar surface. Here we analyze Diviner data for those regions to determine the compositional variability of plagioclase across the Moon.

3:10 p.m. BREAK

3:30 p.m. Cheek L. C. * Donaldson Hanna K. L. Pieters C. M. Head J. W. Whitten J. L.
The Distribution and Mineralogy of Anorthosite in the Orientale Basin: New Perspectives from M^3 Data **[#9022]**
A detailed mineralogic analysis of the Orientale Basin using M^3 data reveals that crystalline anorthosite (shocked to <25 GPa) is abundant, and that the most highly pure examples (> ~98% plagioclase) are concentrated in the Inner Rook Mountains.

3:50 p.m. Wiseman S. M. * Donaldson Hanna K. L. Mustard J. F. Isaacson P. J. Pieters C. M. Jolliff B. L.
Aristarchus Olivine in Context with Circum-Imbrium Olivine Deposits **[#9025]**
We investigate the origin of olivine-bearing deposits in Aristarchus Crater ejecta. Given that spectrally similar olivine is found circum Imbrium, olivine in Aristarchus may represent reexposed Imbrium ejecta or other impact transported deposits.

4:10 p.m. DISCUSSION

Saturday, July 14, 2012
LUNAR METEORITES: ROCKS AND REGOLITH
8:30 a.m. Rooms 233/235

Chairs: **Lars Borg**
Ryan Zeigler

8:30 a m. Korotev R. L. * Jolliff B. L. Zeigler R. A.
What Lunar Meteorites Tell Us About the Lunar Highlands Crust **[#9003]**
Lunar meteorites provide information about the lunar highlands that was not known from studies of the Apollo and Luna samples.

9:10 a m. Warren P. H. *
Let's Get Real: Not Every Lunar Rock Sample is Big Enough to be Representative for Every Purpose **[#9034]**
Distinguishing between impact-mixture rocks and compositionally pristine, endogenously igneous rocks, a key aspect of lunar highland petrology, has been egregiously ignored in some recent meteorite studies. Modes for tiny samples are also unreliable.

9:30 a m. Zeigler R. A. * Korotev R. L. Jolliff B. L.
Feldspathic Lunar Meteorite Graves Nunataks 06157, a Magnesian Piece of the Lunar Highland Crust **[#9033]**
We will discuss one of the compositional end members of the feldspathic lunar meteorite suite, GRA 06157. It is the smallest lunar meteorite (0.79 g), but despite its small size, its highly feldspathic and highly magnesian composition is intriguing.

9:50 a m. Wittmann A. * Korotev R. L. Jolliff B. L. Irving A. J.
Spherules and Glasses in Lunaite Shişr 161 Record Reworked Regolith and a Magnesian Component of the Feldspathic Highlands Terrane **[#9019]**
Feldspathic breccia Shişr 161 contains metamorphosed spherules that likely formed fallback debris into a large lunar impact crater. Together with glass shards, they record broad variations among precursor rocks that generated a magnesian character.

10:10 a m. BREAK

10:30 a m. Gross J. * Treiman A. H. Mercer C. N.
Lunar Feldspathic Meteorites: Constraints on the Geology of the Lunar Farside Highlands, and the Origin of the Lunar Crust **[#9021]**
Lunar feldspathic meteorites are not obviously consistent with predictions of the LMO model and might represent SPA ejecta.

10:50 a m. Borg L. E. * Gaffney A. M. Shearer C. K.
Chronologic Confusion in the Lunar Highlands **[#9008]**
Mechanisms for disturbances to isotopic chronometers are explored and the criteria that can be used to define reliable igneous crystallization ages of lunar highland samples are examined.

Saturday, July 14, 2012
REMOTE SENSING AND INDIVIDUAL ROCKS
1:30 p.m. Rooms 233/235

Chairs: **Bradley Jolliff**
Rachel Klima

1:30 p.m. Isaacson P. J. * Hiroi T. Hawke B. R. Lucey P. G. Pieters C. M. Liu Y. Patchen A. Taylor L. A.
Geologic Context of Feldspathic Lunar Meteorites: Combining Laboratory Spectroscopy with Diverse Remote Compositional Analyses **[#9023]**
We pair laboratory VNIR analyses of feldspathic lunar meteorites with remote sensing observations. This combined approach will constrain the geologic context of these samples of the largely unexplored lunar feldspathic highlands.

1:50 p.m. Crites S. T. * Taylor G. J. Martel L. M. V. Lucey P. G. Blake D. F.
Modal Analyses of Apollo Soils by X-Ray Diffraction and Microscopic Spectral Imaging **[#9030]**
We are using quantitative X-ray diffraction (XRD) and microscopic hyperspectral imaging to determine modal mineralogy of over 100 Apollo soils with an emphasis on testing the petrologic character of geochemical terrains at the Apollo 16 site.

2:10 p.m. Kramer G. Y. * Kring D. A. Pieters C. M.
Deep Crust/Mantle Mineralogy Exposed in the Uplifted Peak Ring and Basin Wall of Schrödinger **[#9013]**
We report our analysis of the mineralogy exposed in Schrödinger's peak ring, which represents material derived from the mantle or crust/mantle interface, and the basin wall, which reveals the composition of the target crust.

2:30 p.m. Srivastava N. * Gupta R. P.
Compositional Diversity Inside Lowell Crater, Orientale Basin: Evidences for Extensive Spinel Rich Deposits **[#9016]**
Extensive exposures of spinel rich rocks have been found inside Lowell Crater (12.9°S 103.1°W) and in other adjoining areas of Montes Rook, Orientale Basin, indicating their pervasive presence in the crust at depth prior to the Orientale impact.

2:50 p.m. BREAK

3:10 p.m. Klima R. L. * Cahill J. T. S. Hagerty J. Lawrence D.
Bullialdus Crater: Excavation and Exposure of an Mg- or Alkali-Suite Pluton? **[#9017]**
The reflectance spectra of Bullialdus Crater suggest an enhancement of OH^- relative to the surroundings. We examine local mineralogy and the spatial distribution of local Th and OH^- signatures to investigate the composition of the excavated pluton.

3:30 p.m. Zanetti M. * Jolliff B. L.
Aristarchus Crater as a Probe of the Lunar Crust's Most Fractionated Rock Types **[#9031]**
We examine the petrogenetically diverse suite of rocks excavated by the Aristarchus Crater impact event through the integration of available spectrographic datasets with photogeologic mapping.

3:50 p.m. Jolliff B. L. * Stopar J. D. Lawrence S. J. Robinson M. S. Hawke B. R.
New Views of Silicic Volcanism on the Moon **[#9037]**
Four examples of compositionally evolved nonmare volcanics on the Moon include the Gruithuisen and Mairan domes, and the Hansteen-Alpha and Compton-Belkovich sites. Despite morphologic differences, these volcanics may have common aspects of origin.

4:10 p.m. DISCUSSION

Saturday, July 14, 2012
POSTER SESSION
5:30 p.m. Ballroom C

Sakai R. Nagahara H. Ozawa K. Tachibana S.
Chemical Composition of Lunar Magma Ocean Constrained by the Conditions of Crust Formation **[#9004]**
The bulk composition of the lunar magma ocean was constrained to satisfy the formation condition of lunar anorthosite crust. We showed that the lunar magma ocean was likely to be enriched in FeO compared to the BSE.

Mills R. D. Simon J. I.
Predicting the Sources and Formation Mechanisms of Evolved Lunar Crust by Linking K/Ca Ratios of Lunar Granites to Analogous Terrestrial Rocks **[#9011]**
We use terrestrial chemical data as a proxy for igneous rocks in the lunar crust that allow us to hypothesize what type of rock may have been parental to granite found in Apollo breccia sample 14321.

Gustafson J. O. Gaddis L. R. Hawke B. R. Giguere T. A.
Analysis of Pyroclastic Deposits Within Floor-Fractured Lavoisier Crater **[#9036]**
We are using LROC WAC and NAC as well as Kaguya TC and MI data to investigate the extent and characteristics of the pyroclastic deposits within Lavoisier Crater.

Head J. W. III
Lunar Orientale Basin: Characterization and Insights into Multi-Ringed Basin Formation **[#9038]**
New data from the armada of recent and ongoing lunar spacecraft are providing multiple datasets, new characterization, and new insights into the origin and evolution of the Orientale Basin.

Arivazhagan S. Anbazhagan S.
Lunar Highland Analog Rocks in Southern Peninsular India **[#9010]**
In south India, there are a number of anorthosite complexes available and studied by numerous authors. In the present work, a comparative study is carried out between South Indian and lunar anorthosites with reference to chemistry and mineralogy.

Hui H. Peslier A. Zhang X. Neal C. R.
Detection of Hydroxyl in Ferroan Anorthosite and Troctolite: Implications for Water Contents in Lunar Magma Ocean and Highlands Upper Crust

Sunday, July 15, 2012
STILLWATER TO THE MOON
8:30 a.m. Rooms 233/235

Chairs: **Francis McCubbin**
Georgiana Kramer

8:30 a m. Treiman A. H. *
Outstanding Problems

8:50 a m. Carli C. * Sgavetti M. Capaccioni F. Serventi G.
Studying Spectral Variability of an Igneous Stratified Complex as a Tool to Map Lunar Highlands **[#9007]**
Moon Mineralogy Mapper data have revealed different portion of magmatic chambers or separate plutons. We analysed Stillwater Complex (SWC) rock suite. Spectral signatures and spectral parameters could help to interpret the new spectral lunar data.

9:10 a m. Kickapoo Lunar Research Team Kramer G. Y. *
Stratified Ejecta Boulders as Indicators of Layered Plutons on the Lunar Nearside **[#9029]**
We tested the leading formation hypotheses for the origin of the stratified ejecta boulders and assessed their plausibility based on our observations and measurements of layer thicknesses and albedos.

9:30 a m. Vaughan W. M. * Head J. W. Hess P. C. Wilson L. Neumann G. A.
Smith D. E. Zuber M. T.
Mini-Magma Ocean Petrology: Differentiation of Massive Impact Melt Sheets on the Moon **[#9018]**
Massive impact melt sheets are mini-magma oceans. We quantitatively treat the differentiation of impact melt in lunar basins of different sizes. The submitted full abstract is a case study of the differentiation of the Orientale impact melt sheet.

9:50 a m. Shearer C. K. * Burger P. V. Guan Y.
Post-LMO Crustal Growth. A Comparison of Apollo 17 Dunites **[#9026]**
There are multiple types of dunites collected from the Apollo 17 site. This comparison of these dunites provides insights into their origin, and the relationships between Mg-suite and mare magmatism.

10:10 a m. BREAK

10:30 a m. Elardo S. M. * McCubbin F. M. Shearer C. K. Jr.
Reopening a Can of Wormy Intergrowths: A New Look at Chromite Symplectites in Mg-Suite Troctolite 76535 **[#9012]**
The origin of symplectites in 76535 has been debated and bears relevance to the extremely low Cr content of its cumulus olivine and parental magma composition. Here we assess symplectite formation mechanisms in the context of Mg-suite petrogenesis.

10:50 a m. McCubbin F. M. * Shearer C. K. Sharp Z. D.
Magmatic Volatile Reservoirs on the Moon and the Chemical Signatures of urKREEP **[#9035]**
Many of the recent findings regarding lunar volatiles are synthesized and expand upon with data from KREEP basalts. The implications of these findings are then discussed in the context of the lunar highlands and chemical signatures of urKREEP.

LUNAR HIGHLAND ANALOG ROCKS IN SOUTHERN PENINSULAR INDIA. S. Arivazhagan[1] and S. Anbazhagan[2]

Centre for Geoinformatics and Planetary Studies, Department of Geology, Periyar University, Salem – 636 011, India.
[1]arivusv@gmail.com & [2]anbu02@gmail.com

1.0 Introduction: Any material derived from natural or synthetic, terrestrial or meteoritic components close to the mineralogy, chemical, mechanical, engineering properties and particle size distributions equivalent of a lunar or other planetary rock/ soil referred as Lunar Soil Simulant or Planetary analog [1]. The development of lunar regolith simulant is insufficient in quantity to support lunar technology projects. Samples of actual lunar regolith are limited and too small for research so that, the scientific value of the lunar soil samples is high. Hence, lunar analogs have been developed to replicate the physical, chemical, mineralogical and geotechnical properties of lunar soil for Earth based studies. Planetary scientists are using terrestrial analogs for various kinds of research and comparative studies between terrestrial and planets. The knowledge of lunar soils and its physical, chemical, mineralogical and geotechnical characteristics were obtained from various Apollo returned samples. Anorthosite, a plagioclase-rich igneous rock with subordinate amounts of pyroxenes, olivine and other minerals, is an important type of fragment found mainly in the breccias and soils at each site and as large rock fragment at the Apollo 15 site [2]. Similar rocks are available on terrestrial, which could provide vital clue about origin and evolution of the Moon. Repeated analog studies are required to understand physical, chemical and spectral properties of lunar rocks and remote mapping of the lunar surface. In southern peninsular India, there are number of anorthosite complexes available as equivalent rocks. In the present work, an emphasis has been given to the chemistry and mineralogy of southern peninsular Indian anorthosites with reference to the lunar anorthosite.

2.0 Analogs from Peninsular India: Anorthosite is a less abundant but fascinating rock composed almost entirely of calcic-plagioclase. Terrestrial anorthosite occurrences fall into a few genetic 'types' or 'associations' such as: (i) Archaean (> 2500 million years (Ma)) megacrystic, (ii) Proterozoic - massif type (2500–500 Ma) and (iii) components of layered mafic and ultramafic igneous plutons [3]& [4]. The Archean anorthosite complexes were considered as analogs to the lunar highland anorthosites. Terrestrial anorthosites grade into gabbroic anorthosites, then into anorthositic gabbros and finally into gabbros. In contrast to terrestrial anorthosites, the lunar anorthosites are much finer-crystalline and feldspars with very high Ca/Na ratios. Anorthosite samples returned from the Apollo missions contain >90% calcium-rich plagioclase [5], as well as minor amount of pyroxene and olivine, which are relatively iron-rich [6]. The plagioclase feldspars in lunar anorthosites are typically ranges from An40 to An98, although most of the rock possess An >70 [7]. Rock samples from the highlands and/ or from depths within the crust are characterized by anorthosites, norites and troctolites are collectively referred as the ANT group [8].

Layered complex of anorthositic and gabbroic rocks (SAC) are located at Sittampundi, Tamil Nadu, India. The Sm-Nd isotopic studies of Sittampundi anorthosites show an age of 2935±60 Ma, indicating the Archean age [9]. The Archean anorthosites (> 2.6 Ga) are primarily of interest because of their closer chemical similarity to highland anorthosites on the moon [10]. Oddanchatram anorthosite complex (OAC) is situated at Dindigul district, Southern region of Tamil Nadu, India and comprises of anorthosite, norite associated with charnockite, quartzite, garnet- sillimanite gneiss and magnetite-quartzite. The zircons separated from the Oddanchatram anorthosite has yielded U-Pb ages of 600Ma [11]. Kadavur anorthosite (KA) mass is a funnel shaped pluton covered about 20 km^2 area. It consists of anorthosite and gabbroic anorthosite with more mafic rocks at the boundaries grading to very coarse anorthosite in the interior. The KA complex lies south of Plaghat-Cauvery Shear Zone in the northern Madurai block (Tamil Nadu state) and crystallized at 829±14 Ma (LA –ICPMS) in a supra-subduction zone settling [12]. The mineralogical attributes (An-content of plagioclase) of the Kadavur and Oddanchatram anorthosites indicate that they represent the Proterozoic massive type anorthosite.

The Chimalpahad anorthosite Complex (CAC) is the largest, deformed and metamorphosed layered Complex in the Precambrian shield of South India [13] located at Khammam District, Andhra Pradesh. It contains a well-exposed stratigraphy of layered anorthosite-leucogabbro-gabbro-ultramafic rocks. The anorthosite body covered 200km^2 area in the Precambrian shield as irregular mass with plagioclase content of 71-86%. [14]. CAC comprised of layered gabbro anorthosite body, ultramafic rocks and massive (Alpine) type chromitite, quartzite, calc-silicate rocks, schist and gneisses. The Kondapalli layered Complex (KLC) located in the state of Andhra Pradesh, India consists of dominant gabbroic and anorthositic rocks, with subordinate ultramafic rocks. It occurs as minor bands and lenses within a region dominated by charnockites and variably deformed and cut by rare meta dolerite dykes. The KLC represents a discontinuous stratiform type complex and its disrupted fragments contain different components [15].

3.0 Chemistry and Mineralogy: The anorthositic body located in various parts of Southern peninsular India were studied and compared in terms of their equivalents with lunar highland anorthosites. The chemistry and mineralogy were considered for such correlation (Table 1 & 2). Anorthosite samples were collected from Sittampundi and Kadavur for chemical analysis. The average composition of anorthosites were compiled and listed in the Table.1. Similarly, the average chemical value of OAC, CAC and KLA were taken from published work. From the chemical values, the mineral constituents were derived using CIPW norm calculation.

4.0 Discussion: Several works have been conducted on terrestrial analogs and considered as equivalent of lunar analogs in terms of chemistry and mineralogy. Battler et al (2006) have located Archean anorthosites body in Canada, which is mineralogically similar to lunar anorthosites, featuring 90% of plagioclase with An75-95%, and 10% of pyroxene, olivine, garnet and minor amphibole. Although amphibole and garnet are not present in the lunar anorthosites, most of the terrestrial anorthosites contain small amounts of hydrated minerals, due to alteration of the pyroxene and/or olivine [23]. Anbazhagan and Arivazhagan (2010) have revealed that Sittampundi anorthosite is chemically and mineralogically equivalent of lunar anorthosite gabbro attributing 73% of plagioclase with An>67% and nearly 14-15% of pyroxene along with 5% of olivine. [19]. The analog from terrestrial may differ from genuine lunar soils in several aspects, mostly due to the effects of micrometeorites and solar wind on the moon.

Analyses of Apollo 11 samples show the anorthosites are deficient in alkalis and phosphorus due to volatilization on the surface. However, the terrestrial analogs have higher alkali contents. There is a widely accepted theory that lunar anorthosites were formed through lunar magma ocean. The anorthosites on the Earth could be the reworked and tectonically modified remnants of an original widespread early anorthositic crust on the earth formed from a global magma ocean? [24].

In the present study, chemistry of five terrestrial anorthosites form Southern peninsular India were taken along with the lunar highland geochemistry for comparison. Silicates, Al_2O_3, CaO, MgO, FeO and Fe_2O_3 are the major oxides noticed in the anorthosites. The major difference between lunar anorthosites and terrestrial analogs are absence

of ferrous iron and presence of hydrated minerals in the later case. Out of five analogs, the chemistry of Sittampundi anorthosite is almost equivalent of lunar anorthosites. The other four terrestrial analogs are remain match with chemistry of lunar anorthosites, particularly with major oxides like SiO_2, Al_2O_3, CaO, MgO. Presence of minor amount of TiO_2 is noticed in all anorthosites.

Plagioclase, clino pyroxene (CPX) and ortho pyroxene (OPX) are the major mineral constituents noticed in the CIPW norm calculation. The other minor minerals are olivine, ilmenite and orthoclase. The content of CPX in lunar highland is ~3-14%, and in the terrestrial analog it fall from 0.35-14%. The CPX content of SAC and KA anorthosites are matches with the LAG. The lunar highland OPX leads up to 32% whereas the terrestrial OPX is restricted to 8%. Presence of olivine noticed in LA, LAG and terrestrial anorthosites SAC, KLC. Olivine is absent in KA, OAC, and CAC. Orthoclase and quartz are represents in the LAN, KA, OAC and CAC, however those are absent in LA and LAG which is supporting the non-completion of differentiation of lunar magma. However, at present most of the research findings are supporting the presence of silicate on the lunar surface [25] & [26]. Among the five analogs, SAC found almost equivalent with lunar highland anorthosites.

References: [1]. Sibille, et al. (2005)Lunar regolith simulant materials, NASA: Marshall Space Flight Center. [2].Wood et al., (1970) Popular Astronomy, 18: Pp.67-72. [3]. Wiebe, (1992). In. Proterozoic Crustal Evolution, p.251. [4]. Ashwal, L. D., Anorthosites, Springer Verlag, Berlin, 1993, p. 422.[5]. Peterson et al., (1997). Lunar Planet. Sci. XXVIII, 1608 #.[6]. Heiken et al., (1991). In: Lunar Source Book–A User's Guide to the Moon, Cambridge Univ.Press, p. 121.[7]. Frondel, J., (2006). Lunar mineralogy. Lunar Planet. Sci. XXXVII, 1622 #.[8]. Short, (1975). Planetary Geology, Prentice – Hall, Inc. p. 197. [9]. Selvan and Subramanian (2001). Geol. of TN and Pondi, GSI pub.[10]. Blatt, et al., (2006). Freeman and company New York.[11]. Ghosh, et al., (1998). J. African Earth Sciences, 27, 86. [12]. Teale, et al., (2011). Jr. of Asian Earth Sci. doi:10.1016.[13]. Leelanandam, (1987). Rec. Res. in Geol., vol. 13., pp. 108–116.[14]. Appavadhanulu et al., (1976) Geol. Surv. Ind. Mis. Pub. 23, 267–278. [15]. Leelanandam, (1991) In IGCP Project 290. [16]. Norman, et al., (2003). *Met. & Planet. Sci.* 38, p. 645-661. [17]. BVSP, 1981., Pergamon Press, p.1286. [18] Heiken, et al., 1991. Lunar Source Book, Cambridge University Press, p. 736. [19]. Anbazhagan, S. and Arivazhagan S. (2010), Planet. and Space Sci. 58 , Pp. 752–760.[20]. Radhakrishna and Naqvi, S.M., (1986), Jr. of Geol. 94, Pp.145-166.[21]. Dharma Rao, et al., (2011). Precambrian Res. doi:10.1016/j.precamres.2011.11.012. [22]. Leelanandam, C., (1997). Gondwana Research, Vol. 1, Pp.95-114.[23]. Battler, et al., (2006). LPSC. XXXVII, 1622 #. [24]. Blatt, et al., (2006). Petrology – Igneous, Sedimentary and Metamorphic, 3rd Edition, W.H. Freeman and Company, New York, P. 530. [25]. Greenhagen, et al., (2010). Science, Vol.329, 1507-1509.[26]. Glotch,et al., (2010). Science, Vol. 329 no. 5998 Pp. 1510-1513.

Table1. Chemistry of lunar and analog anorthosites of Souhern Peninsular India

	LA[16]	LAG[17]	LAN[18]	Terrestrial Anorthosites (Southern India)				
				SAC [19]	KA	OAC[20]	CAC[21]	KLC[22]
Type				Neo Archean (layered)	Massif	Archean	Proterozoic (layered)	Proterozoic (layered)
Age	4.46 Ga [16]			2935±60 Ma [9]	825 ± 17 Ma [12]	2600 Ma [20]	1170 Ma [21]	851±28 Ma [22]
Sio_2	45.0	48.39	45.31	44.79	49.01	54.32	51.5	48.70
TiO_2	0.5	0.9	0.36	0.085	0.71	0.046	0.044	0.16
Al_2O_3	27.2	20.68	20.44	25.69	21.14	28.26	27.15	28.12
Fe_2O_3	-	-	-	3.27	8.54	0.646	1.63	0.86
FeO	5.2	8.85	12.60	-	-	-	-	2.94
MgO	5.7	7.79	6.88	5.78	4.29	0.296	1.439	3.12
CaO	15.7	12.13	14.41	16.52	12.34	11.22	14.89	13.74
Na_2O	-	0.02	0.15	1.37	3.11	4.506	1.729	2.37
K_2O	-	0.01	0.01	0.06	0.53	0.692	0.023	-
P_2O_5	-	0.02	-	0.02	0.01	0.032	0.045	0.03
Total	99.3	98.79	100.16	97.58	99.84	100.90	98.45	100.04

LA- Lunar Anorthosite; LAG-Lunar Anorthositic Gabbro; LGA-Lunar Gabbroic Anorthosite; SAC-Sittampundi; KA-Kadavur; OAC-Oddanchatram; CAC-Chimalpahad; KLC-Kondapalli

Table.2: Mineralogical constitutes of lunar anorthosites and terrestrial analog of Southern peninsular India

Minerals	LA	LAG	LAN	SAC	KA	OAC	CAC	KLC
Quartz	-	-	4.74	-	0.184	1.2	9.01	-
Orthoclase	-	0.059	0.059	0.355	3.132	4.09	0.136	-
Plagioclase	74.21	56.32	56.46	73.13	70.66	92.96	80.88	86.13
Clino pyroxene	2.99	13.71	3.17	13.83	12.86	0.35	5.67	1.52
Ortho pyroxene	20.28	19.45	32.61	-	4.72	0.57	0.95	8.87
Olivine	0.85	9.91	-	5.59	-	-	-	1.87
Magnetite	-	-	-	-	-	-	-	1.24
Ilmenite	0.95	0.68	1.71	-	-	-	0.06	0.3
Hematite	-	-	-	3.27	8.54	0.64	1.63	-
Total	99.28	100.12	98.74	96.17	100.09	99.81	98.33	99.93

THE EFFECT OF INITIAL COMPENSATION STATE ON RETENTION OF SUPERISOSTASY IN LUNAR IMPACT BASINS

Jeffrey A. Balcerski[1], Steven A. Hauck, II[1], and Andrew J. Dombard[2], [1]Dept. of Earth, Environmental, and Planetary Sciences, Case Western Reserve University, Cleveland, OH 44106 (jeffab@case.edu), [2]Dept. of Earth and Environmental Sciences, University of Illinois at Chicago, Chicago, IL 60607

Introduction: Observations by spacecraft recently in orbit around the Moon are fundamentally improving our understanding of its gravity field [e.g.,1-3]. The prospect of these new data has refocused attention on the question of the mechanism(s) responsible for the formation and preservation of large, positive, free-air gravity anomalies in areas of low topography (or "mascons" [4]), which have been observed to be present over many large impact basins. Thus far, these features have resisted a unified and consistent explanation. Of particular relevance to the lunar highlands are those basins that possess little or no evident mare fill and exhibit a strong positive central gravity anomaly surrounded by an annulus of a weaker, negative free-air anomaly. [e.g. 1]. With the results from the SELENE mission and those that will be forthcoming from GRAIL, the gravity map of the far side of the Moon has been refined sufficiently to distinguish several basins located in the Feldspathic Highlands Terrane that possess these characteristics as well as having a well-defined, positive Bouguer anomaly in the center of the basin [1]. Because these features are well-distanced from the elevated heat production in the Procellarum KREEP Terrane, they provide a crucial locale with which to test models of impact crater evolution.

Though the cause of the central Bouguer anomalies in major basins originally was a source of much debate [e.g., 5,6] recent literature has attributed it to the uplift of the crust-mantle interface in the basin center as a consequence of the impact process or subsequent basin collapse and relaxation [e.g., 7-10]. More recently, several studies have variously re-examined the role of impact heat upon the evolution of the lithosphere, particularly in the period of time closely following the impact event [11-13]. The idea that the interior topography may be flexurally uplifted by an annulus of buoyant, thickened crust surrounding the basin has also been investigated [9]. Furthermore, there has been a suggestion that the Bouguer anomaly may not be due to an uplifted Moho, but rather the intrusion of magmatic sills and inflation of the crater floor at some time post-impact [14]. However, the application of this latter model to the lunar highland basins that host positive Bouguer anomalies with little or no observed extrusive mare is challenging.

Approach: Absent from the discussion of the origin and preservation of large central Bouguer gravity anomalies in lunar mascon basins is a thorough treatment of the viscoelastic evolution of these basins. Toward that goal, we have calculated the evolution of a broad suite of impact basins to understand the conditions (if any) under which structural relief along the moho greater than predicted by isostasy (termed superisostasy or overcompensation) can be preserved. We generated a suite of viscoelastic finite-element models representing a range of basin sizes (100-1200 km in diameter) each with an initial degree of compensation from compensated (DC = $[(h_m(\rho_m-\rho_c)/(h_c\rho_c)]$ = 1.0) to highly overcompensated (DC = 3.0), where DC is the degree of compensation, h_m is the height of the Moho, h_c is the topography of the crater, and ρ_m and ρ_c are the mantle and crust densities. The models contain two layers, both with Poisson ratio = 0.25 and Young's modulus = 10^{11} Pa, with crustal (ρ=2900 kg/m^3) and mantle (ρ=3400 km/m^3) rheologies of dry diabase [10] and dry olivine [11] respectively. The nominal crustal depth was fixed at 60 km, with variation inside the basin constrained by the degree of compensation for each particular model and a minimum thickness at the basin center of 30 km. We used the MSC Marc software package to solve each model in 2-D spherical axisymmetry, with a suite of equilibrium conductive temperature distributions with surface heat fluxes varying from 10-50 mW/m^2, and thermal conductivities of 2 W m^{-1} K^{-1} (crust) and 3 W m^{-1} K^{-1} (mantle). The transient heat from the impact event (which our models neglect) diffuses away and is replaced by the background thermal gradient in approximately 500 Myr, which also marks the onset of significant horizontal viscous flow. We place a lower limit on the model viscosity of 10^{18} Pa·s to maintain reasonable simulation completion times, and captures the full range of viscous behavior of the crust and upper mantle.

Results: In all models with initial DC >= 1.5, we find that the degree of compensation of the basin center after evolving for 4 Gyr resists completely relaxing to a state of isostasy. At 50 mW/m^2 surface heat flux (the hottest thermal condition), all basin sizes maintain a state of superisostasy with at least 10% overcompensation (DC >= 1.1). The magnitude of retained superisostasy is determined mainly by an inverse relationship to both basin diameter and surface heat flux [Figure 1]. In addition, we find a smaller, but measurable dependence on the initial degree of compensation. Figure 2 illustrates the results of simulation of a 1200

km diameter basin with a 50 mW/m^2 surface heat flux and different initial degrees of isostatic overcompensation. Though larger in diameter than all farside basins excepting South Pole-Aiken, it provides an upper bound for rate and extent of isostatic adjustment. We note a rapid vertical adjustment and early convergence of the state of compensation regardless of the initial state, but little or no further convergence after 10 kyr. At smaller heat fluxes, the convergence is increasingly delayed (by orders of magnitude), and the effect of the initial state of compensation on the final state is more pronounced.

In the models with the highest heat flux, the effect of horizontal viscous creep, particularly at long time scales is non-negligible. After several hundred Myr there remain sufficient stresses from the surface and Moho topography to drive horizontal flow inward from the periphery of the basin, along the base of the crust and the associated upper mantle. Figure 3 illustrates the change in crustal thickness due to lateral crustal flow for a 1200 km diameter basin at 50 mW/m^2 of surface heat flux after 4 Gyr. This change in crustal thickness is superposed upon the earlier vertical topographic changes and results in a region of thickened crust just medial of the basin rim, surrounded distally by an annulus of thinned crust.

Discussion: Namiki et al. [1] illustrated that the rheological behavior of plagioclase is more resistant to viscous flow than olivine under dry conditions, making lateral relaxation of basin Moho topography difficult at temperatures < 800 K. However, the hydration state of the lunar mantle is the subject of ongoing study [17], and the presence of a wetter crust and mantle would result in greater deformation.

The early isostatic adjustment of the hottest models (50mW/m^2 surface flux) compares reasonably well with other studies that explicitly include the effects of impact heat [13]. Ours differ however, in that they preserve at least 10% overcompensation. This is likely due to a combination of membrane support and the mechanical strength of the lithosphere.

References: [1] Namiki, N., et al. (2009), *Science, 323,* 900. [2] Zuber, M. T., et al. (2012) *LPS 43*, Abs. 1489. [3] Mazarico, E., et al. (2012), *J. Geod.*, 86, 193. [4] Muller, P. M., and Sjogren, W.L. (1968), *Science*, *161, 3842,* 680. [5] Conel, J. E. and Holtrom, G. B (1968) *Science*, *162, 3860*, 1403. [6] Wise, D. U. and Yates, M. T. (1970) *JGR, 75, 2*. [7] Neumann, et al. (1996), *J. Geophys. Res., 101, E7*, 16841–16843. [8] Wieczorek, M.A. and Phillips, R.J. (1999), *Icarus, 139*, 246. [9] Andrews-Hanna, J. C. (2012), *LPS 43,* Abs. 2084. [10] Stewart, S. T. (2011), *LPS 42*. Abs. 1633. [11] Balcerski, J. A., et al. (2010) *LPS 41,* Abs. 2535. [12] Melosh, H. J., et al. (2012), *LPS 43*, Abs. 1633. [13] Kiefer, W. S., et al. (2012), *Early Solar System Impact Bombardment II*, Abs. 4026. [14] McGovern, P. J., et al. (2012), *LPS 43*, Abs. 2937 [15] Mackwell, S., et al. (1998), *JGR, 103*, 975. [16] Karato, S., and Wu, P. (1993), *Science, 260*, 771. [17] Saal, A. E., et al. (2008). *Nature, 454*, 192.

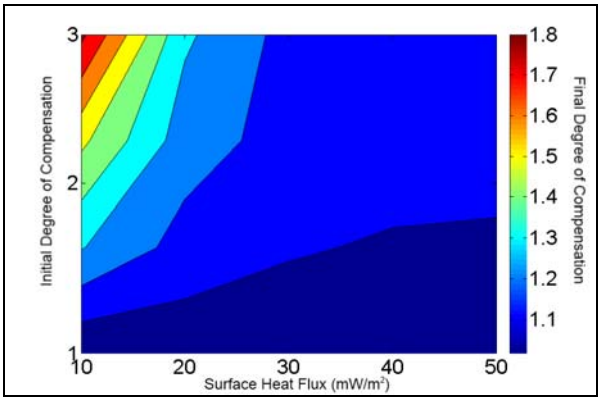

Figure 1. Effect of thermal conditions and initial compensation state on final degree of compensation at the center of a 1200 km diameter basin after 4 Gyr.

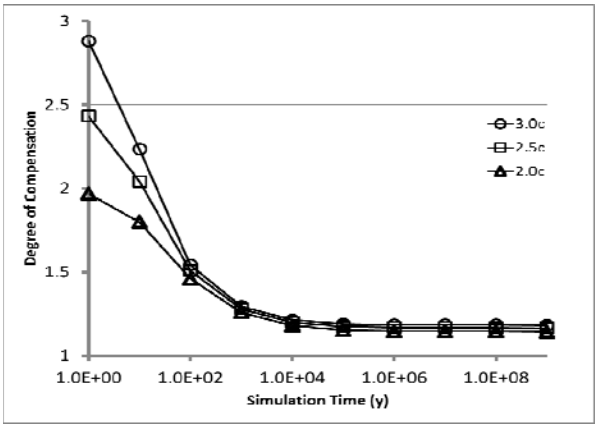

Figure 2. Evolution of the compensation state of the center node of a 1200 km diameter basin with different initial DC for a constant 50 mW/m^2 surface heat flux.

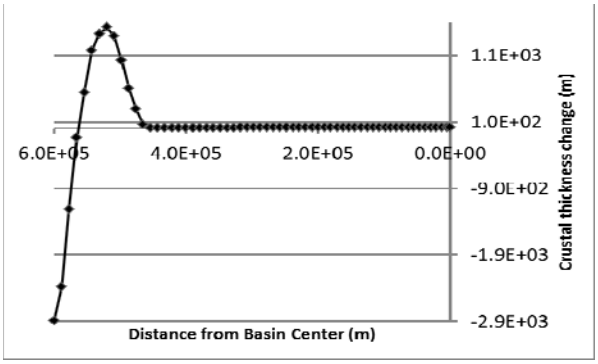

Figure 3. Change in crustal thickess as a function of distance from the center of a 1200 km diameter basin after 4 Gyr . Initial DC=3.0 with constant surface heat flux of 50 mW/m^2.

CHRONOLOGIC CONFUSION IN THE LUNAR HIGHLANDS. L. E. Borg[1], A. M. Gaffney[1], and C. K. Shearer[2]
[1]Chemical Sciences Division, Lawrence Livermore National Laboratory, 7000 East Avenue L-231 Livermore CA USA (borg5@llnl.gov).[2] Institute of Meteoritics, University of New Mexico NM USA.

Introduction: In the absence of detailed stratigraphic information, radiometric age determinations of lunar highland rock suites are the primary mechanism used to elucidate their temporal relationships, as well as to constrain the origin and evolution of their sources [e.g. 1-2]. However, despite their tremendous power, results of radiometric age investigations are often ambiguous because the ages are not reproducible, have large uncertainties, or have internal inconsistencies that suggest they do not represent geologic events [3]. Below we explore the mechanisms for these disturbances and examine the criteria that can be used to define reliable igneous crystallization ages.

Disturbances: The most common chronometers used to date crystallization of highlands rocks are Rb-Sr, Sm-Nd, and U-Pb. In order to account for inherited daughter isotopes, ages are calculated by plotting isotopic data from multiple fractions on isochron diagrams. The slope (or the y-intercept for Pb-Pb) of the isochron defines the age of the sample. Linearity of the fractions on the isochron is the basis for calculating the age uncertainty and is ultimately the main criteria by which the reliability of the age is evaluated.

The isotopic systematic of lunar highlands rocks are strongly disturbed by the late heavy bombardment [e.g. 4]. Experimental investigations of shocked and heated lunar samples demonstrate that Sm-Nd is least mobile during shock metamorphism and therefore is the most reliable recorder of igneous events [4]. In contrast, Ar-Ar, Rb-Sr, and U-Pb systems are more easily disturbed, accounting for the wide range of ages reported for highlands samples [Fig. 1]. However, replicate Sm-Nd ages on single samples are usually discordant. For example, average Sm-Nd ages determined on FANs 60025 and troctolite 76535, are 4.38±0.12 Ga and 4.34±0.18 Ga respectively (see refs in [1]; uncertainties are 2 stdev of ages).

Much of the disturbance to the Sm-Nd isotopic system is likely to reflect the fact that the Moon is a relatively small, water-poor body and consequently crystallizes only a limited number of phases that contain REE. These phases include: plagioclase, pyroxene, olivine, and phosphates. Many rocks contain only two REE-bearing phases so that isochrons produced from these samples are in essence mixing lines. These lines can have chronologic significance, provided fractions are in isotopic equilibrium. The presence of minor amonts of extraneous minerals, however, can produce highly linear "isochrons" (i.e. with small age uncertainties) that have do not temporal significance. Furthermore, the extraneous mineral phases can have very similar mineralogical characteristics to the indegeneous minerals and are therefore very difficult to detect. is difficult to detect [5]. Note that such mixing lines will have inappropriate initial isotopic compositions. ***Thus, isochron linearity is necessary but not sufficient to demonstrate isotope equilibrium.***

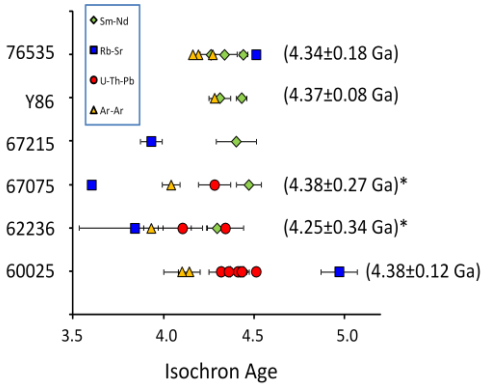

Figure 1. Ages of highlands samples that have been dated multiple times. Ages in parentheses are average Sm-Nd ages. * denotes average Sm-Nd and U-Pb ages.

Criteria: Samples that yield concordant ages from multiple isotopic systems almost certainly record a crystallization event. Ages determined by single chronometers should be considered with caution especially if: (1) multiple isotopic systems yield discordant ages on the same fractions, (2) ages are not reproducible between replicate analyses, and (3) initial isotopic compositions are inconsistent with petrogenetic models for the origin of the samples.

Conclusion: To our knowledge there are only three FAN and Mg-suite rocks that yield concordant ages from multiple isotope systems. These are FANs 67075 (4.47±0.07 Ga, [6]) and 60025 (4.359±0.003 Ga, [1]) and norite 78238 (4.344±0.037, Ga [7]). Clearly, the paucity of reliable ages does not permit the temporal relationship of these highland rock suites to be evaluated rigorously. Furthermore, the existing data indicate that the age distinctions are likely to be small (~50 Ma) between rock suites. Therefore in order to reliably elucidate the temporal relationships between highland samples the application of higher precision chronometers currently being developed will be required.

References: [1] Borg. et al. (2011) *Nature, 477,* 70-2. [2] Carlson & Lugmair (1988) *EPSL. 90,* 119-30. [3] Borg et al. (1999) *GCA. 63,* 2679-91. [4] Gaffney et al. (2011) *MAPS 46,* 35-52. [5] Shearer et al. (2012) LPSC #1421. [6] Nyquist et al. (2010) LPSC #1383. [7] Edmunson et al. (2009) *GCA 73,* 514-27. Prepared by LLNL under Contract DE-AC52-07NA27344.

STUDYING SPECTRAL VARIABILITY OF AN IGNEOUS STRATIFIED COMPLEX AS A TOOL TO MAPS LUNAR HIGHLANDS. C. Carli[1], M. Sgavetti[2], F. Capaccioni[1] and G. Serventi[2], [1]IAPS-INAF (via Fosso del Cavaliere 100, 00133, Rome, Italy; cristian.carli@iaps.inaf.it), [2]Physics and Earth Sciences, University of Parma (via delle Scienze, 157, Parma, Italy).

Introduction: Terrestrial planetary surfaces are characterized by high amount of igneous rocks. The Moon shows highland regions with a composition typical of plutonic basic rocks, and samples from the Apollo missions have confirmed the presence of such cumulitic rocks.

Similar plutonic complexes are present in the Earth, with mineral associations that could be considered as analogues of the lunar rocks. Moreover Moon Mineralogy Mapper (M^3) data have revealed that different portion of a magmatic chamber or separate plutons could be recognized by remote sensing data [1]. Describing spectra variation of samples from cogenetic rocks and quantifying spectral parameters could help to discuss and interpret the new spectral signatures and spectral variability shown by the new data.

Here we propose the analysis of the Stillwater Complex (SWC) rock suite. The spectral characterization of these rocks can represent both the background for understanding the geologic significance of the regolith composition and the starting point for modeling surface alterations. These rocks include ultramafic rocks, norites, gabbro-norites and anorthosites, and have significant analogies with lunar rock suites.

Background: The crusts of terrestrial planets and natural satellites largely consist of magmatic rocks, which are the natural products of magma-rock dynamic systems, controlled by T, P, oxygen fugacity and time. Individual rock-forming mineral assemblages represent well defined equilibrium points in the system evolution. Although initial magma composition and physical constraints could have been different, planets share common origin and genetic processes, whose evolution can be traced starting from rock compositions.

The Moon surface shows a high variability of igneous rocks, both volcanic and plutonic, with variable composition, subdivided in Maria and Highlands. Maria can be subdivided at first approximation in low-Ti, high-Ti, and high-Al composition, whereas highlands can be divided in Ferroan anorthosites, Mg rock suite, and KREEP material [2]. Recently M^3 data indicate unusual rock types (defined as 'OOS') dominated by orthopyroxene (opx), olivine (ol) and spinel (spl) in the Moscoviense region [1]. Although the abundance of plagioclase was not retrived the authors hypothesize that rock types could approach pyroxenite, harzburgite, and spinel rich rock. Moreover those rocks are embedded whithin anorthositic material so OOS could be contemporaneous with crustal products from the cooling magma ocean[1].

The terrestrial rock suites: The Stillwater Complex (SWC) is a cumulitic layered intrusion that was emplaced about 2.7Ga [3].

SWC was built up by two compositionally different magmas: a MgO and SiO_2 rich magma (olivine-saturated) which formed the Ultramafic Series, and a tholeitic magma from which the Banded Series originated. Cumulitic mafic minerals and opaque occur within the Ultramafic Series whereas the plagioclase cumulus occurs within the Banded Series.

Methods: Reflectance spectra were measured on slabs and powders (<125 and <250 μm grain sizes), representative of the Series of the Stillwater Complex. Rock samples of SWC were ground and dry sieved. Total reflectance spectra of slabs were measured using a double-beam, double monochromator spectrophotometer (Perkin-Elmer, Lambda19), with 0.35 – 2.5 μm spectral range and 1 nm spectral resolution. Bidirectional reflectance spectra of powders were measured using a spectrophotometer (Fieldspec pro) mounted on a goniometer, with 0.35 – 2.5 μm spectral range and 1 nm spectral resolution, i=30° e =0°.

We have used Gaussian models (e.g. Modified Gaussian Model [4]) to separate the contribution of Opx and Cpx and to determine the position of band I center (near 0.9 and 1.0 μm, respectively).

Results: *Spectra characterization.* The spectra show four different crystal field absorption bands: a wide 1.25 μm indicative of iron in plagioclase, two well defined bands at circa 1 and 2 μm indicative of Fe^{2+} in M1 and M2 sites of pyroxenes, and a wide 2 μm absorption indicative of Chr-spinel. Samples can be generally grouped in four classes considering different association of the absorptions. Moreover, variation of the position and intensity of the bands can be correlated with the chemistry and modal composition (Fig. 1).

Band minima vs mineral chemistry.

As expected, fitting parameter results for SWC spectra split into two groups, which plot within the high Ca and low Ca pyroxene fields (Fig. 2, after [5]). The systematic variation of band minima with Fs content is shown by the trend for both low Ca and high

Ca pyroxene. Moreover powders and slabs have similar positions, as expected, with a slight shift for rocks with higher amount of Fe^{2+}.

Band depth vs modal composition of rocks.

A good linear relationship exists between pyroxene band I intensity and the modal distribution of Fe^{2+} (Fe^{2+} * px mod. Ab.) within powdered samples and rocks samples belonging to the SWC (Fig.3).

Conclusions and future work: 1) Using a band fitting technique, both mineral chemistry and modal abundance of lunar rock analogues can be estimated with fairly good accuracy for complex mixtures like powdered rocks. 2) Considering the modal distribution of Fe^{2+} also samples with saturated absorption bands of mafic minerals show a linear relationship with the band intensity. 3) Further work is still required in order to simulate or model the weathering effects on these rocks and thus allow comparison with Moon soils.

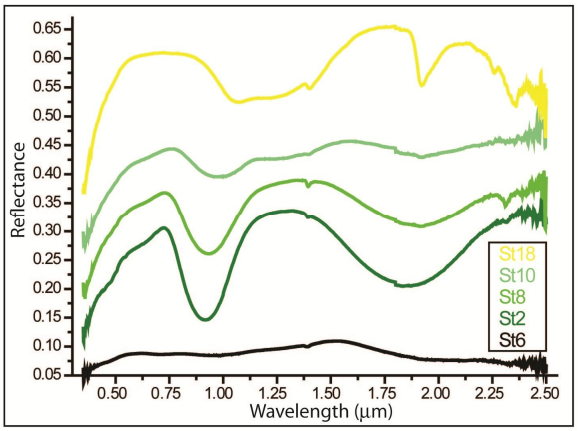

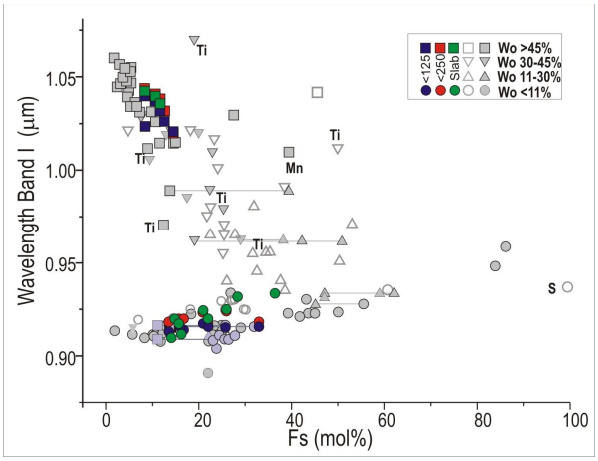

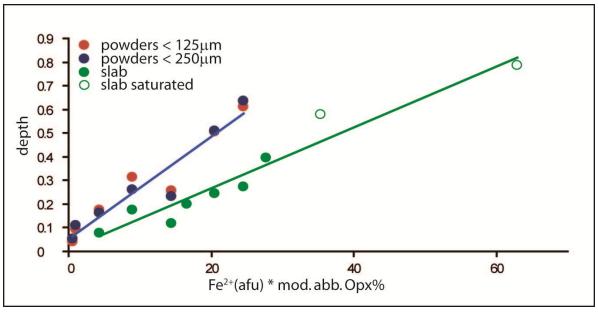

Fig. 1: Spectra of different rock types: St6, Chr-spl rich rock, St2, St8, Px rich rocks, pyroxenite and gabbronorite, respectively, St10, pl rich, px bearing rock, leucogabbro, St18, high pl content, anorthosite. **Fig. 2:** band I position vs molar Ferrosilite in pyroxenes. Modified after [5, 6]. **Fig. 3:** Pyroxene band I depth vs modal distribution of Fe^{2+}, confidence level of 99%.

References: [1] Pieters C. M. et al. (2011) JGR, 116, doi:10.1029/2010JE003727. [2] Lucey et al. (2006) in New views of the Moon, RiMG, 60, 83-220. [3] McCallum I. S. (1996) in Layered Intrusions, Elsevier, 441-483. [4] Sunshine J. et al. (1990) JGR, 95, 6955-6966. [5] Cloutis E. A. and Gaffey M. J. (1991) JGR, 96, 22809-22826. [6] Pompilio L. et al. (2007) JGR, 112, 10.1029/2006JE002737.

THE DISTRIBUTION AND MINERALOGY OF ANORTHOSITE IN THE ORIENTALE BASIN: NEW PERSPECTIVES FROM M³ DATA . L. C. Cheek,[1] K. L. Donaldson Hanna[1], C. M. Pieters[1], J. W. Head[1], J. L. Whitten[1], [1]Dept. of Geological Sciences, Brown University, Providence, RI, 02912 (Leah_Cheek@brown.edu).

Introduction: The Orientale basin is a 930 km multiring impact structure on the western limb of the Moon. Due to the unique preservation of its ring structure, Orientale has been the focus of studies aiming to understand not only the nature of the lunar crust exposed during the impact event, but also the mechanics of large-scale impact processes that have operated throughout the solar system. Orientale's innermost ring, the Inner Rook Mountains (IRM), has long been thought to expose anorthosite from beneath the mixed megaregolith, based on Earth-based telescopic data and Clementine multispectral data [e.g. 1-3]. Anorthosite is a rock type consisting of ≥90% plagioclase that is believed to dominate the upper crust of the Moon as a cumulate from a crystallizing magma ocean early in the Moon's history [e.g. 4]. However, due to limitations in both spatial and spectral resolution, the earlier remote sensing data did not detect the diagnostic plagioclase absorption feature near 1250 nm. Instead, featureless, high albedo spectra in the IRM were identified and attributed to a shocked form of anorthosite, since experimental studies have shown that the plagioclase absorption is erased when the mineral is shocked to pressures greater than 25 GPa [5-7].

Recently, the Multiband Imager (MI; onboard SELENE) and the Moon Mineralogy Mapper (M^3; onboard Chandrayaan-1) have identified the diagnostic plagioclase absorption in a few isolated locations within the IRM [8, 9]. These direct identifications in the IRM have confirmed the previous inferences about their anorthositic nature, and suggest that certain areas within the ring have experienced slightly lesser degrees of shock metamorphism. The high spectral and spatial resolution of these new datasets permits a thorough assessment of the mineralogy and distribution of anorthosite in the Orientale Basin.

Here we present a detailed analysis of the anorthosite exposed in the Orientale Basin using hyperspectral imaging data from M^3. Specifically, we aim to characterize 1) the distribution of "crystalline anorthosite," which retains a plagioclase absorption band and therefore has not been shocked above ~25 GPa, and 2) variations in the "purity," or plagioclase abundance, of anorthosites across the basin, as indicated by the relative strengths of the plagioclase and mafic absorption bands.

Methods: M^3 is a hyperspectral imaging spectrometer that acquired near-global coverage of the Moon in 85 spectral bands from 460 – 3000 nm at a spatial resolution of 140 or 280 m/pixel. Spectral parameters computed for a full-resolution mosaic of Level 2 M^3 data strips for the Orientale Basin were used to identify pixels with absorption features. The spectra from these pixels were classified according to the relative strengths of their diagnostic absorption bands: Class A spectra display only a plagioclase absorption, Class B spectra contain both mafic and plagioclase signatures, but are dominated by the plagioclase feature, and Class C spectra are dominated by mafic absorptions.

Results: Initial results indicate that 1) crystalline anorthosite (i.e. anorthosite shocked to <25 GPa) is pervasive throughout the basin, and that 2) the most highly pure anorthosite (> ~ 98% plagioclase) is concentrated in, though not confined to, the IRM.

Crystalline Anorthosite. The plagioclase absorption feature is identified in many locations throughout the Orientale Basin. Detection of the 1250 nm feature requires that these particular areas have a plagioclase abundance on the order of 85% or more [10] and that they did not experience shock pressures in excess of ~25 GPa. The plagioclase detections are typically small in spatial extent (~1 km), and preliminary analyses of high-resolution LROC NAC images suggests that strong features correspond to fresh craters or rocky areas on massifs.

Spectra from a traverse along a single IRM massif are shown in Figure 1. In this traverse, the spectra displaying a plagioclase absorption (spectra 3 & 4) are surrounded by material with featureless spectra (spectra 1, 2, 5, & 6). The featureless materials are more spatially extensive than the crystalline anorthosite exposures and may be analogous to the shocked anorthosite described in earlier data. Additional analyses will focus

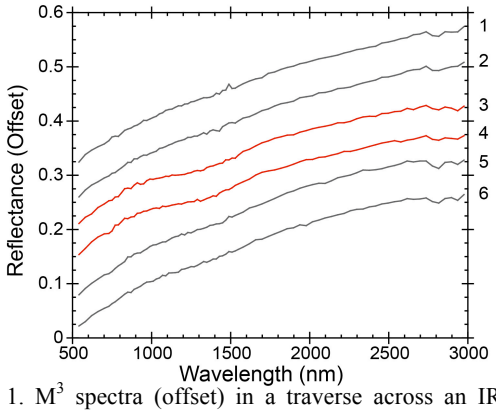

Figure 1. M^3 spectra (offset) in a traverse across an IRM massif. Each spectrum represents 1 pixel, and is separated from the next by 1 pixel. The two spectra showing a plagioclase absorption feature are surrounded by materials with featureless spectra. Spectra 3 and 4 are "Class A".

on characterizing the physical nature of the featureless material using LROC NAC images.

Variations in mafic mineral content. An initial map of the three spectral classes in the Orientale Basin (mare excluded) is shown in Figure 2, illustrating the variations in plagioclase vs. mafic mineral content discerned by qualitatively comparing the relative strengths of the plagioclase (1250 nm) and mafic mineral (1000 nm) absorption bands. In Orientale, the dominant mafic mineral is pyroxene; no definitive olivine detections are reported.

Class A materials (red dots) display only a plagioclase absorption (no pyroxene absorptions are present), constraining their plagioclase content to ~ 98% or greater based on intimate mixing calculations [11]. These highly pure anorthosites are concentrated in the IRM, although a few occurrences are found exterior to the inner ring. Class B spectra (yellow dots) are dominated by the plagioclase feature but also show weak pyroxene absorptions and are predominately located in the IRM. Comparison with mixing calculations suggests that these materials contain around 94-98% plagioclase. Class C materials (purple dots) have spectra dominated by mafic absorptions, suggesting that they are <94% plagioclase. Mafic-dominated spectra are known to sometimes display an absorption near the location of the plagioclase feature (1200 nm) that is due to Fe^{2+} in the M1 site of Ca-rich pyroxenes [12], making it difficult to distinguish if weak absorptions in this range are due to mixtures with plagioclase. The present classification does not attempt to assign the ~ 1200 nm band in mafic-dominated spectra to either plagioclase or pyroxene, and therefore Class C may represent a wide range of mineralogies. Class C materials occur throughout the entirety of the basin but are slightly less common in the IRM.

Conclusions: The presence of crystalline anorthosite in both of Orientale's inner rings suggests that certain locations throughout the basin have been shocked to < 25 GPa. Further, the high purity of the anorthosite in the IRM is consistent with an upper crustal origin, whereas the ORM are distinctly more mafic and therefore may be derived from the overlying mafic megaregolith [13]. The extremely low mafic mineral content throughout the IRM is consistent with plagioclase flotation over large spatial scales, although mechanisms for removing nearly all residual mafic liquids from the plagioclase grains during this process are still unclear.

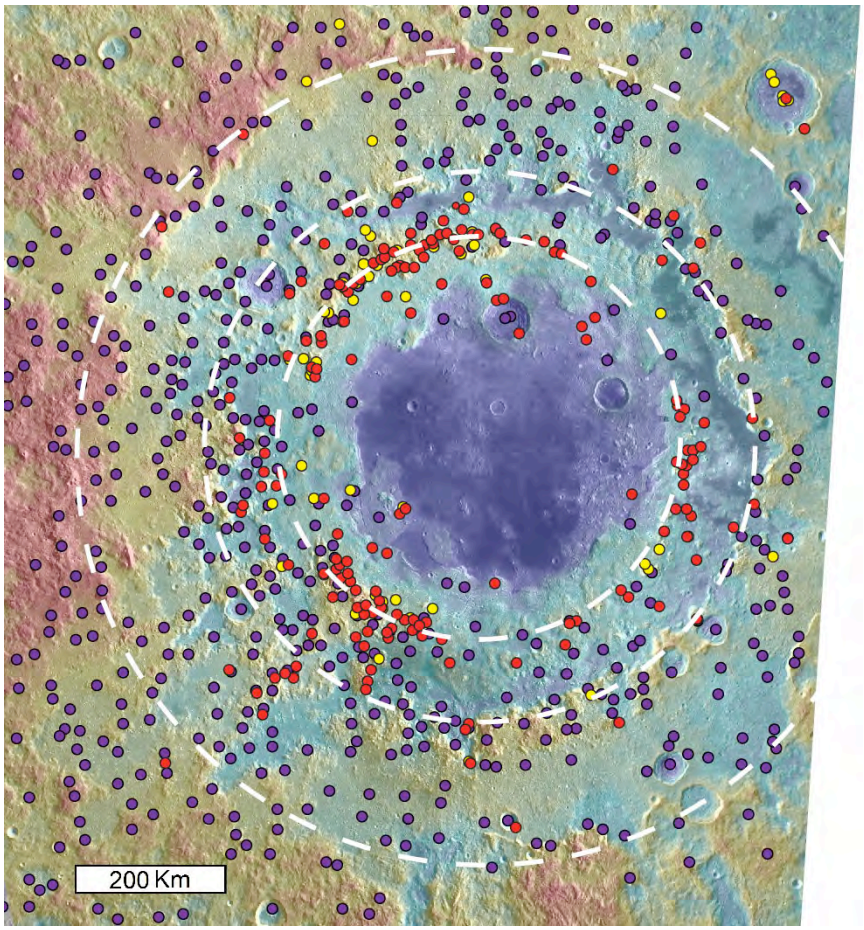

Figure 2 (left). Distribution of plagioclase vs. mafic mineral content in the Orientale Basin (mare excluded). Red dots represent Class A materials that are > ~98% plagioclase. Yellow dots (Class B) are likely ~94-98% plagioclase, and Purple dots (Class C) are < ~94% plagioclase. The classification reveals that the purest anorthosite is concentrated in the IRM.

References: [1] Spudis P. D. et al. (1984) *PLPSC15*, C197-C210. [2] Bussey B. J. and P. D. Spudis (2000) *JGR, 105(E2)*, 4235-4243. [3] Hawke B. R., et al. (2003) *JGR, 108 (E6)*, 5050. [4] Wood et al (1970) *GCA Suppl., 1*, 965-988. [5] Adams J. B. et al. (1979) *LPS X*, Abstract # 1. [6] Johnson J. R. and F. Horz (2003) *JGR 108(E6)*, 5120. [7] Bruckenthal, E. A. and Pieters, C. M. (1984) *LPS XV*, Abstract #96. [8] Ohtake M. et al. (2009) *Nature, 461*, 236-240. [9] Pieters C. M. et al. (2009) *LPS XL*, Abstract # 2052. [10] Crown, D. A. and C. M. Pieters (1987) Icarus, 72, 492-506. [11] Cheek L. C. and C. M. Pieters (2012), LPS XLIII, Abstract # 2731. [12] Klima, R. L. et al., (2010) *MaPS, 43*, 1591-1604. [13] Head, J. W. et al., *JGR, in prep.*

MODAL ANALYSES OF APOLLO SOILS BY X-RAY DIFFRACTION AND MICROSCOPIC SPECTRAL IMAGING. Sarah Crites[1], G. Jeffrey Taylor[1], Linda M.V. Martel[1], Paul G. Lucey[1], and D.F. Blake[2],[1]Hawai'i Institute of Geophys. & Planetology, 1680 East-West Rd., Honolulu, HI 96822, gjtaylor@higp.hawaii.edu, [2]NASA Ames Research Center, Moffett Field, CA.

Introduction: We have launched a project to determine the modal mineralogy of over 100 soils from all Apollo sites using quantitative X-ray diffraction (XRD) and microscopic hyperspectral imaging at visible, near-IR and thermal IR wavelengths. The two methods are complementary: XRD is optimal for obtaining the major mineral modes because its measurement is not limited to the surfaces of grains, whereas the hyperspectral imaging spectroscopy method allows us to identify minerals present even down to a single grain, well below the quantitative detection limit of XRD. The goal is to use this quantitative mineralogy in comparison with reflectance and thermal emission spectra of the same soils and with remote sensing data of the sampling stations to improve our ability to extract quantitative mineralogy from remote sensing observations.

We report here our initial results from analysis of the <150 μm fraction of 30 Apollo 16 soils. We also analyzed 90–150, 45–90, 25–45, and <25 μm fractions from Apollos 12, 14, and 16 for comparison with previous data [1-3]. A bonus of analyzing numerous soils from one site is that it allows us to test ideas for the petrologic character of geologic terrains such as at the Apollo 16 site, specifically the Descartes Mountains and the Cayley Plains.

Methods: For XRD, samples were dry-sieved to obtain >150 and <150 μm fractions. Samples were analyzed in an InXitu Terra XRD instrument using sample masses of ~35 mg; we did replicate analyses of each sample and averaged them. We reduced the data using Reitveld refinement as implemented by the Jade program. Glass abundances were determined by fitting a broad Gaussian to the scattering hump above a linear background. We calibrated the instrument by using mineral mixtures and results from the Lunar Sample Characterization Consortium (LSCC [1–3]). A comparison of our data for three soil samples (25–45 μm fraction) and data from the LSCC are shown in Fig. 1. The dashed line is simply a 1:1 line; a line fitting to the data has a slope of 0.97. The standard deviation of the dataset is 2.8 wt%, which is acceptable for improving remote sensing data, and we expect it to decrease as we analyze more samples that were also studied by the LSCC.

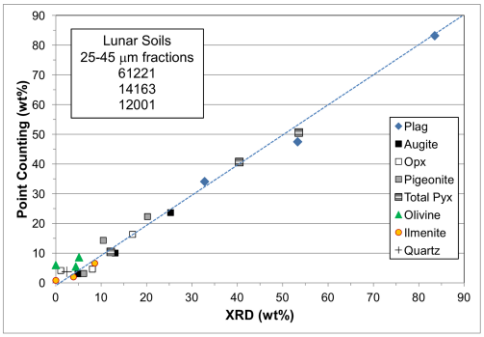

Fig. 1. Our XRD modes vs LSCC results [1–3].

For microscopic thermal imaging we measure wet-sieved soils at a variety of grain sizes as we develop our methodology, to date using 45-75 microns, 75-150 microns, 75-125 microns, and >75 mcrons. Spectral images at 30 micron resolution are measured over fields of 8x30 mm at both near and thermal IR wavelengths using spectrometers built by us. Near-IR data are collected at 10 nm resolution from 900-2500 nm, and thermal IR data at 20 wavenumber resolution from 8 to 14 microns.

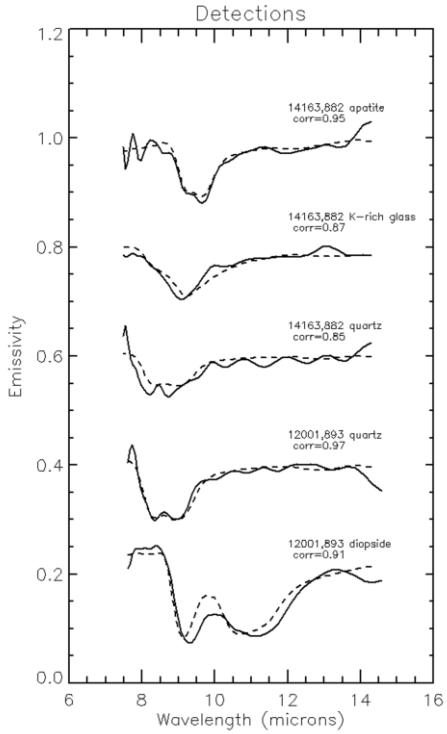

Figure 2. Thermal IR spectra of individual grains in Apollo soils. "Corr" is a correlation parameter indicating similarity with library reference spectra.

Results: XRD: On a glass-free basis, plagioclase ranges from 78 to 94 wt%, with the sites on the Descartes Mountains (Stations 4, 11, and 13) tending to contain more plagioclase (Fig. 3). This is consistent

with previous conclusions that the Descartes highlands are more feldspathic than the Cayley Plains [e.g., 5]. The relative abundance among pyroxenes and between pyroxene and olivine varies throughout the site, with little correlation with sampling location (Figs. 3–5).

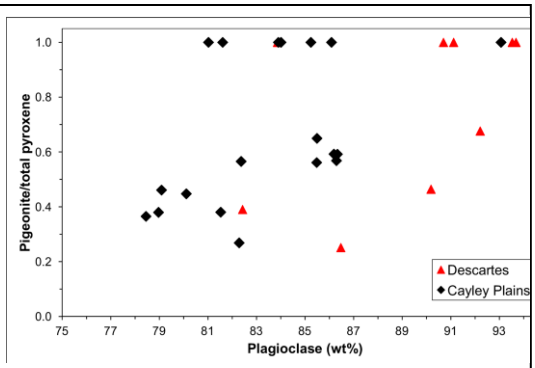

Fig. 3. Normative plagioclase (glass-free basis) vs the ratio of pigeonite to total pyroxene. Note that in general the Descartes sites are richer in plagioclase.

Modal plagioclase is systematically greater than normative plagioclase (Fig. 5). A difference between modes and norms is not unusual, but this substantial difference indicates that the glass in the Apollo 16 regolith is more mafic than the crystalline material. This is consistent with the average composition of impact glass in Apollo 16 samples compared to bulk soils [3]. For example, bulk regolith contains 26–30 wt% Al_2O_3 [literature values], whereas impact glasses on average contain 23–27 wt% [3,6].

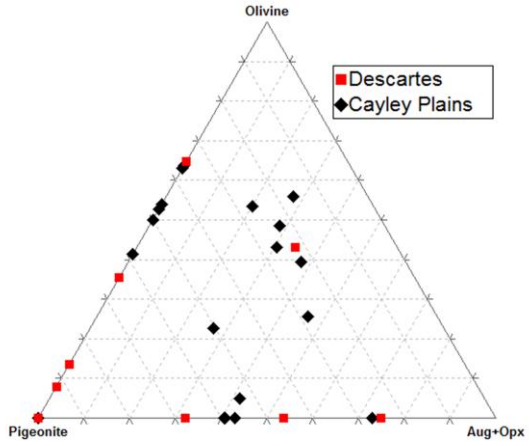

Fig. 4. Relative abundance of mafic silicates in Apollo 16 soils. Although the Descartes sites are richer in plagioclase (Fig. 3), mafic mineralogy is variable.

Spectroscopy: The high resolution imaging capability enables detection of relatively rare components in the soils. To date we have identified quartz, K-rich glass and apatite in soils from various landing sites using thermal IR spectroscopy. Taking the cautions of [4] regarding near-IR microscopic spectral imaging, the samples are arrayed on a glass slide above a first surface mirror to allow dark field measurements that limit the signal to transmitted light. High contrast near-IR spectra are obtained using this method.

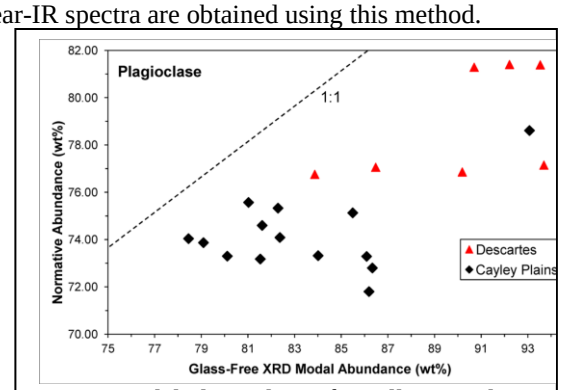

Fig. 5. Modal plagioclase of Apollo 16 soils is greater than normative mineralogy, indicating that the glass component is systematically less feldspathic than is the crystalline component.

Discussion: Our XRD results are consistent with previous studies that concluded that the Descartes highlands, as represented particularly by ejecta from North Ray Crater, are more feldspathic than the Cayley Plains [5–9]. The Cayley Plains are more mafic, probably because of addition from Imbrium [6,10] and other basin [11] ejecta. Additional mafic components may have been added to the site from mare sources [3].

This work re-emphasizes the difference in chemistry between the minerals and glass components of the soils recognized by [1-3]. This has important implications for using these data for calibration of remote sensing data. Methods must be developed to decide how ground truth measurements such as being developed here are to be applied to remote data.

Acknowledgement: Supported by NASA Grants NNX11AE85G and NNX08AZ06G.

References: [1] Taylor, L.A. et al. (1996) *Icarus, 124*, 500-512. [2] Taylor, L.A. et al. (2001) *Meteoritics & Planet. Sci.,, 36*, 288-299. [3] Taylor, L.A. et al. (2010) *JGR ,115*,doi:10.1029/2009JE003427. [4] Klima R.L. and Carle M. Pieters (2006), *JGR, 111*, E01005. [5] Spudis, P.D. and C.M. Pieters (1991) *Lunar Sourcebook*, 595-632. [6] Korotev, R. L. (1996) *Meteor. & Planet. Sci., 31*, 403-412. [7] Taylor, G.J. et al. (1973) *PLSC 4th*, 553-568. [8] Norman, M.D. (1981) *PLPSC 12th*, 235-252. [9] Stoffler, D. et al. (1985) *PLPSC 15th*, C449-C506. [10] Korotev, R.L. et al. (2010) *GCA, 74 7362-7388.* [11] Petro, N.E. and C.M. Pieters (2006) *JGR,111*, doi:10.1029/2005JE002559.

COMPOSITIONAL DIVERSITY OF CRYSTALLINE PLAGIOCLASE IN THE LUNAR HIGHLANDS. K. L. Donaldson Hanna[1], C. M. Pieters[1], B. T. Greenhagen[2], and L. C. Cheek[1], [1]Department of Geological Sciences, Brown University, Providence, RI 02912, (Kerri_Donaldson_Hanna@Brown.edu), [2]Jet Propulsion Laboratory, California Institute of Technology, Pasadena, CA 91109.

Introduction: The anorthositic highlands, the primary crust of the Moon, likely formed by the crystallization and floatation of plagioclase in the late stages of a lunar magma ocean due to the density difference between plagioclase and the remaining mafic liquid [e.g. 1-3]. The impetus for these magma ocean models came from the analysis of pristine samples returned from the Apollo 11, 15, and 16 missions which provided the first evidence of this primary crust in the form of widely distributed ferroan anorthosites (FANs) in the sample suites [e.g. 1,4]. The ferroan anorthosites have distinct characteristics that uniquely identify them from other pristine rock samples including: (1) plagioclase has a small compositional range (An_{94-98}) and (2) relatively low Mg# for co-existing mafic silicates [e.g. 4-6]. However the Apollo ferroan anorthosite samples represent a small portion of the lunar surface; therefore it is unclear whether the range in AN# observed in the Apollo samples represents the AN# range of all ferroan anorthosites on the Moon. Thus the question remains as to how deviations from the An_{94-98} might change current models of the lunar magma ocean.

Recent near infrared (NIR) observations from the SELENE Spectral Profiler (SP) and Multiband Imager (MI) and the Chandrayaan-1 Moon Mineralogy Mapper (M^3) have uniquely identified Fe-bearing crystalline plagioclase in the walls, floor, ejecta, and central peaks of craters as well as lithologies associated with basins like the Inner Rook Mountains of Orientale Basin [7-12]. These results are significant because they validate earlier observations [e.g. 13-14] as well as characterize the widespread distribution of crystalline plagioclase across the lunar surface.

The identification of Fe-bearing crystalline plagioclase in the NIR comes from a broad absorption band at approximately 1.25 μm due to the electronic transition of minor amounts of Fe^{2+} in the crystal structure. While previous NIR lab studies have suggested that the band depth and center position of the 1.25 μm feature may vary with Fe and An content [15-16], the relationship between NIR spectral properties of plagioclase and its composition (AN#) has yet to be quantified. However, new laboratory thermal infrared (TIR) emissivity measurements of varying compositions of the plagioclase solid solution series measured under simulated lunar conditions demonstrate that the position of the Christiansen Feature (CF), an emissivity maximum indicative of composition [17], is linearly related to the AN# [18]. Ca-rich plagioclase compositions like anorthite have CF positions near 7.84 μm while Na-rich compositions like albite have CF positions near 7.6 μm [18]. Thus, regions of spectrally pure crystalline plagioclase (<2% olivine and pyroxene) as identified in NIR spectra are ideal areas to investigate the utility of TIR data to constrain plagioclase compositions [18-19].

Here we use identifications of crystalline plagioclase made with M^3 NIR reflectance data and integrate those observations with Diviner TIR data to better understand the variability of plagioclase compositions across the lunar surface in an effort to constrain thermal and chemical regional variations in the lunar magma ocean or indicate locations of excavated Mg-rich materials (products of the lunar secondary crust) or source regions for Mg-anorthosites identified in feldspathic meteorites [e.g. 20-21].

Data and Methods: M^3 is an imaging spectrometer that acquires images of the lunar surface across 85 wavelengths (0.43 – 3.0 μm) at a spatial resolution of

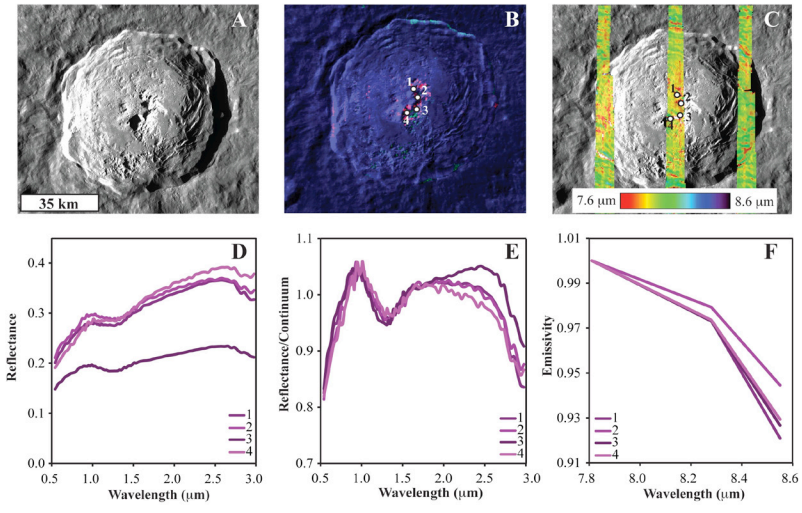

Figure 1. (A) LROC WAC reflectance image of Jackson crater. **(B)** M^3 RGB image overlain on the WAC image where R = IBD at 1.25 μm, G = IBD at 1.0 μm, and B = reflectance at 1.6 μm. Red areas indicate regions identified as pure crystalline plagioclase. Circles indicate where 5 x 5 pixel locations were extracted for spectra. **(C)** Diviner CF map overlain on the WAC image. Areas of short CF positions (red units) indicate plagioclase rich areas. Circles indicate locations where CF values were extracted. **(D)** M^3 reflectance spectra extracted from areas as indicated in **B. (E)** M^3 reflectance spectra where a continuum (anchored at ~1.0 μm and 2.7 μm) has been removed. **(F)** Diviner emissivity spectra extracted from areas indicated in **C**.

140 or 280 m/pixel. An integrated band depth (IBD) used to identify plagioclase is calculated by removing a continuum between 1.03 and 1.7 μm and summing band depths over 27 bands across the broad 1.25 μm absorption. M^3 spectra were also extracted from each of the high IBD value regions to confirm the identification of spectrally pure crystalline plagioclase. Regions are identified as spectrally pure (>98% plagioclase) if mafic absorptions near 1 and 2 μm are absent in the M^3 spectra [11].

Diviner is currently in orbit about the Moon onboard NASA's Lunar Reconnaissance Orbiter has three spectral bands near the 8 μm region chosen specifically to measure the peak of the CF [19]. Diviner radiance data for lunar mid-day over spectrally pure plagioclase regions are converted to emissivity and used to generate a CF map. Diviner TIR emissivity spectra are extracted to confirm the identification of plagioclase.

Results: This survey includes craters where crystalline plagioclase has been identified and Diviner data coverage is good. To date fifteen craters have been analyzed. Analysis of M^3 and Diviner data over each crater shows a nice correlation between the M^3 IBD plagioclase spectral parameter and the Diviner CF map as seen in Figure 1 for Jackson crater. Areas highlighted in red in both maps are areas of spectrally pure plagioclase. M^3 reflectance spectra and Diviner emissivity spectra extracted for these regions confirm the presence of plagioclase. Average CF values for all craters analyzed range from 7.74 – 7.94 μm with standard deviations between 0.01 – 0.07 μm.

Plagioclase samples of known compositions have been measured under simulated lunar conditions and a linear relationship between the AN# of the sample and its CF position (Figure 2). This linear relationship can be used along with the average and standard deviation of the CF values to compute the mean AN# as well as the range of AN#'s for each spectrally pure region. Results for 13 of the 15 craters indicate Ca-rich compositions ($An_{>90}$) similar to plagioclase compositions in the ferroan anorthosite samples while the other 2 highlands craters (Jackson and Humboldt) have more Na-rich compositions (An_{71-84}). AN#'s > 100 are obviously unphysical. This could result from: (1) a lack of terrestrial anorthites with high-Ca contents available for our lab analysis or (2) space weathering of the plagioclase-rich units.

Conclusions: Integrated near- and thermal-infrared analyses provide robust determinations of mineral compositions (AN#) for understanding the origin of lunar crustal rocks. Widespread distribution of crystalline plagioclase of similar compositions supports the idea of a single global differentiation event like a lunar magma ocean. A majority of the crystalline plagioclase identifications suggest that the compositions of plagioclase in ferroan anorthosites are consistent with plagioclase across most of the lunar highlands. Regions with more Na-rich plagioclase compositions suggest: (1) local heterogeneities in magma ocean, (2) regions of Mg-rich materials (secondary crustal products), or (3) source regions of Mg-rich anorthosites found in lunar meteorites.

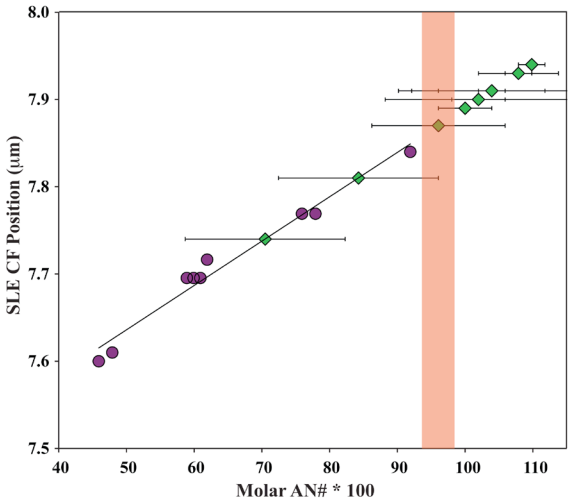

Figure 2. The purple circles represent plagioclase samples of known compositions measured under simulated lunar conditions in the lab. The linear fit is fit to the lab data. The green diamonds are the mean AN# for each spectrally pure plagioclase region while the horizontal line gives the range in AN# for each region. The orange box indicates the AN# range of plagioclase in the ferroan anorthosites.

References: [1] Wood J. A. et al. (1970) *Proc. Apollo 11 Lunar Sci. Conf., 1*. [2] Warren P. H. (1985) *Ann. Rev. Earth Planet. Sci., 13*. [3] Warren P. H. (1990) *Am. Mineral., 75*. [4] Dowty E. M. et al. (1974) *Earth Planet. Sci. Letters, 24*. [5] McGee J. J. (1993) *JGR, 98*. [6] Papike J. J. et al. (1998) *Rev. Min. Geochem., 36*, 1014p. [7] Matsunaga T. et al. (2008) *GRL*, *35*. [8] Ohtake M. et al. (2009) *Nature, 461*. [9] Pieters C. M. et al. (2009) *LPS XL*, Abstract #2052. [10] Donaldson Hanna K. L. et al. (2012) *LPS XLIII*, Abstract #1968. [11] Cheek L. C. and Pieters C. M. (2012) *LPS XLIII*, Abstract #2624. [12] Cheek L. C. et al. (2012) *LPS XLIII*, Abstract #2731. [13] Spudis P. D. et al. (1984) *JGR, 89*. [14] Hawke B. R. et al. (2003) *JGR, 108*. [15] Adams J. B. and Goullaud L. H. (1978) *LPS IX*. [16] Cheek L. C. et al. (2009) *LPS XL*, Abstract #1928. [17] Conel J. E. (1969) *JGR, 74*. [18] Donaldson Hanna K. L. et al. (2011) *LPS XLII*, Abstract #1968. [19] Greenhagen B. T. et al. (2010) *Science, 329*. [20] Korotev R. L. et al. (2003) *Geochim. et Cosmo. Acta, 67*. [21] Takeda H. et al. (2006) *Earth Planet. Sci., 247*.

REOPENING A CAN OF WORMY INTERGROWTHS: A NEW LOOK AT CHROMITE SYMPLECTITES IN Mg-SUITE TROCTOLITE 76535 S. M. Elardo, F. M. McCubbin, and C. K. Shearer, Jr., Institute of Meteoritics, University of New Mexico, Albuquerque, NM 87131 selardo@unm.edu

Introduction: At the Sixth Lunar Science Conference, there was an "animated debate" [1] concerning the origin and significance of symplectites in some olivine-bearing lunar rocks. Mg-suite troctolite 76535 is one such rock. Symplectite assemblages in 76535 consist of Mg-Al-chromite and two pyroxenes [1-5]. These symplectites occur primarily at olivine-plagioclase grain boundaries (e.g. Fig. 1a), but importantly, most grain boundaries are symplectite-free. Previously proposed symplectite formation mechanisms include crystallization of trapped interstitial melt and an olivine-plagioclase reaction which included diffusion of Cr from cumulus olivine and/or remobilization of pre-existing cumulus chromite grains [1-5]; however the topic never saw a substantial resolution.

A characteristic feature of olivine in Mg-suite rocks is that it is significantly depleted in Ni, Co and Cr relative to mare basalt olivine. The low Cr content of the cumulus olivine implies that Mg-suite magmas, and by inference their source material, were also low in Cr [6]. If correct, this would be a curious feature given that 76535 contains significant Cr sporadically, but highly, concentrated in symplectite assemblages. However, the symplectite formation mechanisms above imply that this Cr-depletion may be illusory.

With the goal of better constraining the origin of the symplectites in 76535 and petrogenesis of the Mg-suite, we present a detailed petrologic and textural investigation of symplectites, as well as their relationships to intercumulus and primary cumulus phases. We have also investigated chromite veins (Fig. 1b), olivine-hosted melt inclusions (MIs; Fig. 1c) and intercumulus assemblages (Fig. 1d) in 76535 to determine what information they record in regards to the origin of the symplectites and the magmatic processes that formed the Mg-suite layered intrusions.

Analysis: Sample 76535 has experienced minimal shock and retains original, albeit metamorphic, textures and well-preserved symplectites. Several thin sections were analyzed in this study: 76535,46 ,56 and ,159. Prior to microbeam analyses, samples were documented via optical and electron microscopy to fully understand textural relationships and identify potential targets for subsequent analysis. Olivine, orthopyroxene (OPX), clinopyroxene (CPX), chromite, apatite and merrillite were analyzed for major and minor elements using the electron microprobe at the University of New Mexico.

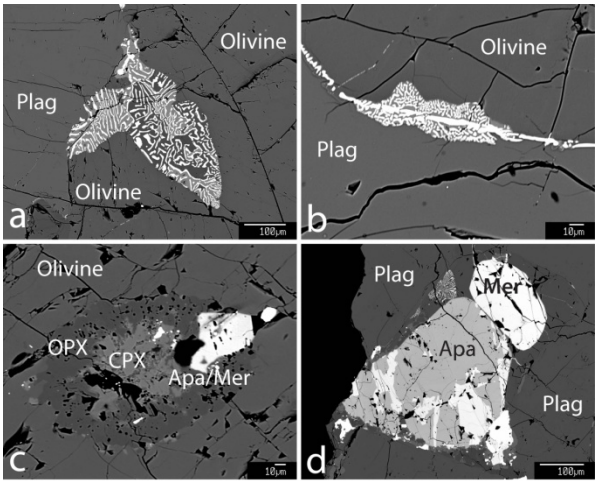

Figure 1: BSE images of a typical symplectite (a), an example of chromite veining with a small symplectite (b), an olivine-hosted melt inclusion (c), and an intercumulus assemblage (d) that contains a small symplectite.

Results: Symplectites occur mostly along olivine-plagioclase grain boundaries, but by far most boundaries are free of symplectites. Figure 1a shows a typical symplectite at such a boundary. Symplectites are sometimes associated with discontinuous chromite veining along grain boundaries. Figure 1b shows a chromite vein with a small symplectite. Chromite veins along olivine-plagioclase boundaries often occur within close proximity to chromite-free olivine-plagioclase boundaries. Chromite was not observed as discrete crystals or as inclusions in cumulus phases.

Multiphase intercumulus assemblages also contain small symplectites (Fig. 1d); however olivine-hosted MIs do not contain chromite. Both the MIs and intercumulus assemblages contain apatite-merrillite intergrowths. Apatite between the two textural occurrences is identical in terms of halogens. Other phases present in intercumulus assemblages include OPX, CPX, baddeleyite, zircon and Fe-Ni metal. Other phases in MIs include OPX, CPX, Fe-Ni metal, a K-Ba-Si-rich phase (probably K-spar), and pyrochlore.

Olivine-hosted melt inclusions (e.g. Fig. 1c) are low in Cr. Whereas OPX and CPX in symplectites contain an average of 7400 and 8100 ppm Cr_2O_3, respectively, OPX and CPX in the melt inclusions contain an average of 900 and 1200 ppm Cr_2O_3, respectively (Fig. 2). Sample 76535 also contains large interstitial OPX grains that are similar in composition, including Cr, to symplectite OPX (Fig. 2).

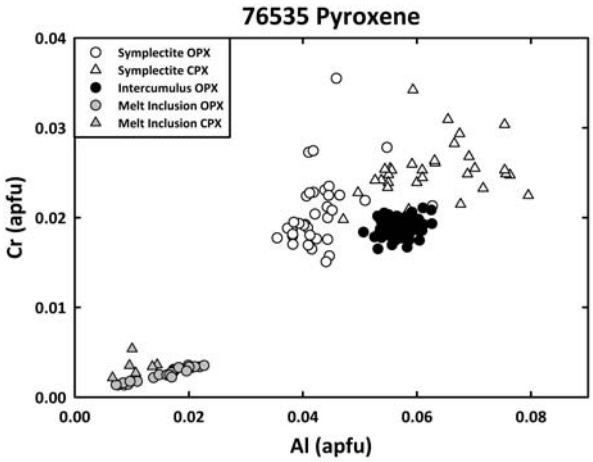

Figure 2: A plot of Cr vs. Al in atoms per formula unit for pyroxenes in troctolite 76535. Melt inclusion pyroxenes are significantly depleted in Cr relative to symplectite and intercumulus pyroxenes.

Discussion: In light of our new data, presented in [7], we have reassessed previously proposed symplectite formation models. The crystallization of intercumulus melt pockets was favored by [3, 5]. This mechanism would require significant adcumulus growth of plagioclase and olivine for a melt pocket to produce the large amount of chromite observed in symplectites. However, the symplectites exhibit textures more consistent with consumption of olivine and plagioclase in a mineral-mineral reaction [i.e. 8], with some symplectites preserving relict grain boundaries. Additionally, symplectites do not contain other minor phases (e.g. apatite, baddeleyite) that are indicative of intercumulus assemblages, which do seem to represent trapped melt pockets [e.g. 1-2, 4]. Based on these observations, we rule out crystallization of trapped melt.

Symplectite formation via a reaction between olivine and plagioclase that included diffusion of Cr from olivine or the remobilization of pre-existing chromite was preferred by [3-4] and [2], respectively. In the diffusion model, Cr in symplectite chromite is derived from originally more Cr-rich cumulus olivine. However, we observe olivine not in contact with and far away from symplectites that is also low in Cr. If olivine lost Cr, we would expect chromite in contact with or surrounding olivine throughout the rock. The low Cr content of the MIs also argues against Cr diffusion (Fig. 2). Furthermore, reduced systems such as lunar magmas can have Cr^{2+}/Cr^{3+} ratios greater than 1 [9-10], and olivine partitions the two valence states roughly equally [10]. Cr diffusion creates the need for a Cr^{2+} oxidation mechanism to create the large amounts of Cr^{3+}-rich chromite. This, combined with the observation that olivine in chromite-saturated melts at low f_{O2} contain 1000's of ppm Cr_2O_3 [9-10], rules out diffusion of Cr from olivine.

The remobilization of pre-existing chromite is argued against by the high-Cr content of olivine in equilibrium with chromite-saturated melts, low Cr-content of MIs, and lack preserved primary chromite. If the parental melt was saturated in chromite, the olivine should be much richer in Cr, and diffusional loss of that Cr is argued against above. We would also expect at least some cumulus chromite to be preserved as discrete grains or as inclusions, which is not the case.

Failure of these symplectite formation mechanisms implies that open system addition of Cr to 76535 is required. We have evaluated three potential models for Cr addition: solid state addition of chromite, Cl-rich fluid metasomatism [i.e. 4], and metasomatism by a melt. Solid state addition may come in the form of differential settling of dense chromite from higher regions of the 76535 pluton. However, there are no chromite–rich samples of the Mg-suite that may represent such a region, and the mechanism by which chromite settles through a partially molten intrusion and stalls in the troctolite layer is unclear. A Cl-rich fluid has the potential to mobilize the typically fluid immobile Cr^{3+} [e.g. 11]; however, such a fluid should also have re-equilibrated intercumulus apatite to more Cl-rich compositions than MI apatite. This is not the case and seems to rule out an exogenous Cl-rich fluid.

Chromite is, however, a near liquidus phase in many lunar basalts. Metasomatism of the 76535 pluton by a chromite-saturated melt provides a mechanism for adding Cr to the rock along cracks and grain boundaries (i.e. melt pathways). Chromite would be deposited locally, resulting in the symplectite forming olivine-plagioclase reaction. Most olivine is unaffected and the shielded MIs retain their low Cr content. Although speculative, melt metasomatism is the model we feel best fits the available data [see 7 for more detail]. If correct, it would imply that the Mg-suite parental magmas were extremely low in Cr compared to mare basalts, a condition that would require further explanation [i.e. 6]. Furthermore, if the intimate interaction of migrating melts with early lunar crustal rocks was a widespread phenomena, it would likely delay closure of or reset radiogenic isotopic clocks, and could help explain the Mg-suite-FAN age overlap [7].

References: [1] Bell et al. (1975) *LSC VI,* 231-248. [2] Gooley et al. (1974) *GCA* ***38****,* 1329-1339. [3] Dymek et al. (1975) *LSC VI,* 301-341. [4] McCallum and Schwartz (2001) *JGR* ***106****,* 27,969-27,983. [5] Albee et al. (1975) *LSC VI,* 1-3. [6] Elardo et al. (2011) *GCA* ***75****,* 3024-3045. [7] Elardo et al. *GCA* In Press [8] Kushiro and Yoder (1966) *J. Petrol.* ***7****,* 337-362. [9] Roeder and Reynolds (1991) *J. Petrol* ***32****,* 909-934. [10] Hanson and Jones (1998) *Am. Min.* ***83,*** 669-684. [11] Klein-BenDavid et al. (2011) *Lithos* ***125****,* 122-130

LUNAR FELDSPATHIC METEORITES: CONSTRAINTS ON THE GEOLOGY OF THE LUNAR FARSIDE HIGHLANDS, AND THE ORIGIN OF THE LUNAR CRUST. J. Gross[1,2], A. H. Treiman[2,3], and C. Mercer[4]; [1]American Museum of Natural History, New York NY 10024; [2]NASA Lunar Science Institute, Houston TX 77058; [3]Lunar and Planetary Institute, Houston TX 77058; [4]USGS Denver Federal Center, Denver, CO 80225 (jgross@amnh.org).

Introduction: The Lunar Magma Ocean (LMO) hypothesis holds that, early in its history the Moon was wholly or mostly molten [1,2]. Mafic minerals (olivine and pyroxene) crystallized first from the magma and sank to form the mantle, enriching the remaining magma in Fe and incompatible elements. Later, plagioclase floated in the dense Fe-rich magma [3,4], and concentrated at the Moon's surface to form a global crust of ferroan anorthosite. The LMO residue became strongly enriched in incompatible elements and produced abundant ilmenite and residual melt enriched in KREEP to form new basaltic magmas that then intruded the global ferroan anorthosite, now represented by Mg-suite plutonic rocks and mare basalts.

This global LMO hypothesis is consistent with most petrologic and geochemical data from the Apollo returned samples. Most Apollo anorthosites are ferroan. Crystallization ages of the anorthosites are ancient [2,5], consistent with formation early in the Moon's history. Orbital remote sensing shows that all of the Moon's highland crust is anorthositic [6-8], as required by the LMO model. Mare basalts show a strong Eu depletion, complementary to the strong Eu enrichment of ferroan anorthosites[9], and consistent with flotation and thus removal of plagioclase from the mare basalts' source regions.

Lunar meteorites, ejected from the lunar surface by impact events, provide additional tests of the global distribution of LMO products. The meeorites come from random sites across the lunar surface [10]. About 2/3 of the meteorites are feldspathic, 1/3 are basaltic, consistent with the proportion of the lunar surface covered by highland material and mare basalts [10]. Feldspathic lunar meteorites, such as ALHA81005 and NWA 2996, represent these highland materials.

Samples and Method Meteorites ALHA81005 and NWA2996 are feldspathic, polymict, regolith breccias composed of rock and mineral fragments from the lunar highlands [11,12] with very little (NWA2996) to no (ALHA81005) KREEP component [13,14]. In thin section both meteorites contain fragments of anorthosites, 300μm to 3.5mm in diameter (Fig. 1), with 90-98 vol% plagioclase and 2-10 vol% olivine, low- and high-Ca pyroxenes, and/or accessory ilmenite.

Quantitative mineral analyses were obtained with a Cameca SX100 at NASA Johnson Space Center. Operating conditions were: 15kV accelerating voltage, 20nA beam current, 1μm beam diameter for olivine and pyroxene, and 5μm for plagioclase.

Geochemistry: Mineral compositions are uniform within each clast in these meteorites, but vary widely among clasts: plagioclase ranges from An_{96-99}; Mg# range from highly magnesian (Mg#=86) in both meteorites, to hyper-ferroan (Mg#=39) in ALHA81005 (Fig. 2A), a far larger range than the 'typical' Apollo ferroan anorthosites (Mg#=50-70; Fig. 2A). The range of Mg#s in anorthosites in both meteorites spans the gap between the Apollo ferroan anorthosite suite and Mg-suite (Fig. 2A), and is concentrated in this gap (Mg# 65-85). These meteorites also contain mineral fragments and granulites with the same Mg# range as the anorthosites, impact glasses, and basalts. Fragments of Mg-suite rocks are very rare.

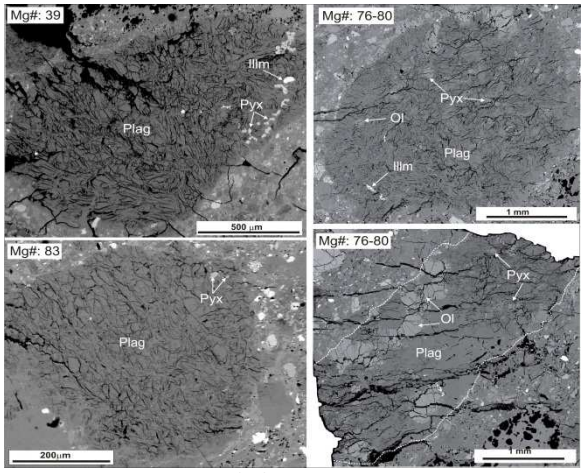

Fig. 1: BSE images of four typical anorthosite clasts in ALHA81005 (left side) and NWA2996 (right side).

Lunar Magma Ocean products?

ALHA81005 and NWA2996 and most lunar feldspathic meteorited [26] are not obviously consistent with predictions of the LMO model.

1) Most Anorthosite clasts in lunar feldspathic meteorites are too magnesian (Mg#>70) to have formed from flotation cumulates on a global LMO. Of the 43 known feldspathic lunar meteorites, data on 19 are adequate to evaluate the composition of their anorthosites [11]. Of those 19 about 2/3 contain magnesian anorthosites (Mg# >70; Fig. 2B), and the reminder 1/3 contain ferroan Anorthosite clasts comparable to those of the Apollo sites.

2) No known lunar meteorite is a 'pure anorthosite' (>95% plagioclase), and 'pure anorthosite' clasts are rare in feldspathic breccias [24]. Thus, 'pure anorthosite' may not be widespread across the lunar surface as suggested by remote sensing [25].

3) Most feldspathic meteorites contain little KREEP, consistent with the Th distribution on the lunar surface (concentrated in the nearside Procellarium KREEP Terrain, PKT). This alone suggests that a hallmark of LMO models KREEP, is not globally distributed.

4) Clasts of Mg-suite rock are rare in lunar feldspathic meteorites. Nearly all clasts that plot in the Apollo Mg-suite field (Fig.2) are magnesian anorthosites and noritic anorthosites that appear continuous with the range of other anorthositic clasts. Very few clasts in the feldspathic meteorites fall along the Mg-suite trend of decreasing An and Mg# (Fig.2).

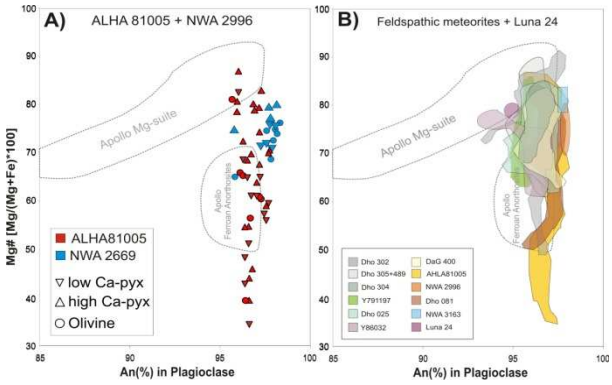

Fig. 2: A) Graph of anorthite (mol%) in plagioclase versus Mg# in mafic minerals in lunar samples. A) Anorthosite clasts in ALHA81005 (red symbols) and NWA2996 (blue symbols); B) Fields of anorthosite clasts in some feldspathic lunar meteorites and Luna 24, each color represents a different meteorite.

Lunar Farside Highlands: The lunar feldspathic meteorites suggest that magnesian anorthositic rock is a major component of the lunar highland crust and is the dominant material over most of the Moon. Only 1/3 of the feldspathic meteorites are ferroan, which is approximately the same as the proportion of the lunar highlands that is affected by the continuous Imbrium ejecta [3,16]. Only the Luna 20 and 24 missions returned samples from outside the continuous ejecta of Imbrium, and their highlands materials are dominated by magnesian anorthositic rocks, not ferroan anorthosites [17]. Thus, it seems reasonable to suggest that ferroan anorthosite, as well as KREEP and Mg-suite rocks, reflects processes localized in the Imbrium area and that magnesian anorthositic material is characteristic of the remaining 2/3 of the lunar crust. So, how did that remaining 2/3 form? By analogy with the Imbrium ejecta, and by impact modeling [27], that surface is likely underlain by ejecta from the South-Pole-Aitkin basin (SPA). SPA is the largest and oldest recognized lunar impact basin, and its ejecta blanket was kilometers thick over the whole lunar surface [27]. This ejecta, mostly of mid- and deep-crustal material, should be dominant at the lunar surface, except where covered by younger deposits (basin ejecta or basalt). Thus, it seems reasonable that the materials of most feldspathic highlands meteorites should be principally derived from mid- and deep crustal materials of the SPA target, and the remainder of highlands meteorites should consist mostly of Imbrium ejecta.

If the surface of the lunar highlands as we see it today is a continuous blanket of the Imbrium and SPA ejecta then **how did the original lunar crust form and evolve?** The long-standing alternative to the LMO hypothesis is serial magmatism – that the observed lunar crust is the product of multiple intrusions of basaltic magma, each differentiating during and after emplacement so that any primordial LMO crust is obscured[18,19]. In that model, plagioclase-rich cumulates from intrusions that rise into the crust as diapirs [18,20-22], while the complementary mafic layers sank back to the mantle [18]. Our data and the literature data are consistent with a modified version of this model, in which layered intrusions are emplaced close to the surface, differentiate and rise continuously over time. Each diapir is expected to have its own unique chemistry, Mg# range and plagioclase composition, depending on the physical and chemical characteristics of its source region and the duration of ascent and fractionation of interstitial melt within the diapirs [23]. During the SPA impact event those diapirs, close to the lunar surface, were then distributed onto and over the lunar surface.

Acknowledgements: Supported in part by NASA Cosmochemistry Grant NNX08AH78G to AHT and an NLSI/CLSE subcontract to J.Gross.

References: [1] Wood, J.A. et al. (1970) *Proc. 1st Lunar Sci. Conf.*, 965-988. [2] Shearer, C.K., et al. (2006) *Rev. Min. Geochem.* 60, 365-518. [3] Warren, P.H. (1990) *Am. Min.* 75, 46-58. [4] Elkins-Tanton, L.T et al. (2011) *EPSL* 304, 326–336. [5] Borg, L. et al. (1999) *Geochim. Cosmochim. Acta*, 63, 2679-2691. [6] Lucey, P.G. (2004) *GRL* 31, L08701. [7] Prettyman, T.H. et al. (2006) *J. Geoph. Res.* 111, E12007 [8i] Greenhagen, B.T. et al. (2010) *Science* 329, 1507-1509. [9] Warren, P.H. (1985) *Ann. Rev. Earth Planet. Sci.* 13, 201-240. [10] Korotev, R.L. (2005) *Chemie der Erde* 65, 297–346. [11] Korotev, R.L. (2011) <http://meteorites.wustl.edu/lunar/moon_meteorites_list_alumina htm>. [12] Goodrich, C.A., et al. (1984) *Proc. 15th Lunar Planet. Sci. Conf.*, C87-C94. [13] Kallemeyn, G.W. & Warren, P.H. (1983) *Geophys. Res. Let.* 10, 833-836. [14] Korotev, R.L. et al. (2009) *Meteor. Planet. Sci.* 44, 1287–1322. [16] Spudis, et al. (2011) *42nd LPSC*, Abstract #1365. [17] Taylor G.J., et al. (1973) *Geochim. Cosmochim. Acta* 37, 1087-1106. [18] Longhi, J. & Ashwall, L.D. (1985 *Proc. 15th Lunar Planet. Sci. Conf.*, C571-C584. [19] Longhi, J. (2003) *J. Geophys. Res.* 108, #5083. [20] Ashwal, L.D. (1993) *Anorthosites.* Springer, 422 p. [21] Longhi, J., et al. (1999) *J. Petrol.* 40, 339-362. [22] Vander Auwera, et al. (2006) *Lithos* 89, 326-352. [23] Haloda, J et al. (2009) *Geochim. Cosmochim. Acta*, 73, 3450-3470. [24] Korotev R.L. et al. (2010) LPSC 41, abstr. Xxxx. [25] Ohtake et al, 2010; *Nature;* [26] Gross J. et al. (2012) *LPSC 43*. [27] Petro and Pieters (2008).

ANALYSIS OF PYROCLASTIC DEPOSITS WITHIN FLOOR-FRACTURED LAVOISIER CRATER. J.O. Gustafson[1], L.R. Gaddis[2], B.R. Hawke[3], and T.A. Giguere[4]. [1]Dept. Earth & Atmospheric Sciences, Cornell University, Ithaca, NY 14853; [2]Astrogeology Program, U.S. Geological Survey, Flagstaff, AZ 86001; [3]Hawaii Institute of Geophysics and Planetology, University of Hawaii, Honolulu, HI 96822; [4]Intergraph Corporation, Kapolei, HI 96707.

Introduction: Numerous localized pyroclastic deposits have been identified within the pre-Nectarian floor-fractured crater Lavoisier (D=70 km), located in the highlands northwest of Oceanus Procellarum (38.2°N, 81.2°W), as well as adjacent floor-fractured craters Lavoisier F (D=33 km) and Lavoisier H (D=29 km) [1-3]. Recent data from the camera subsystems aboard the Lunar Reconnaissance Orbiter (LRO) and SELENE/Kaguya spacecraft [4-6] enable more detailed analysis of these pyroclastic deposits and associated small effusive deposits. We are using high-resolution monochrome data from the LRO Narrow Angle Camera (NAC; resolution ~0.5-2.0 m/pixel) and the Kaguya Terrain Camera (TC; resolution ~10 m/pixel) to examine deposit morphologies, surface textures, and potential source vents. We are also using multispectral data from the LRO Wide Angle Camera (WAC; two ultraviolet (UV) and five visible (VIS) wavelengths from 320-690 nm; resolution ~400 m/pix in the UV and ~75 m/pix in the visible) and the Kaguya Multiband Imager (MI; five VIS and near-infrared (NIR) wavelengths from 415-1000 nm; resolution ~20 m/pixel) to constrain deposit compositions and to look for differences in mineralogy and/or glass content between deposits.

Our goals for this investigation included not only further characterizing the Lavoisier pyroclastic deposits, but also assessing the efficacy of using the combined LRO and Kaguya camera data in the analysis of localized pyroclastic deposits.

Discussion: A number of pyroclastic deposits are associated with the annular floor fractures visible within Lavoisier, Lavoisier F (southeast of Lavoisier), and Lavoisier H (northeast of Lavoisier). The dark tone of these deposits stands in contrast to the surrounding highlands deposits, as seen in the Clementine multispectral mosaic (Figure 1). Some of these deposits may also contain an effusive component. An LROC NAC mosaic of the deposit along the western wall of Lavoisier reveals a broad irregular depression that could be a source vent, as well as a possible flow lobe (Figure 2). At the edge of the depression and across the possible flow lobe are several smaller, possibly endogenic craters that could be smaller vents. We also plan to examine both the LROC WAC and Kaguya MI multispectral data for these deposits; a single-band image from the Kaguya MI shown in Figure 3 provides an example of level of resolution available from this instrument.

Summary/future work: Our preliminary review of the LROC and Kaguya camera data for Lavoisier indicates that these data will enable a more detailed assessment of extent and characteristics of these deposits than was previously possible. We plan to continue our investigation of Lavoisier crater by examining additional LROC NAC and Kaguya TC images to locate possible source vents, identify likely effusive deposits, and determine the extent and approximate thickness of the pyroclastic deposits. LROC WAC and Kaguya MI multispectral data will be examined to constrain the composition of the deposits and to search for compositional heterogeneity among deposits. Once we have completed this assessment, we plan to extend our analysis to pyroclastic deposits found within other floor-fractured craters across the Moon.

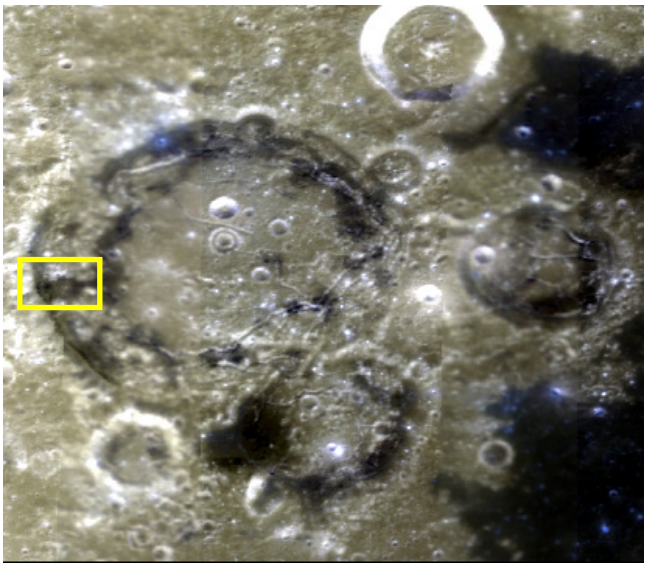

Fig. 1: Clementine multispectral mosaic of Lavoisier Crater. Yellow box indicates location of Figs. 2 and 3. Image width is 110 km (USGS).

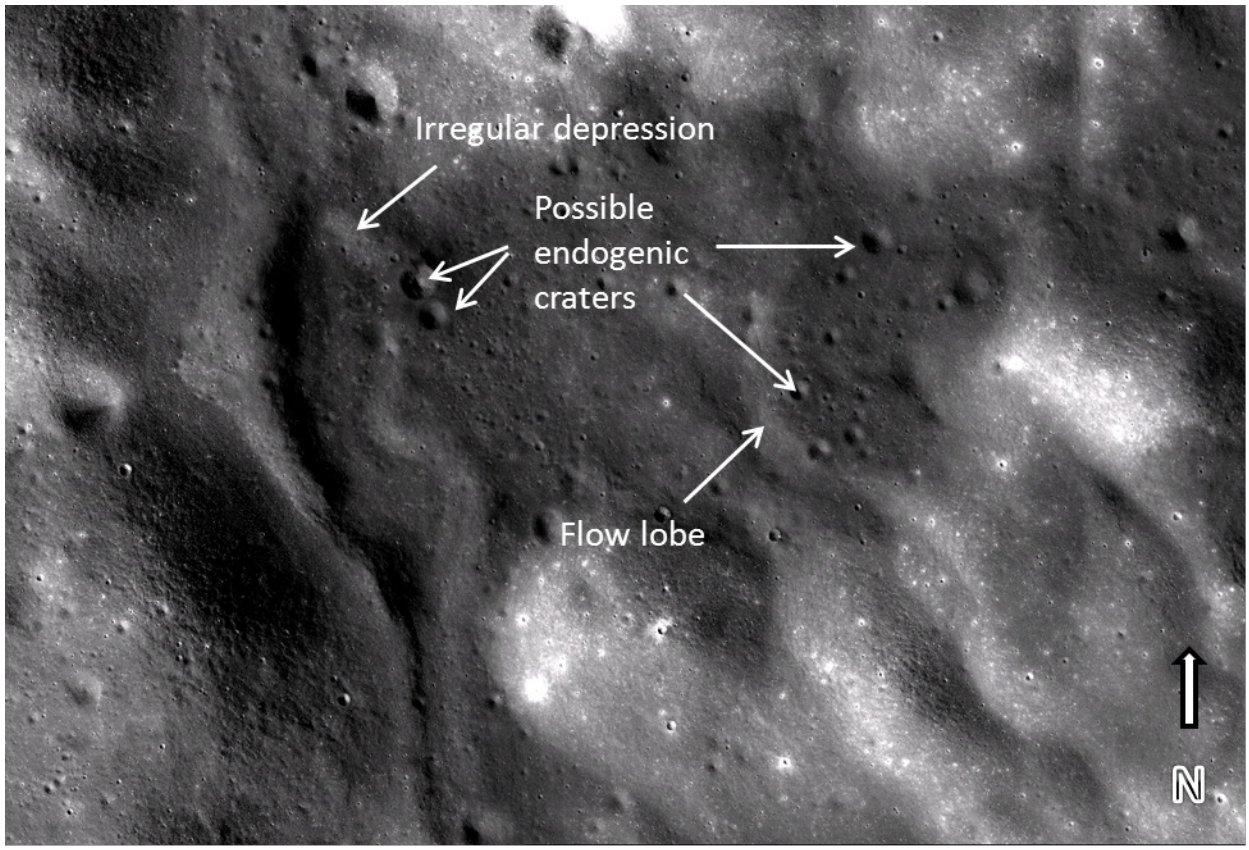

Fig. 2: NAC mosaic of the western edge of Lavoisier crater. Image width is 16 km. NAC image M105055584l/R (NASA/GSFC/ASU).

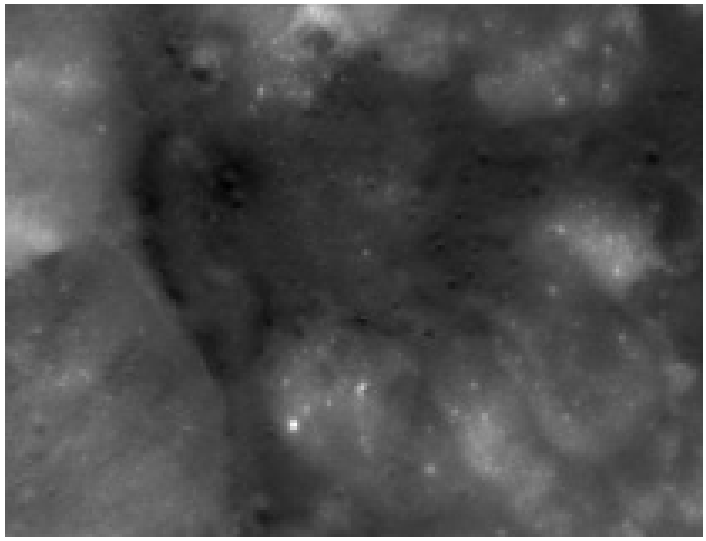

Fig. 3: Single band of Kaguya MI image from the western edge of Lavoisier Crater (JAXA)

References: [1] Schultz, P.H. (1976), *Moon 15*, 241-273. [2] Coombs, C.R. et al. (1993), *PLPSC 23rd*, 249-250. [3] Rosanova et al. (1998), *PLPSC 29rd*, abstract #1710. [4] Robinson M.S. *et al*. (2010) *Space Sci. Rev.* 150, 81-124. [5] Haruyama et al., 2008, Adv. Sp. Res. 42, 310-316. [6] Ohtake et al., 2010, Space Sci. Rev. 154, 57-77.

MEGAREGOLITHS, CATACLYSMS, AND HIGHLANDS: A SYNOPSIS. W. K. Hartmann (Planetary Science Institute, 1700 E Ft Lowell Rd Ste 106, Tucson AZ 85719-2395 USA; hartmann@psi.edu).

Lunar highlands preserve saturation-levels of cratering, and this means that their surface materials typically involve "megaregolith." This in turn means that samples available on lunar highland surfaces are strongly controlled not just by "productive" histories of magma oceans, crustal formation processes, or even impact melt production rates, but also by simultaneous "destructive" processes of brecciation, pulverization, and ejecta-blanket formation. Numbers of surviving early impact melt samples, for example, are not proportional to numbers of impacts, as can be demonstrated directly from impact glass age statistics. Four decades after the first lunar landings, our community still faces exciting challenges and controversies in understanding the consequences of these facts.

Highland evolution has been confused by the idea of a lunar (or solar-system-wide?) impact-related "cata- clysm." The confusion is not because the concept is necessarily wrong, but because it has meant different things to different people at different times. Some (bi- ased?) highlights follow, based on the philosophy that we are all in this together. (Salient terms for highland cratering are in quotes and italics.)

- 1965-6 "Early Intense Bombardment". Mare lavas average 3.5 Gy old, and therefore cratering rate in pre-lunar-mare time had to average order $10^2 \times$ post-mare cratering rate, based on highland crater statistics. (1)
- 1972 "Terminal Lunar Cataclysm". Lack of >4.0 Gy Apollo samples implies a "cataclysm" around 3.9 Gy ago. The cataclysm was due to (a) Imbrium basin; or (b) many basins forming at that time, or (c) a global metamorphic event on the Moon. (2)
- Ca. 1972-4 Wasserburg gives talks with a Gothic cathedral placed on the graphs of sample-number vs. time around 3.9 Gy, to emphasize uniqueness of event around that time.
- 1973-5 Term "megaregolith" is coined for deep brecciation of lunar crust due to impact saturation effects. Scarcity of >4.0 Gy samples thus might be caused by intense pre-4.0 Gy cratering. (3)
- 1989-90 "Late Cataclysm". Lack of >4.0 Gy impact melts said to prove near-zero impact rate prior to 3.9. Large spike (~half the samples) ~3.85-4.0Gy ago said to prove impact cataclysm at that time. (4)
- 1998 Dominance of 3.9 Gy ages in Apollo samples reflects primarily the Imbrium impact, whose effects dominate frontside samples. (5)
- 2000 "Lunar Cataclysm". Lack of >4.0 Gy impact melts in KREEP-poor lunar meteorites interpreted as affirming a cataclysm at 3.9 Gy ago. (6)
- 2001 Virtually all observed lunar multi-ring basins formed in 150 My period around 3.8 to 4.0 Gy ago. (7)
- 2003 Lunar and asteroidal meteorite data show no spike at 3.9 Gy, but a broader peak in impact events, thus disagree with "cataclysm." (8)
- 2006 "Nice Model 1.0" predicts a sudden wave of impacts at uncertain date. If date is 3.9 Gy ago, then it "confirms" the cataclysm model. (9)
- 2011-12 Increasing reports of 4.2, 4.3 Gy impact melt clasts in highland breccias. (10, and various LPSC presentations)
- 2011 "Nice model 2.0" extended wave of pre-4.0 Gy cratering, matches asteroidal meteorite data. (11)
- 2012 "Nice model 3.0" Basin-scale post-3.9 Gy impacts in Earth-Moon caused by impacts from inner asteroid "E-belt." (12)

Some interpretations (2, 4, 6, 7, 9) are frankly ca- tastrophist, in terms of invoking a unique event or pro- cess at 3.9 Gy ago to explain the observations. Other interpretations (1, 3, 5, 8, 10, 11, 12) tend more toward uniformitarianism, in terms of invoking ongoing impact processes and non-unique events from before 4.1 to~3.8 Gy ago.

In summary, highland evolution models that have been lumped under the rubric of "cataclysm," are surprisingly inconsistent, ranging from pre-4.0 Gy intense cratering, to a tight spike in impacts at 3.9 Gy, to a more extended wave of cratering from ~4.3 to 3.7 Gy. The "Gothic cathedral" version of the concept, with virtually all lunar basin formation concentrated in a unique solar-system-wide, 150 My-long episode of cratering (2, 4, 7, 9) is inconsistent with published evidence from asteroids, lunar meteorites, and highland breccia (6, 8, 10, 11, 12), and is thus probably wrong.

References: (1) Hartmann, W. K. 1966. Icarus 5, 406-418. (2) Tera, F., D.A. Papanastassiou, and G. J. Wasserburg 1974. Earth Planet. Sci. Lett. 22, 1-21. (3) Hartmann, W. K. 1973. Icarus 18, 634-636; also, 1975. Icarus, 24: 181-187. (4) Ryder, G. 1989. Lunar Planet. Sci. 20, 934-935 (Abstract); also, 1990. EOS Trans. AGU, 71, 313. (5) Haskin, L. A. et al. 1998. MAPS 33, 959-975. (6) Cohen, B. A., T. D. Swindle, D. A. Kring 2000. Science 290, 1754-1756. (7) Stöffler, D., G. Ryder, G. 2001, in Chronology and Evolution of Mars, Kluwer Academic Publishers, Netherlands, pp. 105-164. (8) Hartmann, W. K. 2003. MAPS 38, 579-593. (9) Morbidelli, A., W. F. Bottke 2006. First Internatl. Conf. on Impact Cratering in the Solar System (Noordwijk: ESTEC) (Abstract). (10) Norman, M., Nemchin, A. 2012. Early Solar System Impact Bombardment II Conference, LPI, Abstract 4013. (11) Bottke, W. F. 2011 EPSC-DPS meeting abstract EPSC-DPS2011-1884. (12) Bottke, W. F. et al. 2012. Nature 485, May 3 (letter).

LUNAR ORIENTALE BASIN: CHARACTERIZATION AND INSIGHTS INTO MULTI-RINGED BASIN FORMATION. J. W. Head[1], [1]Brown Univ., Providence, RI (james_head@brown.edu),

Introduction: The 930 km diameter Orientale basin is the youngest and most well-preserved large multi-ringed impact basin on the Moon [1-10]; it has not been significantly filled with mare basalts [20], as have other lunar impact basins, and thus the nature of the basin interior deposits and ring structures are very well-exposed and provide major insight into the formation and evolution of planetary multi-ringed impact basins [1-10] (Fig. 1). New data from the armada of recent and ongoing lunar spacecraft are providing multiple data sets, new characterization, and new insights into the origin and evolution of the Orientale basin [11-15].

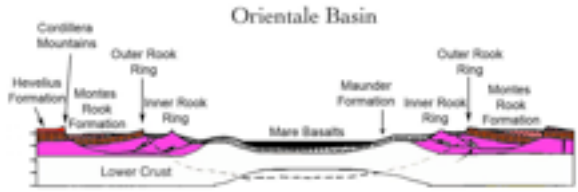

Fig. 1. Schematic cross section of the Orientale basin illustrating the relation of the basin rings to basin deposits (interior and exterior) [4].

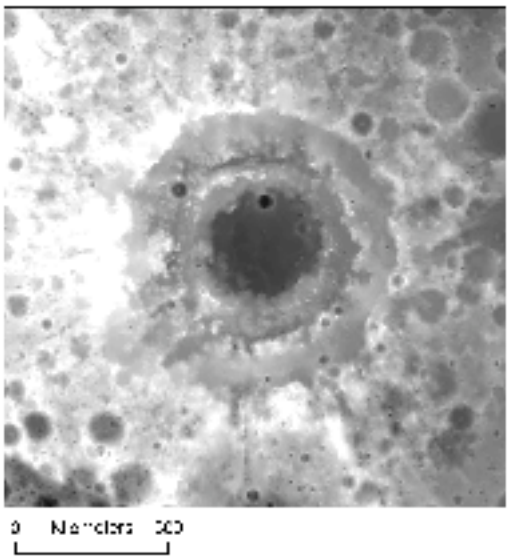

Fig. 2. LOLA altimetry map of the Orientale basin region (1/16th degree resolution).

Lunar Orbiting Laser Altimeter Data: Acquisition of new altimetry data for the Orientale basin from the Lunar Orbiting Laser Altimeter (LOLA) on board the Lunar Reconnaissance Orbiter (Fig. 1,2) has permitted characterization of the pre-basin, basin and ring topography, and we have previously outlined several implications for basin formation and evolution.

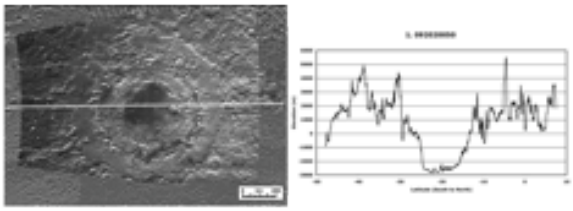

Fig. 3. LOLA profile 092020050 through the center of the Orientale basin and into the pre-Orientale Mendel-Rydberg basin to the south (left).

Pre-basin topography: There is a broad W-E decrease in elevation, consistent with regional changes in crustal thickness [15]. Pre-basin topography had a major effect on the formation of Orientale; we have mapped dozens of impact craters underlying both the Orientale ejecta (Hevelius Formation-HF) (Fig. 2; see rough terrain between -5 and +10 degrees in Fig. 3) and the unit between the basin rim (Cordillera ring-CR) and the Outer Rook ring (OR) (known as the Montes Rook Formation-MRF) (Fig.1), ranging up in size to the Mendel-Rydberg basin just to the south of Orientale (Fig. 2;3-left); this crater-basin topography has influenced the topographic development of the basin rim (CR), sometimes causing the basin rim (see peaks in Fig. 3) to lie at a topographically lower level than the inner basin rings (OR and Inner Rook-IR). LOLA data show the pre-Orientale Grimaldi basin (Fig. 2, upper right) and several crater-basin structures in excess of 200 km. Several ghost craters are observed in LOLA data between the Cordillera and the Outer Rook ring [1], but not inside the Outer Rook. A dark ring previously thought to represent a crater partly located inside the IR [16] is now known to be a pyroclastic deposit from an eruption plume [17]. The deposits inside the OR are dominated by the Maunder Formation (MF) (Fig. 1) which consists of smooth plains (on the inner basin depression walls and floor) and corrugated deposits (on the IR plateau); this topographic configuration supports the interpretation that the MF consists of different facies of impact melt.

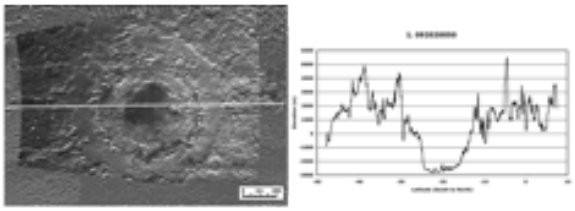

Fig. 4. LOLA profile 092012251 through the center of the Orientale basin and the 55 km diameter crater Maunder on the northern part of the inner basin floor (right).

Basin Interior Topography: The total basin interior topography is highly variable and typically ranges ~6-7 km below the surrounding pre-basin surface, with signifi-

cant variations in different quadrants (Fig. 1-4). The CR consists of linear and cuspate inward-facing scarps; continuity is interrupted by radial crater chains, and amplitude varies due to pre-existing topography (very high in southern quadrant due to M-R basin rim; lower in east quad due to intersecting pre-existing basin and crater interiors). Between the OR and CR, topography dips away from the OR to the base of the CR; lowest depressions are often filled with mare. The OR is generally continuous topographically and consists of a set of asymmetrical massifs with steeper scarps facing inward, prominent near-rim crest topography, and transitioning outward to the outward sloping MRF surface. Compared to the CR, the OR is often much more sinuous in outline, with numerous re-entrants. The IR ring is characterized by a ring of peaks and massifs situated on a broad plateau between the inner depression and the OR, surrounded and sometimes covered by Maunder Formation, interpreted to be impact melt. The plateau itself is very rough (Fig. 2-4) and LOLA data reveal the presence of a narrow 10-25 km wide deep depression between the plateau and the base of the OR ring. This depression is often over a km deep, and is floored by impact melt and mare deposits.

The topography of the western quadrant is highly variable compared to the rest of the basin interior; here the CR and OR rings are much less distinctive, the topography between the CR and MR is higher and radial structure is more prominent, and the IR is subdued except for a very prominent arrow-shaped massif at ~225° (Fig. 2). This asymmetry is paralleled in the HF in that secondary crater chains are much more prominent in the western than eastern quadrant.

Nature of the inner basin depression: The inner basin depression is about 2-4 km deep below the IR plateau (Fig. 2,4); although some of this topography is due to post-basin-formation thermal response to impact energy input and uplifted isotherms [5], a significant part of it may be related to the initial short-term collapse of an inner melt cavity, as outlined in the nested melt cavity model of ringed basin formation [18-19]. The inner depression is floored by tilted mare basalt deposits surrounding a central pre-mare high of several hundred meters elevation and deformed by wrinkle ridges with similar topographic heights (Fig. 4). We have explored the possibility that the very sharp boundary scarp of the inner depression is due to thermal stresses due to cooling of the melt sheet; these data suggest that the melt sheet may be in excess of 10 km [21].

Location of the basin rim and excavation cavity: In contrast to some previous interpretations [see summary in 16], the distribution of these features and deposits supports the interpretation that the OR ring (Fig. 1) is the closest approximation to the basin excavation cavity. The prominence of the pre-Orientale craters right up to the Cordillera ring, the outward-sloping surface of the MRF, the ghost craters between the Cordillera and Outer Rook, all support the model that the Cordillera ring represents failure of the rim crest (Outer Rook ring) at the structural uplift hinge line, and collapse inward to form a megaterrace [1,4,19].

Post-basin impact craters and sampling depths: The depth of the 55 km diameter post-Orientale Maunder crater, located at the edge of the inner depression, is in excess of 3 km (Fig. 4); this depth permits the quantitative assessment of the nature of the deeper sub-Orientale material sampled by the crater. The mineralogy of the Orientale deposits favors the interpretation that the Orientale basin sampling depth was largely confined to the upper crust [13-15]; the mineralogy of the central peaks of the post-Orientale 55 km diameter Maunder crater, located in the basin interior depression inward of the IR (Fig. 4), are somewhat enriched in low-Ca pyroxene apparently sampling noritic lower crust, but not mantle [15].

Origin of basin rings in multi-ringed basins: These new data for the Orientale basin provide insight into basin ring formation, supporting a model that includes the expansion of a peak-ring basin by addition of an outer (Cordillera) ring by inward collapse at the edge of structural uplift along the base of the displaced zone, and the addition of an inner depression formed from an expanding nested melt cavity, and its collapse [18,19]. The newly documented annular depression at the base of the OR is interpreted to be formed during the inward collapse of the peak-ring bounded inner melt cavity.

References: 1. J. Head, Moon 11, 327, 1974; 2. K. Howard et al., RGSP 12, 309, 1974; 3. J. McCauley, PEPI 15, 220, 1977; 4. J. Head et al., JGR 98, 17149, 1993; 5. S. Bratt et al., JGR 90, 3049, 1985; 6. P. Spudis et al., JGR 89, C197, 1984; 7. B. Hawke et al., JGR 108, 5050, 2003; 8. B. Hawke et al., GRL 18, 2141, 1991. 9. C. Pieters et al., JGR 98, 17127, 1993; 10. B. Bussey & P. Spudis, GRL 24, 445, 1997; JGR 105, 4235, 2000; 11. T. Matsunaga et al., GRL 35, L232012008, 2008; 12. M. Ohtake et al., Nature 461, 236, 2009; 13. C. Pieters et al., LPSC 40, 2052, 2157, 2009; 14. S. Kumar et al., LPSC 40, 1584, 2009; 15. M. Wieczorek et al., Rev. Min. Geochem., 60, 221, 2006; 16. P. Spudis, Geology of Multi-Ringed Basins, 263 p., 1993; 17. J. Head et al., JGR, 107, 1413, 2002; 18. M. Cintala and R. Grieve, MAPS, 33, 889, 1998; 19. J. Head, GRL, *37,* L02203, 2010; 20. J. Whitten et al., JGR, *116,* E00G09, 2011; 21. W. Vaughan et al., LPSC 43, 2012.

GEOLOGIC CONTEXT OF FELDSPATHIC LUNAR METEORITES: COMBINING LABORATORY SPECTROSCOPY WITH DIVERSE REMOTE COMPOSITIONAL ANALYSES. P. J. Isaacson[1], T. Hiroi[2], B. R. Hawke[1], P. G. Lucey[1], C. M. Pieters[2], Y. Liu[3], A. Patchen[3], and L. A. Taylor[3] [1]Hawaii Institute of Geophysics and Planetology, University of Hawaii, Manoa, Honolulu, HI, 96822, [2]Dept. of Geological Sciences, Brown University, Providence, RI, 02912, [3]Planetary Geosciences Institute, Dept. of Earth & Planetary Sciences, University of Tennessee, Knoxville, TN, 37996, [isaacson@higp hawaii.edu].

Introduction: Returned lunar samples from the Apollo and Luna programs have provided the major data-base upon which our present-day knowledge of lunar science is based, yet several unsolved questions remain [1-3]. However, due to the limited sampling of the lunar surface (~6-8 %) by manned exploration, the discovery of numerous lunar meteorites has provided "new-sample science" and expanded the areas of the Moon from which we have samples. These meteorite collections have inherent limitations in that their provenances have been speculated on but are largely unknown. However, unlike much of the Apollo and Luna collections, several of these meteorite samples have evidence of originating from outside the anomalous geochemical region from which the returned samples were collected [2-4].

Most lunar meteorite samples are complex polymict breccias made up of a number of different lithologic components, the result of the weathering of the regolith. Bulk measurements of such polymict breccias present only high-level "averages" of the distinct components that form the rocks. Whereas pristine rocks can provide clear indications to formational processes and petrologic evolution [e.g., 5, 6], bulk measurements of complex breccias cannot reveal specifically the evidence provided by the individual lithologic components of the breccia.

Visible to near-infrared (VNIR) reflectance spectroscopy is a powerful tool for investigating the mineralogy of planetary materials, because the properties of absorptions in VNIR spectra are diagnostic of mineralogy and mineral composition [7]. With the advent of high-quality orbital VNIR datasets for the Moon, such absorption features can be analyzed globally. Interpretation of such VNIR data relies largely on ground truth from lunar samples and analogues in which information from laboratory investigations is used to interpret remote observations [e.g., 8].

Here, we present results of laboratory spectroscopy measurements on individual lithologic components (minerals and clasts) of two feldspathic breccias (Allan Hills (ALH) A81005 and Queen Alexandra Range (QUE) 93069). These components contain signatures of the geologic processes that formed the minerals and rocks from which the clasts were sourced, and it is these parent rocks and minerals that are observed through orbital remote sensing as distinct "outcrops" on the lunar surface (the clasts are assumed to represent small samples of larger outcrop-scale deposits). Comparisons between the laboratory spectra of the clasts and orbital measurements provide constraints on the geologic context of the clasts.

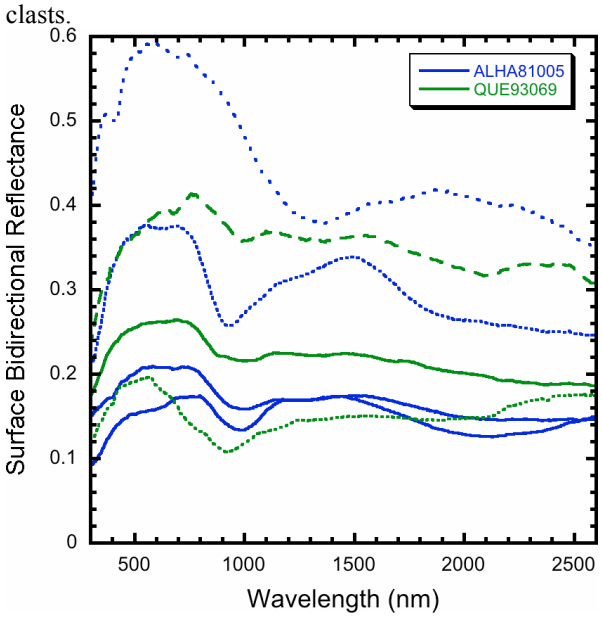

Figure 1: Laboratory visible to near-infrared (VNIR) reflectance spectra of lunar feldspathic regolith breccia clasts. These spectra were analyzed with the Modified Gaussian Model (MGM) to enable direct comparisons with remotely-sensed observations of the lunar surface, which in turn provide constraints on the geologic context of the clast materials.

Methods: We acquired laboratory reflectance spectra of selected clasts in the two samples following the approach of Hiroi et al. [9]. Some of these results were presented by Isaacson et al. [10]. The remote spectra evaluated were acquired and processed as part of a separate project focusing on large crater central peaks [11]. As direct comparisons between laboratory reflectance spectra and remotely-acquired spectra is very challenging and requires a number of assumptions, we employed band parameter analysis in which the basic properties of the diagnostic absorption features (strength, width, and position) were captured by a fitting approach. The laboratory spectra were analyzed with the Modified Gaussian Model (MGM) [12], and

the remote spectra were evaluated with a quadratic polynomial fitting approach [11]. After obtaining these parameters, more direct comparisons can be made between the laboratory results and the remotely-sensed results. To date, we have only compared the laboratory results with large-scale regional averages over specific lunar craters (typical areas are circular with radii from ~30 to >100 km).

We are also employing other remote compositional datasets to provide additional constraints on the geologic context of these clasts and samples. Global maps of various elements were produced by the Lunar Prospector Neutron and Gamma Ray Spectrometers [13-15], and we are using these datasets as additional constraints. This approach suffers from the relatively low spatial resolution of these datasets and the lack of geochemical data for the specific clasts analyzed in the laboratory (which necessitates the use of bulk sample measurements). However, we have also conducted electron microprobe (EMP) analyses of subsets of the breccia samples [16], which should enable more extensive use of the orbital elemental abundance datasets.

Current Results: Reflectance spectra of clasts in the two feldspathic breccia samples are presented in Figure 1. There is substantial diversity in these spectra, including pyroxene-rich lithologies, clear evidence of crystalline plagioclase, and possible olivine-rich signatures. However, several of these spectra exhibit little more than a pronounced negative ("blue") continuum slope. These are very challenging laboratory measurements to make, due to both our measurement geometry (they were measured in chip rather than particulate form) and to the nature of the samples (highly complex and fragmented, with relatively small clasts and abundant glassy, absorbing matrix material). QUE93069 is particularly challenging, as it contains abundant glassy matrix material. Results for these spectra should be evaluated with caution. An example MGM fit to one of these spectra is illustrated in Figure 2. The pronounced blue continuum slope is readily apparent.

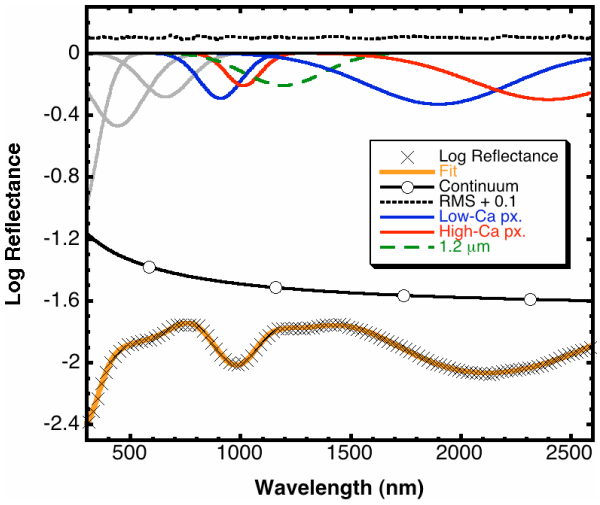

Figure 2: 2-pyroxene MGM fit to one of the ALHA81005 clast spectra. The results of MGM fits to laboratory spectra (band position, strength, and width) are compared to comparable fits of remotely-sensed spectra to identify candidate matches and constrain geologic context.

Discussion: Previous analyses of lunar meteorites have attempted to pair laboratory analyses with remote sensing observations to constrain the source region/geologic context of the samples [e.g., 17, 18, 19]. However, to our knowledge, this study represents the first attempt to add the element of VNIR spectroscopy. The addition of VNIR spectroscopy offers great potential advances, because it can provide much higher spatial resolution than elemental remote sensing techniques such as gamma ray, neutron, and x-ray spectroscopy. There are still a number of issues to be addressed before this approach can provide insight into source regions, not least of which is that this analysis only focuses on large craters, while lunar meteorites may actually derive from relatively small craters [20]. However, the combined application of diverse remote sensing and laboratory techniques should enable significant new insight into the geologic context and potentially into source regions of these important samples of unexplored regions of the lunar crust.

Acknowledgments: The authors acknowledge the support of NASA grant NNX08AY89G to CMP/PJI. RELAB is a multiuser facility supported by NASA grant NNG06GJ31G.

References: [1] Papike, J.J. et al., in *Planetary Materials*, 5.1-5.234. [2] Warren, P.H. (2005) *MAPS*, **40**, 477, 10.1111/j.1945-5100.2005.tb00395 x. [3] Korotev, R.L. (2005) *Chemi der Erde*, **65**, 297-346. [4] Korotev, R.L. et al. (2003) *GCA*, **67**, 4895-4923, 10.1016/j.gca.2003.08.001. [5] Warren, P.H. (1993) *AM*, **78**, 360-376. [6] Dymek, R.F. et al. (1975) *PLSC*, **6**, 301-341. [7] Burns, R.G. (1993) *Mineralogical applications of crystal field theory*. [8] Isaacson, P.J. et al. (2011) *MAPS*, **46**, 228-251, 10.1111/j.1945-5100.2010.01148 x. [9] Hiroi, T. et al. (2011) *Pol. Sci.*, **5**, 337-344, 10.1016/j.polar.2011.06.002. [10] Isaacson, P.J. et al. (2012) *LPSC*, **43**, 1668. [11] Isaacson, P.J. et al. (2011) *LPSC*, **42**, 2556. [12] Sunshine, J.M. et al. (1990) *JGR*, **95**, 6955-6966, 10.1029/JB095iB05p06955. [13] Feldman, W.C. et al. (1998) *Science*, **281**, 1489. [14] Lawrence, D.J. et al. (1998) *Science*, **281**, 1484, 10.1126/science.281.5382.148. [15] Lawrence, D.J. et al. (2002) *JGR*, **107**, 5130, 10.1029/2001je001530. [16] Isaacson, P.J. et al. (2010) *LPSC*, **41**, 1927. [17] Joy, K.H. et al. (2008) *GCA*, **72**, 3822-3844, 10.1016/j.gca.2008.04.032. [18] Joy, K.H. et al. (2010) *Meteoritics & Planetary Science*, **45**, 917-946, 10.1111/j.1945-5100.2010.01067 x. [19] Arai, T. et al. (2010) *GCA*, **74**, 2231-2248, 10.1016/j.gca.2009.11.019. [20] Warren, P.H. (1994) *Icarus*, **111**, 338-363, 10.1006/icar.1994.1149.

NEW VIEWS OF SILICIC VOLCANISM ON THE MOON. B. L. Jolliff[1], J. D. Stopar[2], S. J. Lawrence[2], M. S. Robinson[2], and B. R. Hawke[3] [1]Department of Earth & Planetary Sciences, Washington University, St. Louis, MO 63130; [2]School of Earth and Space Exploration, Arizona State University, Tempe, AZ 85287; [3]Hawaii Institute of Geophysics and Planetology, University of Hawaii, Honolulu, Hawaii 96822 (blj@wustl.edu)

Introduction: Spectral "Red Spots" on the Moon have been known for many years [1,2,3]. Some of these spots correspond to domes that are thought to be volcanic in origin. Relatively steep topographic slopes, coupled with other morphologic and compositional evidence indicate that these features are occurrences of silicic or "felsic" volcanism, e.g., rhyolite [3,4,5].

Data collected by remote sensing missions of the past two decades have produced a body of evidence to suggest that large-scale occurrences of felsic rocks exist on the Moon, perhaps the same rock types that are present only as small bits and pieces of breccia clasts and regolith rock fragments in the Apollo collections. A key set of evidence came from the Lunar Prospector (LP) gamma-ray spectrometer (GRS) [6], which revealed substantial concentrations of naturally radioactive thorium (Th), coupled with analyses of felsic Apollo samples that showed strong Th enrichment to be a compositional signature of such rocks [7,8]. Thorium "anomalies" or "hot spots" were identified and correlated to several of the "red spots" [3,6], as well as to ejecta from several nearside impact craters such as Aristarchus (42 km), Aristillus (55 km, and possibly Mairan (40 km), as well as Oresme V (51 km) on the far side. The GRS had a broad spatial response function, over a hundred km, thus correlations to specific small-scale geologic surface units requires caution and spatial deconvolution.

Nevertheless, the global Th map produced by the LP team showed clearly where the major hot spots occur, and it showed several new ones, most notably the Th hot spot that became known as the Compton-Belkovich site [9]. Although Clementine data showed that a relatively high albedo feature might occur at the center of this hot spot [10], it was the high-resolution Lunar Reconnaissance Orbiter Camera (LROC) Narrow Angle Camera (NAC) images that revealed clear evidence of a volcanic terrain at the center of the anomaly [11]. Moreover, the LRO Diviner instrument, whose spectra include three bands in the region of the Christiansen Feature (CF) (~8 microns), shows direct evidence for silica enrichment at this site, corresponding to morphologies and Th concentrations [12,13]. The evidence for multi-km-scale silicic magmatism and volcanism on the Moon at the Compton-Belkovich site and other sites is now firm.

Morphologies and Spatial Scales: Figure 1 compares the topographic and morphologic expression of several of the silicic volcanic complexes, Gruithuisen and Mairan domes, and the Compton-Belkovich (C-B) and Hansteen-Alpha (H-A) volcanic complexes, using digital terrain models (DTMs) derived from LROC Wide Angle Camera (WAC) images. The diversity of morphologies among these occurrences is striking. The Gruithuisen domes claim the largest volcanic constructs, with the δ and γ domes each over 10 km across and ~1700-1800 m high [5,14]. The Mairan domes range in size, with the largest volcanic constructs being the "middle" and "T" domes, on order of 5-8 km base widths and at least 800 m of vertical relief, and the T dome has a distinctive summit depression [14,15]. The C-B volcanic complex has both large and small volcanic constructs. The α dome is the largest, having a base width of ~6 km and vertical relief of ~800 m [11,14]. The overall complex is a broad dome, ~25×35 km across, with irregular depressions [11]. The H-A complex is a rough-textured triangular mound some 25 km on a side, the margins of which stand ~700 m above the surrounding mare surface and exhibit average slopes of 16-18° [16]. The summit of the arrowhead is ~1 km above the regional mare surface.

Each of these volcanic constructs has regions with relatively steep slopes, ranging from 12° to about 25°, although some of the small topographic features seen in NAC-derived DTMs at H-A and C-B are little more than low-relief circular bulges (e.g., 200-800 m across). In the C-B example, these small bulges also feature distinctive, dense boulder populations [17]. The features with high slopes have been interpreted to represent volcanic cumulo-domes formed from relatively silicic and viscous lavas [e.g., 5, 11, 14, 15]. The low–relief bulges may represent blister-like extrusions of highy viscous lava [18]. Whether the latter features occur at Gruithuisen and Mairan is unknown because mare basalts embay the large domes and cover any low-relief features that might have existed with them.

Origin: Although we have no direct samples of any of these silicic, Th-enriched volcanic hot spots, we do have in the Apollo sample collections numerous small samples of felsic rocks, variably referred to as granite, felsite, or rhyolite. These materials are especially abundant in samples from Apollo 12, 14, and 15. Apollo 12 samples contain an especially diverse set of these materials, including the largest granitic sample, 12013, which is actually a granitic breccia containing two lithologies, granitic material and a mafic, KREEP-rich phase [18].

Arguments can be made for an origin of the granitic phase by silicate-liquid immiscibility during fractionation of KREEP-rich parent magmas, but it

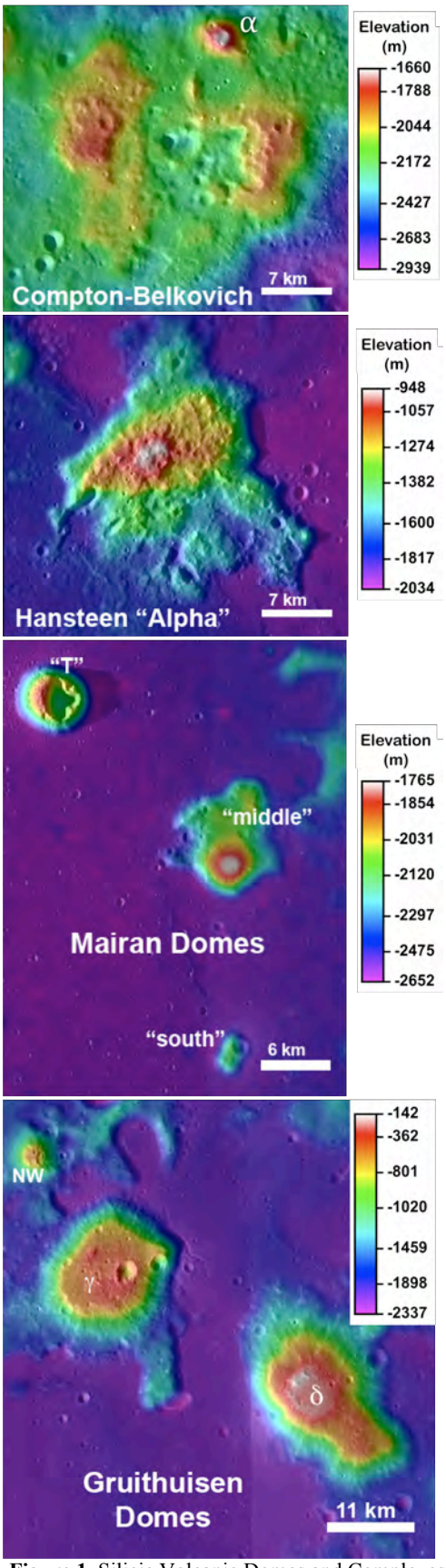

Figure 1. Silicic Volcanic Domes and Complexes; colors represent topography (derived from LRO WAC GLD100 [21].

remains unclear that this process could or did occur on a large enough scale to source volcanic constructs such as the large domes described above. Perhaps KREEP-rich magmas stalled near the surface and underwent fractional crystallization, producing variably evolved differentiates, some of which were extruded to the surface (e.g., C-B [18]). Among the samples, very high Th concentrations and relatively silica-rich compositions occur in granitic samples and quartz monzogabbro (aka monzodiorite). KREEP basalt itself does not have especially high SiO_2 (<50 wt%) [20], so fractionation is needed to yield the distinctive silica enrichment. High proportions of silica plus K-feldspar in lunar granite could account for the observed SiO_2 enrichment.

Another mechanism that has been proposed is heating of an already KREEP-rich source by basaltic underplating [3], which presumably could produce felsic partial melts directly or could generate KREEP-rich melts that intrude to shallow levels where they further differentiate to produce evolved lavas. So far, among the lunar samples, rocks of intermediate composition between KREEP basalt and rhyolite, such as dacite, are not found. The common process may be the local heating of a KREEP-rich source, which is not difficult to imagine in the central to northern Procellarum region of the Moon where volcanism was extensive, especially in the Aristarchus-Gruithuisen-Mairan triangle. The H-A and C-B occurrences may have involved heating of deeper, KREEP-rich sources, generating KREEP-rich melts that intruded to near the surface before stalling and differentiating. The isolation of C-B favors this interpretation. All of these silicic volcanics have in common that they occur where the crust is relatively thin and the surface is below the lunar mean.

Acknowledgements: We are grateful to the LROC Science & Operations Team and to NASA for support of the LRO Project.

References: [1] Malin M. (1974) *EPSL* **21**, 331. [2] Bruno B. et al., (1991) *PLPS* **21**, 405. [3] Hagerty J. et al. (2006) *JGR* **111**, E06002. [4] Head J. & McCord T. (1978) *Science* **199**, 1433. [5] Head J. & Wilson L. (1999) in *Wkshp on New Views of Moon II*, 23. [6] Lawrence D. et al. (2003) *JGR* **108**, 6-1. [7] Jolliff B. (1998) *IGR* **10**, 916. [8] Seddio S. et al. (2010) *LPS* **41**, #2688. [9] Lawrence D. et al. (1999) *GRL* **26**, 2681-2684. [10] Gillis J. et al. (2002) *LPS* **33**, #1967. [11] Jolliff B. et al. (2011) *Nat. Geoci.* **4**, 566. [12] Glotch T. et al. (2010) *Science* **329**, 1510. [13] Greenhagen B. et al. (2010) *Science* **329**, 1507. [14] Tran T. et al. (2011) *LPS* **42**, #2228. [15] Glotch T. et al. (2011) *GRL* **38**, L2120. [16] Hawke B. et al. (2012) *LPS* 43, #1754. [17] Accardo N. et al. (2012) *LPS* **43**, #1656. [18] Jolliff B. et al. (2012) *LPS* **43**, #2097. [18] Seddio S. et al. (2011) *LPS* **42**, #2381. [19] Lawrence, D. et al. (2007) *GRL* 34, L03201. [20] Meyer C. (1977) *Phys. Chem. Earth* **10**, 239. [21] Scholten F. et al. (2012) *JGR* **117**, E00H17.

STRATIFIED EJECTA BOULDERS AS INDICATORS OF LAYERED PLUTONS ON THE LUNAR NEARSIDE. Kickapoo Lunar Research Team[1] and G. Y. Kramer[2], [1](A. Beason, A. Delawder, V. Wilson, and R. D. Snyder) Kickapoo High School, 3710 S. Jefferson Ave, Springfield, MO 65807 rsnyder2@spsmail.org, [2]Lunar and Planetary Institute, 3600 Bay Area Blvd. Houston, TX 77058 kramer@lpi.usra.edu.

Introduction: Among the wealth of amazing imagery and new observations of the lunar landscape captured by the the Lunar Reconnaissance Orbiter's high-resolution Narrow Angle Camera (NAC), the stratified ejecta boulders first reported by [1] offer an unexpected glimpse into igneous processes and heterogeneity of the lunar crust. Several hypotheses have been put forward to explain the formation of these thick sequences of crust with multiple layers of alternating albedo. The purpose of this research was to test these hypotheses to determine the most plausible origin of these boulders.

Methodology: We searched over 500 NAC images near mare-highland contacts for striped boulders including those at Aristarchus discovered by [1]. For each stratified boulder we measured its overall size and the thickness and albedo of each layer. Here we report our observations of twenty-four examples located at Aristarchus Crater and Mare Undarum that best demonstrate the variety of layer thicknesses, albedos, and bedding morphologies (Fig. 1). All analyzed boulders clearly derive from beneath the target crust, excavated by the craters which they surround.

Results: Layer thicknesses can be approximated by a Gaussian distribution having a median between 1 and 2 meters and tails that extend out to 10 meters and below the spatial resolution of NAC imagery (~50 cm). The measured thicknesses of alternating light and dark material showed no consistent patterns compared between boulders from a single nor from geographically distinct regions. In addition, the ratio between adjacent light and dark layer thicknesses demonstrated no observable relationship even within a single boulder. This last point reflects the fact that several of the boulders demonstrate cross-bedding, trough-shaped layering, tapered layering and cumulate enclaves.

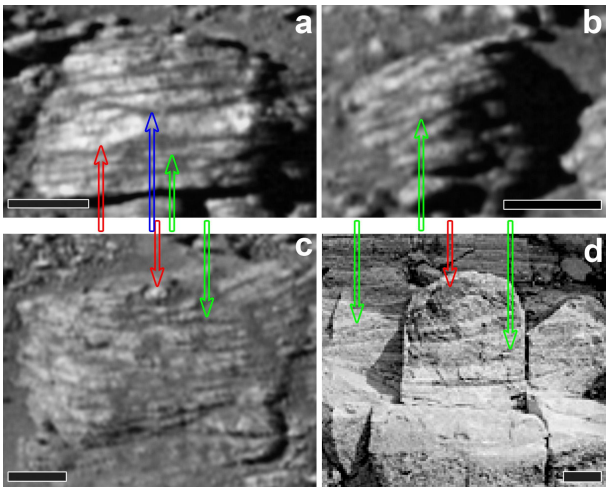

Figure 1: Examples of boulders and bedding features measured in this study. Arrows indicate locations of bedding morphologies: red arrows show cumulate enclaves, blue arrow shows trough-shaped layering, and green arrows show tapered layering and cross-bedding. Figures a, b, and c are from NAC image M120161915L; scale bars = 10 m. Figure d is an analog example from the Coastal Batholith, Ilo, southern Peru; Scale bar = 10 cm (from [2]).

Albedo variations between the layers did demonstrate a more consistent relationship between different layers within a single boulder and, at least for Undarum, between different boulders. In general, measurements of light and dark strata in both regions have albedo values between that of anorthositic highlands and mare basalts measured from the same respective NAC image (Fig. 2). Some of the variation in albedos among dark layers as well as light layers may be due to the accumulation of fine coatings of dust, which would reduce albedo contrast. The lack of any layers with albedos that exceed the endmember values demonstrates that the layers have compositions that fall between, if not actually approximated by these two endmembers.

Discussion: We tested the leading formation hypotheses for the stratified boulders (Fig. 3) and assessed their plausibility based on our measurements and observations.

Scenario A: Pyroclastic Deposits: This hypothesis postulates that the dark layers are pyroclastic deposits atop lighter mare basalt layers [1]. The hypothesis predicts that the thicknesses of the pyroclastic dark layers should be between 10 and 30 meters [4]. Our measurements of layers thickness are significantly below 10-30 meters, arguing against this hypothesis, or at least this particular prediction of the hypothesis. Measured albedos of the layers falls roughly midway between those of the highlands and mare, with the lighter layers having a difference from that of the highlands about equal to the difference between the dark layers and mare. If

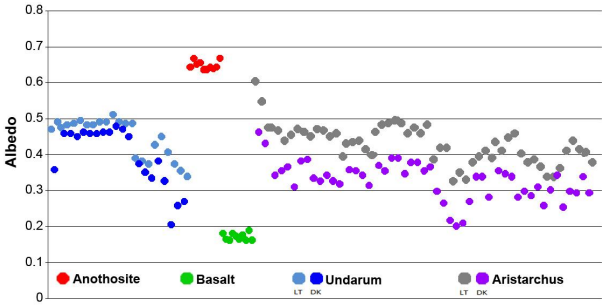

Figure 2: Measured albedos of layers in boulders demonstrate that the layers do not actually have a strong albedo contrast. All layers have albedos lower than that of anorthositic highlands and higher than that of mare basalts.

the layering were the result of alternating dark mare basalt flows and darker pyrocastic deposits we would expect to see the distribution of albedos shifted closer to the basalt endmember in Figure 2.

Scenario B: Impact Gardening: A second hypothesis states that the alternating layer albedos reflect the development of regolith atop periodic mare basalt flows [1]. The rate of regolith production is ~1 cm/10 million years [5]. To build up the number of layers observed in some boulders, the period of time between flows would have to be geologically short, in which case, only a very thin layer of regolith could develop. As a result of this slow rate, the thicknesses of dark lava flow layers would always greatly exceed the thicknesses of the lighter regolith layer. However, the lighter layers are not consistently thinner than the darker ones, and both have thicknesses ranging from 1-5.5 meters - too great to be regolith build-up.

Scenario C: Vesiculated Crust: Upon exposure to the cooler, ambient surface temperature, the surface of a lava flow quenches, forming a thin, glassy rind [1]. This rind acts as an insulator to the remaining melt, allowing time for some of the gases to exsolve. Trapped beneath the glassy rind, the gases inflate the upper surface, forming a vesiculated crust, ~10% of the height of the flow [6]. None of the measured boulders exhibit a ratio between the light and dark layer thicknesses consistent with this hypothesis.

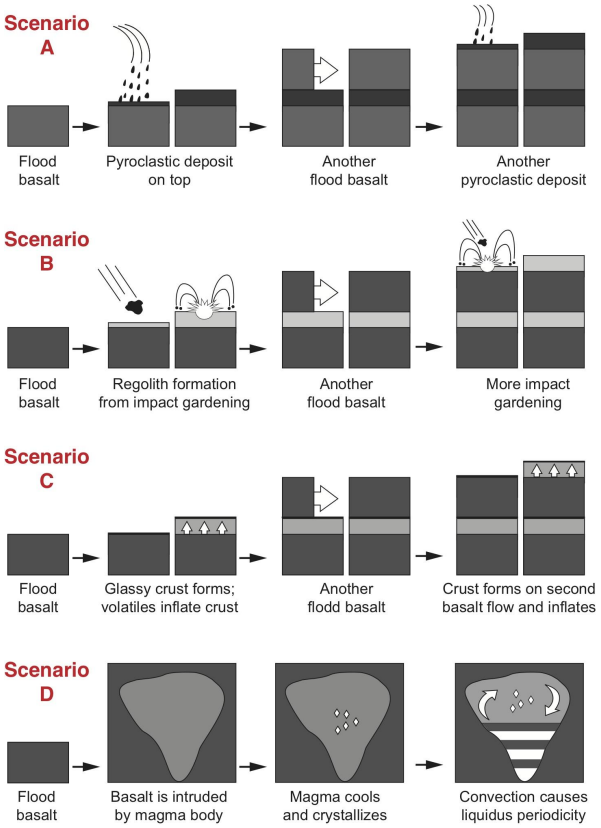

Figure 3: Summary of the four hypotheses for the origin of the stratified boulders. See text for details. Figure after [3].

Scenario D: Layered Pluton: Alternating sequences of felsic (light) and mafic (dark) mono-mineralic layers are common enough on Earth, and are interpreted to be the result of periodic changes in the composition of the liquidus due to convection or magma recharge in a cooling intrusive body [7,8,9]. Layer thicknesses are a function of the magma composition and thermal gradient, so have no prescribed ratio between light and dark layers. Crystallization on the walls of the pluton can lead to cross-bedding features, and cumulate fragments broken off of the chamber walls and entrained by the convecting magma can manifest as cumulate enclaves in the cooled, layered intrusion [2].

Our observations support the hypothesis that the stratified boulders derive from layered igneous intrusions in the lunar crust [10]. Measurements of light and dark layers have albedos that lie between anorthositic highlands and mare basalts, respectively (Fig. 2). In the absence of fluvial or aeolian forces, observed bedding morphology, such as cross-bedding, cumulate enclaves, and tapered layering can be explained by convection or magma recharge in a cooling intrusive body.

Conclusions: The relative thicknesses of dark and light layers show no relationship consistent with recurrent episodes of mare volcanism separated by episodes of pyroclastic deposits, regolith gardening, or formation of a vesiculated crust. We observed bedding morphology (crossbeds, trough-shaped layers, tapered layers, and enclaves) often attributed to sedimentary deposits involving the movement of water or air. The only plausible means of generating such bedding features and alternating layers of mafic and felsic lithologies on the Moon is crystallization in a convecting igneous intrusion. We conclude that these layers are the result of periodic changes in the composition of the liquidus due to convection or magma recharge in a cooling intrusive body. Fragments of these plutons were excavated by large impacts that penetrated overlying mare basalts and, in some cases, anorthositic crust.

References: [1] Zanetti M. et al. (2011) *LPS XLII,* Abst. #2262; [2] Barbey, P. (2009) *Geologica Belgica*, **12**; [3] Malaska, M. (2011, 3/29). [Figure in web blog message]. Retrieved from http://planetary.org/blog/article/00002980/; [4] Weitz, C. M. et al. (1998) *JGR*, **22**; [5] Quaide, W. & Oberbeck, V. (1975) *The Moon*, **13**; [6] Self, S. et al. (1997) *Geophys. Monograph*, **100**; [7] Poldervaart, A. & Taubeneck, W. H. (1969) *Bull. Geol. Soc. Am.*, **70**; [8] Maaloe, S. (1978) *Mineralogical Magazine*, 337-347; [9] Conrad, M. E., & Naslund, H. R. (1984) *J.Pet.*; [10] Pieters, C. M. (1991) *GRL*, **18**

Density and Porosity of Lunar Feldspathic Rocks and Implications for Lunar Gravity Modeling

Walter S. Kiefer[1], Robert J. Macke[2,3], Daniel T. Britt[2], Anthony J. Irving[4], and Guy J. Consolmagno[5], [1]Lunar and Planetary Institute, 3600 Bay Area Blvd., Houston TX 77058, kiefer@lpi.usra.edu , [2]Dept. of Physics, University of Central Florida, Orlando FL, macke@alum.mit.edu, britt@physics.ucf.edu, [3]Boston College, Chestnut Hill MA, [4]Dept. Earth and Space Sciences, University of Washington, Seattle WA, irving@ess.washington.edu, [5]Vatican Observatory, V-00120 Vatican City State, gjc@specola.va.

Introduction

Lunar gravity observations provide our primary tool for understanding lateral variability in the structure of the Moon's crust and mantle. Accurate gravity models require the use of densities and porosities for geologically appropriate compositions. Although many bulk density measurements were reported in the Apollo-era literature, they commonly had errors of 10% or more or had no reported uncertainty [1] and are not useful for geophysical modeling. A small number of samples were measured hydrostatically by immersion in toluene [e.g., 2]. However, toluene commonly failed to fully penetrate the pore space and the reported densities have errors of up to 5% [3]. Thus, there remains an important need for accurate measurements of density and porosity of lunar rocks.

We previously reported density and porosity results for 13 lunar samples covering a broad range of compositions [3]. Here, we analyze measurements of bulk density, grain density, and porosity for feldspathic highland rocks, including 3 Apollo samples and 21 lunar meteorites (4 of these samples were included in [3]). The inclusion of lunar meteorites makes the results more globally representative than for Apollo samples alone [4]. Our results show a strong dependence of density on composition and can be combined with remote sensing observations to estimate densities for highland units that have not been sampled. These results are an important new constraint for interpreting lunar gravity observations, such as from the on-going GRAIL mission.

Methods

We measured both the bulk density, ρ_{bulk}, and the grain density, ρ_{grain} [5,6]. The bulk density is based on the entire volume of the sample, including any pore space. The grain density is based solely on the solid material, excluding the pore space. Bulk density is important for calculation of gravity anomalies, and grain density is used for studying systematic trends in density as a function of rock composition. Porosity is calculated as $P=1-(\rho_{bulk}/\rho_{grain})$. These measurements are fast, non-destructive and non-contaminating. The bulk volume is measured by immersion in glass beads, approximating an Archimedean fluid. Grain volume is measured by helium pycnometry. Errors are determined by repeated measurements of each sample and are typically 10-30 kg m^{-3} (< 0.9%) for grain density and 1-3% for porosity provided that the sample mass exceeds 10 gm.

Results

The upper part of the Moon's highland crust is composed predominantly of plagioclase, averaging 80 volume per cent, with a smaller amount of mafic minerals [7,8]. The mafic minerals have varying relative abundances of Mg and Fe. Differences between Apollo samples and lunar meteorites suggest the possibility of regional variability in Mg# [9] , which is the molar ratio of MgO/(MgO + FeO).

The samples reported here are all composed predominantly of calcium-rich plagioclase (anorthite), which we interpret as samples of the Moon's feldspathic highland crust. They vary in bulk composition between 22 and 35 weight percent Al_2O_3, with values between 26 and 30% being most common. These rocks are thus 60-95% anorthite, and by igneous classification are anorthosites, noritic anorthosites, and anorthositic norites [10]. The mafic content varies between 0.5 and 18.9 weight percent FeO+MgO, with Mg# between 44 and 80 [9, 11-16]. Rocks in the Moon's upper crust have experienced 4+ billion years of impact processing, and each of the samples we measured has experienced substantial post-igneous crystallization processing, such as brecciation, shock melting, thermal annealing, and addition of meteoritic material [14, 17-20]. We did not consider regolith breccias or meteorites that are mingled mixtures of feldspathic and basaltic material in this work, regardless of composition. We also did not consider samples that are interpreted to be ejecta units from large basins, such as the Fra Mauro Formation.

Grain density and porosity results are shown in Figure 1. Grain densities are a strong function of the abundance of mafic minerals, with the most plagioclase rich rocks, such as 60025, being the least dense and the most mafic rocks, such as 15418 and NWA 5744, being the densest. We are currently developing a model that predicts grain density from bulk composition such as Al_2O_3, FeO, and MgO, similar to work

we did for mare basalts [3]. Combining such a model with remote sensing observations [21-23] will allow us to estimate how the highland crust density varies with location across the Moon. In turn, improved knowledge of the lateral variations in crustal density will improve global models of crustal thickness estimated from gravity inversions [24, 25]. Porosities range from effectively 0 to 20%, although most are in the range 7-13%. Some of the low porosity values are due to thermal annealing to a granulite texture [16, 17] and are indicated by gray circles in Figure 1. Meteorite regolith breccias have been proposed to have low porosity due either to the effects of ejection from the Moon or landing on Earth [26]. A similar process might contribute to the low porosities of some meteorites in Figure 1, although it is unclear how this might be affected by differences in strength between regolith breccias and other types of lunar rock.

For gravity modeling, bulk density is the essential parameter. Most of the samples (63%) reported here have bulk densities between 2350 and 2650 kg m^{-3}, with a mean of 2580±170 kg m^{-3}. However, high porosity samples have bulk densities as low as 2200 kg m^{-3} [27]. Low porosity samples, such as granulites, have bulk densities up to 2840 kg m^{-3}, which approach their grain densities.

Acknowledgements: This work was supported by NASA grant NNX11AF70G and by NASA Cooperative Agreement NNX08AC28A.

References [1] Talwani et al., Apollo 17 Prelim. Sci. Rpt., 1973. [2] Horai and Winkler, Proc. LPSC 11, 1777-1788, 1980. [3] Kiefer et al., GRL, 39, L07201, doi:10.1029/2012GL051319, 2012. [4] Korotev, Chemie der Erde 65, 297-346, 2005. [5] Consolmagno et al., Chemie der Erde 68, 1-29, 2008. [6] Macke et al., Planet. Space Sci. 58, 421-426, 2010. [7] Warren, Am. Mineral. 78, 360-376, 1993. [8] Taylor, Elements 5, 17-22, 2009. [9] Korotev et al., GCA 67, 4895-4923, 2003. [10] Stöffler et al., Proc. Lunar Highland Crust, 51-70, 1980. [11] Cahill et al., MAPS 39, 503-529, 2004. [12] Korotev et al., GCA 70, 5935-5956, 2006. [13] Sokol et al., GCA 72, 4845-4873, 2008. [14] Korotev et al., MAPS 44, 1287-1322, 2009. [15] Kuehner et al., LPSC 41, abstract 1552, 2010. [16] Hudgins et al., GCA 75, 2865-2881, 2011. [17] Nord et al., Moon 17, 217-231, 1977. [18] Ryder, GCA 46, 1591-1601, 1980. [19] Daubar et al., MAPS 37, 1797-1813, 2002. [20] Irving et al., LPCS 39, abstract 2168, 2008. [21] Prettyman et al., JGR 111, 2005JE002656, 2006. [22] Lucey et al., LPSC 43, abstract 1736, 2012. [23] Ohtake et al., LPSC 43, abstract 1977, 2012. [24] Neumann et al., JGR 101, 16,841-16,863, 1996. [25] Hikida and Wieczorek, Icarus 192, 150-166, 2007. [26] Warren, JGR 106, 10,101-10,111, 2001. [27] Jeanloz and Ahrens, Proc. LPSC 9, 2789-2803, 1978.

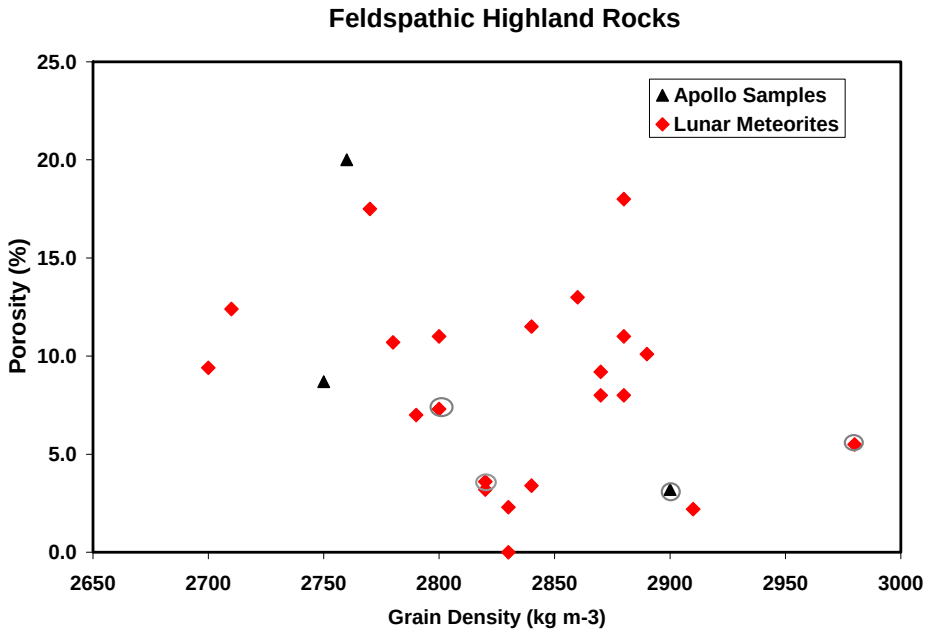

Figure 1: Grain densities and porosities for the feldspathic lunar rocks measured in this study. Apollo samples are shown as black triangles and lunar meteorites are red diamonds. Gray circles indicate rocks with granulitic textures.

BULLIALDUS CRATER: EXCAVATION AND EXPOSURE OF AN MG- OR ALKALI- SUITE PLUTON?

Rachel L. Klima (Rachel.Klima@jhuapl.edu)[1], Joshua T. S. Cahill[1], Justin Hagerty[2] and David Lawrence[1], [1]Johns Hopkins University Applied Physics Laboratory, Laurel, MD 20723, USA; [2]USGS Astrogeology Science Center, Flagstaff, AZ, USA.

Introduction: The central peak of Bullialdus Crater has long been recognized as having a reflectance spectrum dominated by a strong noritic signature (e.g., 1-4). Results of spectral fits to the central peak of Bullialdus suggest a relatively high Mg# (>Mg_{75}) in the low-Ca pyroxenes (5), within the range of values observed for Mg-suite lunar samples (e.g., 5). Centered at -20.7°, 337.5° in Mare Nubium, Bullialdus Crater lies within the high-thorium Procellarum KREEP Terrane (e.g., 6). In fact, based on orbital gamma-ray data, Bullialdus is the location of a clear thorium (Th) enhancement, which is important because Th commonly serves as a proxy for detecting KREEP-rich materials on the lunar surface (e.g., 6-8). We examine the mineralogy of Bullialdus crater and the spatial distribution of the Th signature associated with it to investigate the character and composition of the excavated pluton.

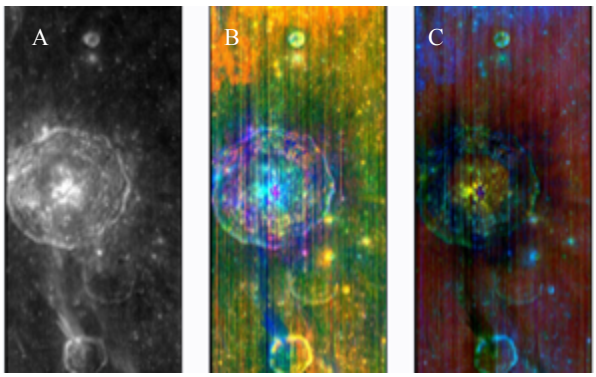

Fig. 1. Mineral diversity in Bullialdus crater. (A) 0.75 μm albedo map. (B) Mafic mineralogy depicted using an RGB composite where R=integrated 1 μm band depth; G=integrated 2 μm band depth, and B=reflectance at 1.5 μm. In this color scheme, fresh material appears bright, with deep blue generally indicating feldspathic material, red indicating an enhancement in olivine, and orange and yellow indicating pyroxenes. Low-Ca pyroxene often appears as cyan, due to the overall brightness and narrow 1 μm band. (C) Pyroxene diversity map depicted using an RGB composite where R = 1.9 μm band depth, G = integrated 2 μm band depth, and B = integrated 1μm band depth. This color scheme highlights low-Ca pyroxene as yellow, and fresh high-Ca pyroxene as cyan. Anorthositic material and highly space-weathered material appear as black.

Bullialdus Region Mineralogy: Bullialdus crater and the local mineralogy are shown in Fig. 1, and representative spectra from Bullialdus and the surrounding region are shown in Fig. 2. Strong pyroxene bands indicative of a noritic composition dominate the central peak. Anorthositic material, excavated by Bullialdus, is exposed in the crater rim and proximal ejecta (Fig. 1). Portions of the walls exhibit a gabbroic signature, potentially olivine-bearing. Fresh craters in Mare Nubium exhibit a typical basaltic spectral signature, while both mare and highland soils in the region are generally spectrally featureless.

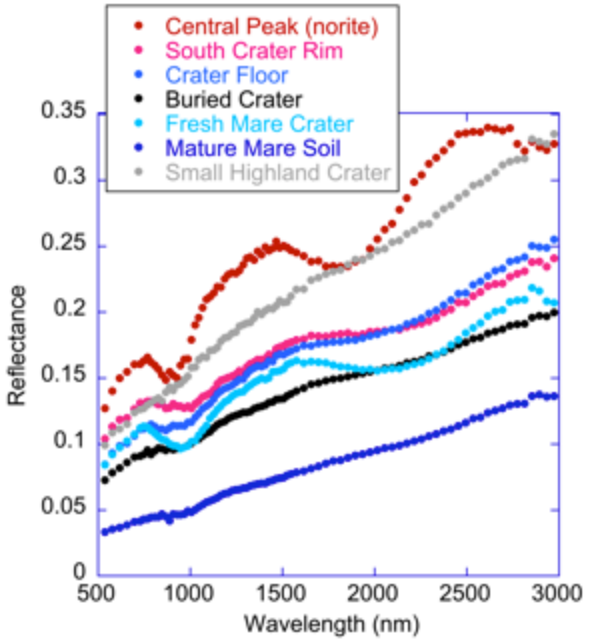

Fig. 2. Representative spectra from within and around Bullialdus crater.

Bullialdus Crater, KREEP and Hydroxyl: Shown in Fig. 3 is the deconvolved Lunar Prospector Th content around Bullialdus crater. There is a clear Th enhancement (~6-7 ppm Th) centered on Bullialdus crater and its northern wall outer flanks (9). However, if the source of the Th is only the material excavated in the central peak, the Th content is higher, and closer to the range of Alkali suite norites (10).

In addition to providing a window into the complex petrology of the lunar crust, Bullialdus crater may also provide insight into the distribution of native lunar volatiles and the minerals that bear them. Multiple lunar data sets have demonstrated that some lunar

surface materials exhibit a 2.8 – 3.0 μm absorption band, indicative of a hydroxyl or water component (e.g., 11-13). An increasing number of studies also suggest that the lunar mantle may have contained more water than originally assumed (14-16) and some of this water may be related to KREEP materials (17). Observations of the central peak of Bullialdus crater indicate that the pyroxenes exhibit a distinctive 2.8 μm band absorption that is significantly stronger than the immediate surroundings, possibly indicating the presence of a hydroxyl component, as illustrated in Fig. 4. The hydroxyl signature persists through multiple viewing geometries and illumination conditions, suggesting that it is not transient, like the lunar surface water previously observed (11-13).

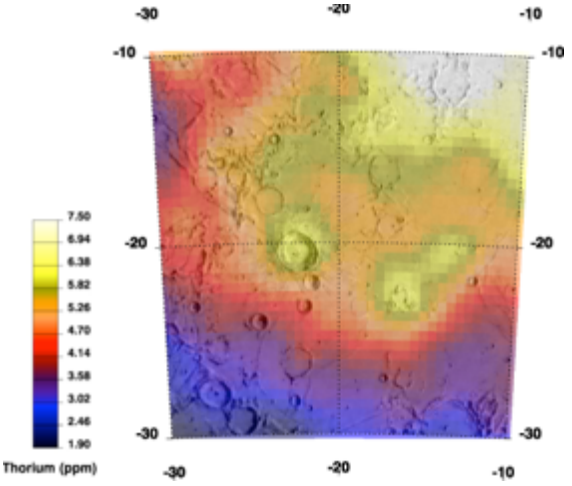

Fig. 3. Lunar Prospector Th, spatially deconvolved and overlain on the regional topography.

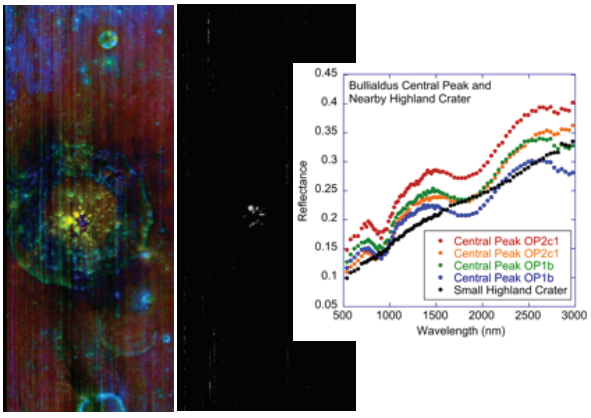

Fig. 4. Bullialdus crater pyroxenes (left) and 2.8 μm band depth (middle). (Right) Example spectra for the central peak taken during different optical periods with different illumination and viewing geometry are provided. A small, fresh highland crater from a similar latitude is provided for comparison.

We will explore the geology in and around Bullialdus in more detail, examining relationships between lithology, Th content, and hydroxylated material. In particular, we investigate the specific compositions and spectral properties of the pyroxenes in these exposures to determine whether they can provide further information about the crustal source region and distribution and character of KREEP within the lunar crust.

Acknowledgements: We are extremely grateful to the M^3 and Chandrayaan-1 teams for providing reflectance data for this project. We also thank the APL NSLI node and LASER grant #NNX10AH62G for supporting mapping and lab work for this project. PMDAP grant #NNH09AL42I provided support for JJH.

References: [1] C. M. Pieters, 1991, GRL 18, 2129. [2] S. Tompkins et al., 1994, Icarus 110, 261. [3] J. T. Cahill and P. G. Lucey, 2007, JGR 112, E10007, doi:10.1029/2006JE002868. [4] Cahill et al., 2009, JGR 114, 9001. [5] Klima et al., 2011, JGR 116, E00G06, doi:10.1029/2010JE003719. [6] Papike et al., 1998, in Planetary Materials, 5-1. [7] B. L. Jolliff et al., 2000, JGR 105, 4197. [8] D. J. Lawrence et al., 2003, JGR 108, 5102. [9] Lawrence et al., 2007, GRL 34, 3201. [10] Klima et al., 2012, in prep. [11] R. N. Clark, 2009, Science 326, 562. [12] C. M. Pieters et al., 2009, Science 326, 568. [13] J. M. Sunshine et al., 2009, Science 326, 565. [14] A. E. Saal et al., 2008, Nature 454, 192. [15] F. M. McCubbin et al., 2010, PNAS 107, 11223. [16] E. H. Hauri et al., 2011, Science 333, 213. [17] A. E. Saal et al., 2011, "A Wet vs. Dry Moon" workshop.

WHAT LUNAR METEORITES TELL US ABOUT THE LUNAR HIGHLANDS CRUST. R. L. Korotev[1], B. L. Jolliff[1], and R. A. Zeigler[2], [1]Dept. of Earth & Planetary Sciences, C/B 1169, Washington University, 1 Brookings Dr, Saint Louis MO 63130, [2]NASA Johnson Space Center, KT, 2101 NASA Pkwy, Houston TX 77058 korotev@wustl.edu.

The first meteorite to be found[1] that was eventually (1984) recognized to have originated from the Moon is Yamato 791197 [1]. The find date, November 20, 1979, was four days after the end of the first Conference on the Lunar Highland Crust [2]. Since then, >75 other lunar meteorites have been found, and these meteorites provide information about the lunar highlands that was not known from studies of the Apollo and Luna samples.

1: Of 50 feldspathic lunar meteorites (>20% Al_2O_3; Fig. 1), all breccias, the average *Mg'* (mole % MgO/[(MgO + FeO] of the nonmetal phases) is significantly greater (66.4 ± 1.5; 95% confidence interval) than that of the FAS (ferroan-anorthositic suite [3]) rocks of the Apollo collection (60.1 ± 2.5; Fig. 1). Mare basalt and glass (low *Mg'*, low Al_2O_3) occur in many of the "highlands" breccias of Fig. 1, thus the nonmare components of the feldspathic lunar meteorites have even greater *Mg'* than the figure implies. For 11 of the feldspathic meteorites, *Mg'* is in the range of magnesian-suite plutonic rocks (>70), yet the meteorites are much more feldspathic than the high-*Mg'* norites, troctolites, and dunites of the Apollo collection and poorer in KREEP elements. These 11 meteorites are much more mafic (mean: 75% normative plagioclase), however, than Apollo FAS rocks. The meteorites tell us that magnesian troctolitic and noritic anorthosites are an important component of the crust at some locations in the feldspathic highlands [4–7].

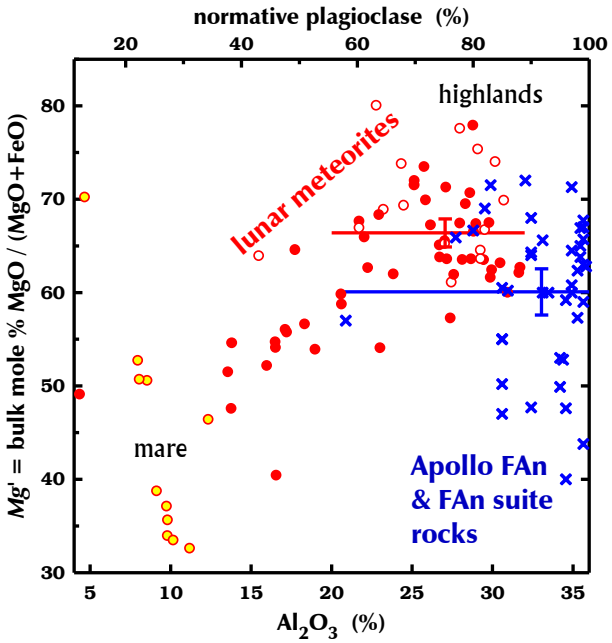

Figure 1. Comparison of *Mg'* in lunar meteorites (red, from whole-rock analysis) to mafic minerals in Apollo ferroan anorthosites and ferroan-anorthositic suite rocks (blue, 41 samples with pristinity "confidence class" >6 [22]). The horizontal lines represent the average *Mg'* for samples with Al_2O_3 >20; the error bars are 95% confidence intervals positioned at the mean Al_2O_3 concentration. For the lunar meteorites, red-filled symbols represent regolith, fragmental, and glassy-matrix breccias, unfilled symbols represent impact-melt and granulitic breccias, and yellow-filled symbols represent igneous rocks.

[1] Calcalong Creek may have been found before Y-791197, but the find date is not actually known [20]. It was not recognized to be a lunar meteorite until 1991 [21].

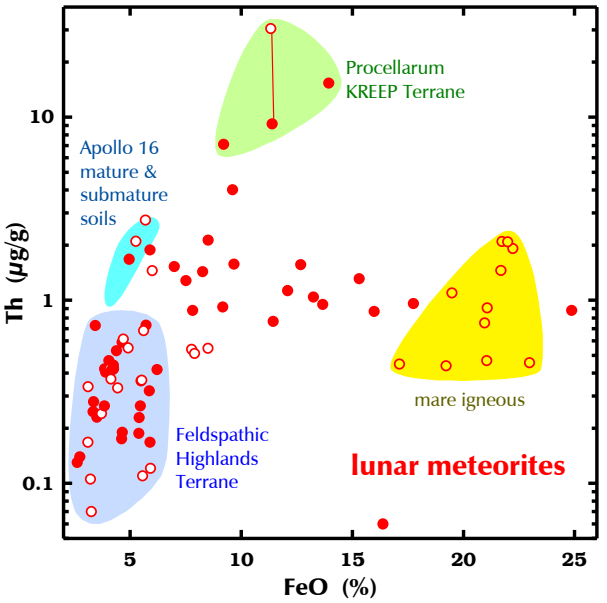

Figure 2. Th and FeO concentrations in lunar meteorites. All meteorites plotting outside the "mare igneous" field are breccias. At least three lunar meteorites are almost certainly from the PKT. (The two lithologies of SaU 169 are plotted as two points connected by the red line.) Most of the feldspathic lunar meteorites (<7% FeO) have <0.8 µg/g Th (mean of 40 meteorites in FHT field: 0.34 µg/g). This value is significantly less than that of Apollo 16 soils (mean of 36 surface and trench soils with I_s/FeO >30: 2.0 µg/g Th).

2: The most feldspathic of the meteorites has "only" 89% normative (~91 vol%) plagioclase. This value compares with 87% for the "prebasin" components of the Apollo 16 regolith [8, Tables 6 & 7]. On average, the meteorites are 3× more mafic than Apollo FAS rocks (Fig. 1). Clasts of highly feldspathic ferroan anorthosite are not common in most of the meteorites [9]. The meteorites are telling us that the Apollo 16 site is unusual in having such a high proportion of highly feldspathic ferroan anorthosite in the regolith and that the highlands megaregolith is more mafic, on average, than the ubiquitous ferroan anorthosites of Apollo 16.

3: Some lunar meteorites with intermediate FeO concentration (8–15%, Fig. 2, or 14–23% Al_2O_3, Fig. 1) and low Th concentrations (<2 µg/g) are polymict breccias consisting of FHT material and mare basalt with little or no KREEP. Others, however, appear to contain little mare material on the basis of petrographic descriptions. (Most of these are woefully understudied with respect to detailed petrography, however.) The lunar meteorites tell us that there are regions of the nominally feldspathic highlands that are moderately mafic (noritic, gabbroic).

4: Most feldspathic lunar meteorites have lower concentrations of incompatible elements than does the Apollo 16 regolith because the Apollo 16 regolith (Fig. 2) contains a substantial component of Th-rich material from the PKT (Procellarum KREEP Terrane) as Imbrium ejecta [9,10]. Along with orbital geochemistry [5,11], the meteorites tell us that, with regard to incompatible elements, the Apollo 16 site is not as typical of the FHT (Feldspathic Highlands Terrane) as was assumed in the immediate post-Apollo era and that the meteorites provide a better picture of the composition of the feldspathic highlands [4].

5. Lithologies like alkali anorthosite and magnesian-suite norite, troctolite, and dunite are found in the Apollo collection but are nearly absent as clasts in the feldspathic lunar meteorites. These rocks occur in the Apollo collection because they were formed in the PKT, not the FHT, and the Apollo sites are all in or near the PKT [10,12]. There is no evidence that any high-*Mg'* clasts in feldspathic lunar meteorites crystallized from KREEP-rich magmas, as did the Apollo magnesian-suite rocks [13,14]. The lunar meteorites tell us that magnesian-suite plutonism of the style that leads to mafic cumulates was rare in the FHT. (A few clasts of spinel troctolite have been found in feldspathic lunar meteorites, however [15,16].)

6. The composition, particularly the high Th/Sm ratio, of some brecciated lunar meteorites of intermediate FeO concentration (Fig. 3) cannot be explained as mixtures of the materials of the FHT (as represented by the feldspathic lunar meteorites), materials of the PKT, and mare basalt; they (pink) plot outside the triangle defined by these components (yellow-blue-green) in Fig. 3 [17]. These meteorites evidently contain some lithic component(s) that differ from rocks of the Apollo collection. Most of these meteorites have concentrations of FeO and Th consistent with an origin in the South Pole-Aitken basin, and at least a few probably do originate from SPA [17]. The lunar meteorites tell us that there are moderately mafic regions of the nonmare (but perhaps not "highlands," in the literal sense) crust that differ from the nearside highlands sampled by Apollo.

7. Ages of clasts of impact-melt breccias in lunar meteorites have been determined [18,19]. The lunar meteorites tell us that the age spectrum of meteorite impacts on the lunar surface is more complicated than the ubiquitous 3.9 Gy obtained from most Apollo samples.

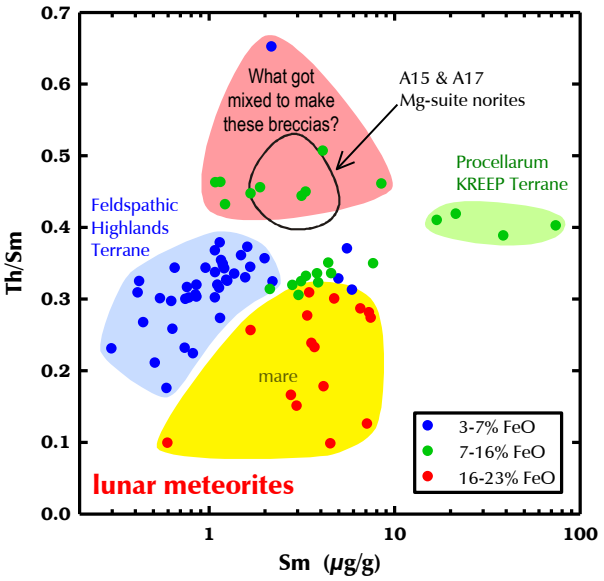

Figure 3. Ten lunar meteorites (pink field), all breccias with 6-12% FeO, have greater Th/Sm than any mixture of feldspathic breccias (blue, <7% FeO), KREEP breccias (green), and mare basalts (yellow, >16% FeO). Among Apollo samples, magnesian-suite norites are similar. The blue point in the "What got mixed to make these breccias?" field represents Dhofar 1528 with *Mg'* = 74, a value consistent with a magnesian-suite norite (mean *Mg'*: 79; range: 71–88; 17 samples of confidence class >6 [3]). The mean *Mg'* of the other 9 (green points), however, is 64 (range 54–69), well below the range of magnesian-suite norites. (Other 9: Calcalong Creek, Dhofar 1527, Dhofar 1528, Dhofar 925/ 960/ 961, NWA 4819, NWA 4932, SaU 300, SaU 449, Y-983385, and an unnamed NWA stone.) The igneous precursors of these breccias must include some that differ geochemically from rocks of the Apollo collection and rocks typical of the feldspathic highlands.

This research was funded by NASA grants NNX10-AI44G and NNX11AB26G.

References: [1] Yanai K. & Kojima H. (1984) *Mem. National Institute Polar Res., Special Issue* **35**, 18–34. [2] Merrill R. B. & Papike J. J., eds. (1980) *Proc. Conf. Lunar Highlands Crust*, 505 pp, Pergamon Press. [3] Warren P. H. (1990) *Am. Min.* **75**, 46–58. [4] Korotev R. L. et al. (2003) *GCA* **67**, 4895–4923. [5] Korotev R. L. et al. (2006) *GCA* **70**, 5935–5956. [6] Takeda H. et al. (2006) *EPSL* **247**, 171–184. [7] Treiman A. H. et al. (2010) *M&PS* **45**, 163–180. [8] Korotev R. L. (1997) *M&PS* **32**, 447–478. [9] Korotev R. L. et al. (2010) *LPS 41*, #1440. [10] Korotev R. L. (2000) *JGR* **105**, 4317–4345. [11] Lawrence D. J. et al. (2000) *JGR* **105**, 20,307–20,331. [12] Wieczorek M. A. & Phillips R. J. (2000) *JGR* **105**, 20,417–20,430. [13] Snyder G. A. et al. (1995) *JGR.* **100**, 9365–9388. [14] Shearer C. K. and Papike J. J. (2005) *GCA* **69**, 3445–3461. [15] Gross J. & Treiman A. H. (2011) *LPS 42*, #2620. [16] Takeda H. et al. (2004) LPS35, #1222. [17] Korotev R. L. et al. (2009) *M&PS* **44**, 1287–1322. [18] Cohen B. A. (2008) *LPS 39*, #2532. [19] Fernandes V. A. et al. (2004) LPS 35, #1514. [20] Wlotzka F. (1991) *Meteoritics* **26**, 255–262. [21] Hill D. H. et al. (1991) *Nature* **352**, 614–617. [22] Warren P. H. (1993) *Am. Min.* **78**, 360–376.

DEEP CRUST/MANTLE MINERALOGY EXPOSED IN THE UPLIFTED PEAK RING AND BASIN WALLS OF SCHRÖDINGER. Georgiana Y. Kramer[1], David A. Kring[1], and Carle M. Pieters[2] [1]Center for Lunar Science and Exploration, Lunar and Planetary Institute, 3600 Bay Area Blvd, Houston, TX 77058, [2] Brown/MIT NLSI, Brown University, Providence, RI 02912, kramer@lpi.usra.edu.

Introduction: Schrödinger basin is 315 km in diameter, has an average depth of ~4-5 km, and is located at 75°S, 132.5°E, which places it on the western rim of the oldest and largest lunar basin, South Pole-Aitken (SPA). More precisely, Schrödinger is nestled between SPA's two prominent rings [1, 2], in what is probably equivalent to the modification zone. Schrödinger is one of the youngest lunar basins, only marginally older than Orientale [3, 4]. These unique conditions mean Schrödinger basin provides a window into the stratigraphy of the lunar crust in the vicinity of SPA near the end of the basin-forming epoch. We have probed Schrödinger with the Lunar Reconnaissance Orbiter, Moon Mineralogy Mapper (M^3), and crater-scaling relationships. Here we focus on the material exposed in Schrödinger's peak ring, which represents material derived from the greatest stratigraphic depth, and the basin wall, which reveals the composition of the target crust.

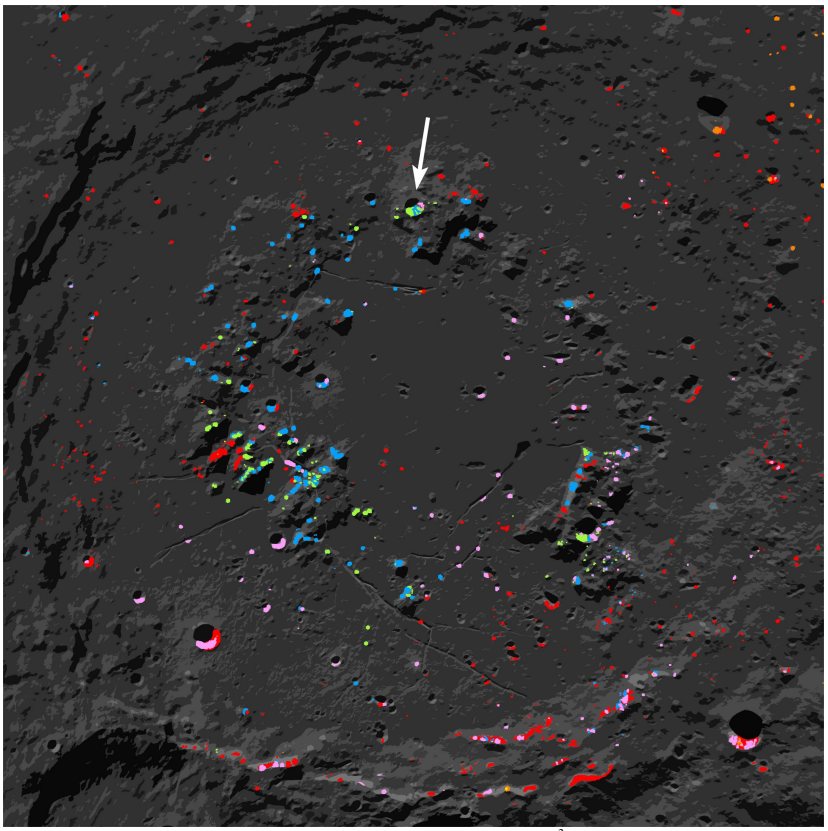

Figure 1: Locations of different lithologies identified from M^3 spectra in Schrodinger Basin. Green = olivine (dunite and/or troctolite), blue = anorthosite (>97% anorthite), magenta = pyroxene-bearing anorthosite (3-10% pyroxene + 90-97% plagioclase), red = norite (>10% orthopyroxene + <90% plagioclase), orange =gabbro (>10% clinopyroxene + <90% plagioclase). Arrow points to crater featured in Fig. 2.

Data & Methodology: We used M^3 level 2 reflectance data for this analysis. Schrödinger is located at high latitudes, which means there are low signal levels as a result of the low sun angle. The low illumination conditions dictate that the best locations from which data can be extracted and still exhibit identifiable spectral features are in the sun-facing sides of steep slopes, such as crater walls and mountain scarps. Sampling from these surfaces also provides a means to observe optically immature material representative of the pristine lithology beneath the mature surface regolith.

Results: M^3 spectral data distinguish five distinct lithologies made up of coarsely crystalline material in the peak ring and basin wall (see caption Fig. 1). These mineral associations are consistent with those recently identified and mapped in the peak ring by Yamamoto et al. [5] using Spectral Profiler (SP) and Multiband Imager (MI) data from Kaguya.

The spatial resolution of the M^3 data used to make the Schrödinger mosaic is 280 m/pixel. To be identifiable in the spectrum, the mineral must spatially dominate the area observed in the pixel. Therefore, the outcrops mapped in Figure 1 represents massive exposures (>280 m^2) of diverse lithologies.

Schrödinger's peak ring is a 125 km diameter mountain range composed of massive blocks of structurally competent material that rises 1 to 2.5 km above the basin floor. Deep faults have cut into the peak ring, creating steep cliffs and chasms between vertically offset massifs. Schrödinger's peak ring is the most mineralogically intriguing and complex of the region. Massive monomineralic outcrops occur in isolated peaks and are juxtaposed next to other massive monomineralic exposures (Fig. 1). Such massive accumulations of dense, coarsely crystalline material suggests a deep, high-pressure origin, such as the lower crust or upper mantle.

Interpretations: Yamamoto et al. [5] surmised that SPA impact melt flooded the area where Schrödinger formed and differentiated to produce

an olivine-rich unit below a pyroxene-rich unit, both of which were emplaced on top of the original Lunar Magma Ocean (LMO) plagioclase-rich crust. In this scenario, the olivine in Schrödinger's peak ring is derived from a relatively shallow impact melt unit deposited by SPA.

In contrast, peak rings are usually interpreted as being collapsed central peaks that were uplifted from great depths. In a structure the size of Schrödinger, a peak ring should be derived from depths up to 50 km (based on equations from [6]), which is far deeper than the ~5 km-thick sequence of SPA ejecta expected at the Schrödinger target site (based on equations from [7]). Thus, we interpret the coarsely crystalline lithologies exposed in Schrödinger's peak ring to be evidence of a deep, stratified lower crust and possibly upper mantle origin. The peak ring material likely represents cumulates of the LMO and subsequent intrusions into the crust.

Some regions of the peak ring (e.g., in the south and southwest) could be interpreted as layered intrusive bodies rather than mantle cumulates. However, higher resolution studies, if not field work, will be needed to test that possibility or whether the juxtaposition of those lithologies is a consequence of the movement of blocks from depth. The crystalline lithologies in the peak ring were derived from regions of the LMO that survived the excavation of SPA. The origin of the peak ring material was also not affected by the adjacent basin, Sikorsky-Rittenhouse, but may have been marginally affected by the Amundsen-Ganswindt Basin.

An intriguing example of this mineral complexity is found in an 8 km-wide impact crater that was produced in the middle of the northern rise of the peak ring (Fig. 2). On the sunlit side of this crater, four distinct lithologies can be seen: olivine-rich (dunite or troctolie), anorthosite, >90% plagioclase + pyroxene, and orthopyroxene. Of the five different types of mineralogies exposed in the Schrödinger region, only clino pyroxene is not found in the peak ring, although there is one exposure in the southern wall. Olivine was found only in the peak ring.

The spectra of fresh material exposed in scarps and fresh craters in Schrödinger's rim and wall are dominated by orthopyroxene, although a few scarps in the south basin wall contain isolated patches of anorthosite and pyroxene-bearing anorthosite, and in one location a pigeonite-bearing material was identified (Fig. 1). Virtually all of the strong spectral exposures in Schrödinger's southern wall occur at the summit of a terrace, and can be distinguished up to half-way downslope. Since these strongly crystalline spectral signatures in the southern wall are mostly confined to within the upper 1 km of a basin terrace wall, it can be argued that these are blocks of Schrödinger ejecta, and therefore derive from the maximum depth of excavation, ~20 km.

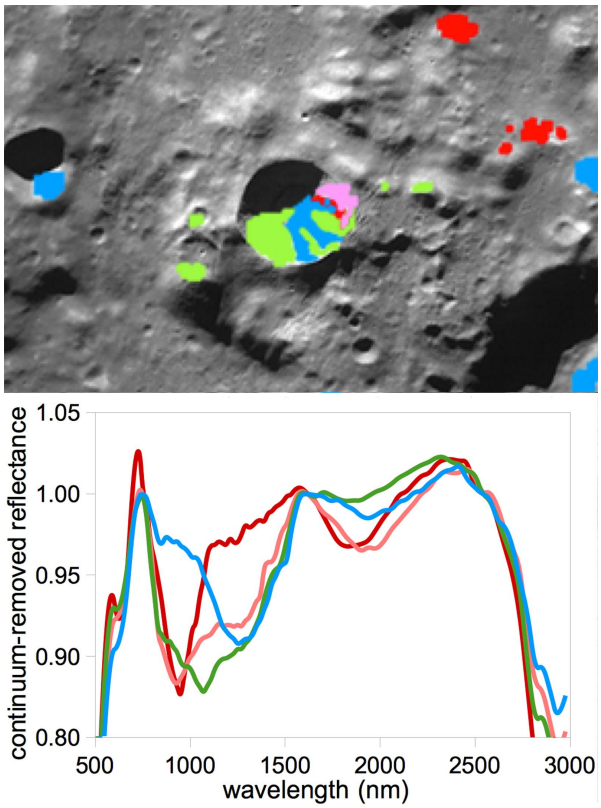

Figure 2: (a) Close-up of 8 km diameter crater in northern part of the peak ring of Schrodinger. (b) M^3 spectra showing four distinct lithologies in the wall of the crater.

Conclusions: The associated exposures of olivine are key to determining whether the uplifed peak ring entrained only crustal lithologies or whether it also entrained mantle material. If the olivine outcrops are true dunites, a mantle origin interpretation is reasonable, although not conclusive. The Ca abundance and Mg# of the olivine would be a more precise indicator. However, the tools necessary to quantify this chemistry are not currently available from orbit at the latitudes of Schrödinger. To conclusively determine the origin of the peak ring might require a sample return mission. Until such time as we can sample and quantitatively determine its origin, the relative contributions of mantle and crustal components that make up Schrodinger's peak ring exists in a state of uncertainty.

References: [1] Garrick-Bethell and Zuber (2009) *Icarus*, **204**; [2] Uemoto et al. (2011) *LPSC 42*; [3] Wilhelms (1987) *USGS Prof. Paper 1348*; [4] Shoemaker et al. (1994) *Science*, **266**; [5] Yamamoto et al. (2012) *Icarus*, **218**; [6] Cintala & Grieve (1998) *Met. Planet. Sci.*, **33**; [7] McGetchin et al. (1973) *EPSL*, **20.**

IMPACT MODIFICATION OF THE LUNAR HIGHLANDS CRUST DURING THE BASIN-FORMING EPOCH. David A. Kring[1,2], [1]Center for Lunar Science and Exploration, Lunar and Planetary Institute, Universities Space Research Association, 3600 Bay Area Blvd., Houston, TX 77058 (kring@lpi.usra.edu), [2]NASA Lunar Science Institute.

Introduction: The lunar crust was heavily modified by impact events during the basin-forming epoch. Here I examine the chronology of those events, discuss how they modified the crust (e.g., by wholesale remelting), and how those same events can be used to probe relatively unaltered portions of the lower crust.

Chronology of Basin-Forming Modification: Ages of thermally altered Apollo samples indicate impact cratering was particularly severe in the Earth-Moon system during the first billion years of its evolution. A concentration of ages circa 3.9-4.0 Ga suggests there may have been a spike in the impact flux in an event called the lunar cataclysm [1,2], but the total duration of the basin-forming epoch is still uncertain. Thus far, we only have one solid age and five tentative ages for the 15 basins produced during the Nectarian and Early Imbrian periods of time. The ages of the final two basin-size events (Schrödinger and Orientale) are among those still uncertain. Based on the available data, estimates for the duration of the lunar cataclysm range from a few tens to a few hundred Ma. We have no ages for ≥29 older, pre-Nectarian basins and, thus, little idea if they are part of a lunar cataclysm or are instead part of an extended period of bombardment that may have lasted as long as 700 million years.

This period of bombardment is also seen among impact-modified samples from planetesimals that existed between the orbits of Mars and Jupiter (now the main asteroid belt). Thus, the lunar cataclysm is sometimes called the inner solar system cataclysm [3]. Based on age spectra among meteorites (e.g., [4-6]), we have detected collisions (e.g., [7]) during the epoch of planetary accretion between ~4.4 and 4.5 Ga. After many of those small planetary relicts were consumed by large collisions or ejected from the solar system, there was a significant decline or absence of impact degassed samples produced between ~4.4 and 4.1 Ga. At ~4.1 Ga, however, the orbits of asteroids were pumped up by resonances sweeping through the belt (e.g., [8,9]), causing a large number of impact-reset ages ~4.1 to 3.5 Ga. The bulk of the excited population was eventually consumed, leaving relatively quiet conditions that produced very few impact ages between ~3.5 and 1 Ga.

Collectively, the existing lunar and meteoritical data reveal a dramatic series of events in the collisional evolution of the early solar system. Yet, the precise chronology of the events that shaped the Moon is still vague. We do not know the duration or magnitude of the terminal cataclysm. Nor can we confidently define the pace of basin-forming events at the tail end of the accretional epoch and during the interval between accretion and the terminal cataclysm.

To determine the tempo of impacts during the basin forming epoch, we need to recover impact melt samples from basins that are representative of the flux in both space and time [10]. As discussed elsewhere [11,12], the highest priority target is unaltered impact melt from the South Pole-Aitken (SPA) basin. Because SPA is the oldest and largest basin, it will define the beginning of the basin-forming epoch. If this basin is part of the cataclysm, then the magnitude of the lunar cataclysm event is far greater than previously proposed, involving ~3 times the number of basin-forming impact events. If SPA has instead a much older age (say 4.4 Ga), then pre-Nectarian basins with successively younger relative ages need to be sampled to determine if a cataclysm began in the pre-Nectarian and, if so, when it began in that basin-forming sequence. The best location for an SPA sample may be within the Schrödinger basin [13], because we could obtain samples of both the oldest and the second youngest basins at that locality, effectively bracketing the entire basin-forming epoch.

Those same impact melt samples can be used to determine the source of projectiles and their chemical compositions. This will, in turn, test proposed mechanisms for the impact flux. These data can also be used to calculate the delivery of biogenic elements during the bombardment and the environmental consequences of the impact events, particularly on neighboring Earth.

Resurfacing the Moon: Geologic mapping [14] indicates that the basin-forming epoch resurfaced most of the Moon. Those processes also dramatically altered topography. The collisional processes excavated large topographic lows (e.g., the floor of South Pole-Aitken basin is ~13 km deep), while producing stacked layers of ejecta kilometers thick that partially buried the original igneous crust of the Moon.

Modifying the Composition of the Crust: The basin-forming processes excavated material from all depths within the crust and created a megaregolith that apparently has a noritic composition created by mixing lower and upper crustal components [15].

Those same events melted immense volumes of the Moon's crust and, in some cases, the underlying man-

tle. A recent calculation [16] indicates that ~10^8 km^3 of impact melt was produced (Fig. 1). Approximately half (if not more) of the impact melt volume was produced by the largest basin-forming event (that of the SPA basin). The largest fraction of the melt stayed within the central melt pool. If we cautiously extrapolate from studies of smaller complex craters [17], then 25 to 45% of that melt may have been ejected.

Differentiating Impact Melt Pools: Melt remaining in the largest basins may have differentiated, producing a new series of layered lithologies. To illustrate the processes involved, let's continue to examine SPA. In this case, impact melting may have been dominated by mantle lithologies [18]. If the surface of the central melt pool cooled to form a "lid" like the surfaces of the central melts sheets at the Chicxulub and Sudbury basins on Earth, it would have a composition similar to that of the bulk melt; i.e., it would have crystallized to form an olivine- and pyroxene-rich rock. As the underlying melt pool cooled, olivine may have crystallized and settled downward (see the illuminating work of [19]). Progressive crystal fractionation would drive the remaining liquid towards noritic compositions. Those magmas may have occasionally pierced the solidified top of the melt pool, erupting to form noritic lava flows. Potentially, rafts of the olivine- and pyroxene-rich roof of the melt pool may have been mobilized and re-exposed on the surface (e.g., potentially like mafic mound). Plagioclase may have eventually crystallized and floated to the top of the melt pool, where it may have been largely trapped as an anorthositic horizon beneath the solidified roof of the melt pool. These differentiation processes may have mimicked those associated with the older, lunar magma ocean (LMO), and partially erased the signatures of the LMO in places like the center of SPA.

Probing the Deep Crust: As outlined above, basins will be the target of future sample return missions, because they provide a means of testing the lunar cataclysm hypothesis and determining the age of the oldest basin on the Moon [e.g., 6].

Impact basins are also excellent probes of the entire lunar crust. Normal faults in the modification zones and along the walls of the basins expose subsurface lithologies and their stratigraphic relationships. Uplifted peak rings in the centers of the basins expose even deeper levels in the Moon's crust. Furthermore, clasts of subsurface lithologies are entrained in impact melt breccias deposited within the basins and beyond the basin rims. Thus, by combining observations of modification zones, central uplifts, and impact breccias, one can generate a cross-section of the lunar crust that may be kilometers to 10's of kilometers deep. The volume of material beneath an impact site that is melted extends to an even deeper level than the material that is excavated. Because that melt is mixed, samples of it will provide an average chemical composition of the crustal (and potentially upper mantle) volume affected by an impact event. Consequently, while collecting samples to determine the impact flux to the lunar surface, one is also collecting samples of the deep lunar crust and potentially the underlying mantle.

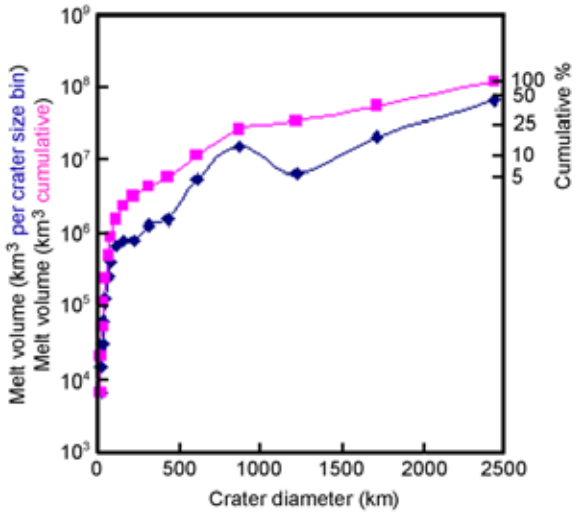

Fig. 1. Melt volumes for ancient lunar highland crater populations in crater size bins ranging from 8 to 2500 km. From [15].

References: [1] Turner G. et al. (1973) *Proc. 4th Lunar Sci. Conf.*, 1889-1914. [2] Tera F. et al. (1974) *Earth & Planet. Sci. Letters, 22*, 1-21. [3] Kring D.A. and Cohen B.A. (2002) *J. Geophys. Res., 107*, doi: 10.1029/2001JE001529. [4] Bogard D. D. (1995) *Meteoritics, 30*, 244-268. [5] Bogard D. D. (2011) *Chemie der Erde, 71*, 207-226. [6] Swindle T. D. et al. (2009) *Meteoritics & Planet. Sci., 44*, 747-762. [7] Weirich J. R. et al. (2011) *Meteoritics & Planet. Sci., 45*, 1868-1888. [8] Gomes R. et al. (2005) *Nature, 435*, 466. [9] Strom R. G. et al. (2005) *Science, 309*, 1847–1850. [10] Kring D. A. (2007) *Lunar Reconnaisance Orbiter Science Targeting Meeting*, Abstract #6037. [11] NRC (2007) *The Scientific Context for Exploration of the Moon*, 107p. [12] Kring D.A. (2008) *LPS XXXIX*, Abstract #1251. [13] O'Sullivan K. M. et al. (2011) *GSA Special Paper, 477*, 117–128. [14] Wilhelms D. E. (1987) *USGS Prof. Paper 1348*. [15] Hawke B. R. et al. (2003) *J. Geophys. Res., 107*, doi: 10.1029/2002JE001890. [16] Kring D. A. et al. (2012) *LPS XVIII*, Abstract #1615. [17] Cintala M. J. and Grieve R. A. F. (1998) *Meteoritics & Planet. Sci., 33*, 889–912. [18] Potter R. W. K. et al. (2010) *LPS XXXXI*, Abstract #1700. [19] Morrison D. A. (1998) *LPS XXIX*, Abstract #1657.

LUNAR HIGHLAND MINERAL MAPS INTEGRATING THERMAL AND NEAR INFRARED MULTISPECTRAL IMAGING. P.G. Lucey[1], B.T. Greenhagen[2] and the LRO Diviner Lunar Radiometer Experiment Team, [1]Hawaii Institute for Geophysics and Planetology, 1680 East West Road, POST 602, Honolulu, HI 96822; [2]Jet Propulsion Laboratory, California Institute of Technology, Pasadena, CA, USA; Email: lucey@higp hawaii.edu

Introduction: Multispectral thermal imaging data from LRO's Diviner Lunar Radiometer Experiment have been used to remotely detect silicic minerals and seek candidates for mantle exposures [1,2]. The compositional capability relies on characterizing the position of the Christiansen Feature (CF), a spectral feature sensitive to silicate mineralogy. The CF is an emission maximum near 8 microns that for silicates that is related to the position where the real index of refraction equals one in pure minerals. The wavelength of the CF in rocks is close to the average of the CFs of the constituent minerals, weighted by their modal abundances [3]. Because the CF is a single parameter, specific minerals are not uniquely detected (except at the extremes), but the CF is a powerful constraint on mineralogy. The CF is complementary to near-IR spectroscopy, which is most sensitive to the relative abundances of the mafic minerals but less sensitive to the abundance of plagioclase where mafic minerals are only moderately abundant. Incorporating the CF as a constraint greatly increases confidence in plagioclase-mafic ratios. Mineral maps have been developed from near-IR data alone (Clementine) with only FeO as an independent constraint, furthermore, these maps were derived from the least mature 5% of the lunar surface and interpolated to a continuous grid [4].

Here we present new mineral maps at 16 pixel per degree resolution (about 2 km at the equator) that combine the spectral constraint of the CF and near-IR spectral properties to produce refined mineral maps.

DATA: Global CF mosaics were produced by topographically projecting and binning Diviner thermal emission data at 16 pixels per degree. The CF for each bin was calculated using the method of Greenhagen et al., [1], which estimates the CF position from a quadratic fit to Diviner's three 8-micron channels' data. The global CF mosaics where normalized to equatorial noon illumination conditions using the method of [5]. Because global mosaics from SELENE or M3 (level 2) were not available for the production of these preliminary maps, Clementine data were used for this proof of concept. Clementine data have significant limitations, among them km level deviations from the current cartographic reference used by Diviner (and LROC and SELENE), but multiple studies have shown these data contain useful spectral information and were the basis for prior global mineral maps.

METHOD: The previously published mineral maps used a multistep process that readily allows adding of the CF constraint. The process begins with calculation of a lookup table of spectra computed from Hapke theory over the system plagioclase, olivine, orthopyroxene and clinopyroxene at 10% steps in composition. Ten lookup tables are produced, each with constant Mg-number for all mafic minerals, with the tables covering a range of Mg from 50 to 90 at 10 unit intervals. The prior method [4] tested each unknown spectrum against each table selecting the best match, yielding a best match at each Mg-number. The final answer was selected by computing the stoichiometric iron content of each best fit model, and selecting the Mg-number fit showing the closest agreement of stoichiometric iron and remotely determined iron content. For this project, the best fit is sought not over the entire lookup table, but only from those compositions that have model CF values within .04 microns of the measured CF of the unknown location, so therefore all solutions are consistent with Diviner measurements. The 0.04 microns range permitted is the approximate uncertainty in the current CF data. The final values for Mg-number and mineral modal abundance is still selected based on the best agreement for calculated stoichiometric iron and measured iron for that location

Because the lunar CF shows some dependence on space weathering [1], we correct the CF for this effect using the optical maturity parameter OMAT:

$$CF_{corrected} = CF_{uncorrected} + (OMAT - 0.4)$$

Table 1. Christiansen Feature values used	
Anorthite	7.85
OPX	8.12
CPX	8.13
Fo90	8.76
Fo80	8.84
Fo70	8.92
Fo60	8.99
Fo50	9.08

This correction shifts the CFs to the approximate units and range of pure minerals. Anorthite, orthopyroxene, and clinopyroxene CF values were taken from [6]. The change in CF position for olivine with composition was taken from [7] and tied to the the Donaldson-Hanna et al. value of forsteritic olivine. Model CF values are determined from the values in Table 1, weighted by the modal abundance input into each model.

RESULTS: Unsurprisingly, the dominant mineral is plagioclase, with a global modal highlands abundance of 80 %. This value is higher than derived from previous global mineral maps, but the derived abundance of aluminum (Al2O3) content of 28 wt.% is well within the range of previous estimates [8,9,10]. This alumina value is much less than that estimated for the crust by [11], but they included the apparent increase in plagioclase content with depth in the upper crust based on ubiquitous detection of anorthite in a large sample of craters larger than 35 km.

Of the mafics, orthopyroxene is widespread in the highlands as expected (but in contrast to previous maps that appeared to overestimate clinopyroxene abundance [4]), and similar to previous work, olivine is widely distributed at low abundances, consistent with the need for a stoichiometric olivine component in geochemical mixing models (12). Clinopyroxene, at this global scale, appears confined to the maria; however, we have not examined the many locations where isolated outcrops of clinopyroxene are reported in the highlands [13,14,15].

The Mg-number map derived from the process is in general agreement with the Lunar Prospector GRS-derived data of Prettyman et al.[16], with a slightly lower average highland Mg of 70. As expected, maria values are much lower, near 50. Interestingly, the Mg-number we report, and that of Prettyman et al., is at the high end of ferroan anorthosite (FAN) Mg-values, superficially suggesting the presence of more magnesian anorthositic material than the Apollo collection. However, if FAN is as mafic poor as suggested by Ohtake et al. [11] our Mg-number estimate would be dominated by that of the mafic contaminant that causes lunar surface iron to be higher than pure anorthosite, not the anorthosite itself. There is one critical caveat regarding these interpretations: The derived Mg and plagioclase content is sensitive to the specific CF value assigned to anorthite, which is in turn derived from terrestrial minerals measured in a simulated lunar environment[6]. Considerable ground truth effort will be required to lend confidence to these results.

CONCLUSIONS AND FUTURE WORK: The above results are broadly consistent with prior work, but new data can substantially improve many aspects of the data product. Data from M3 and the SELENE Multiband Imager and Spectral Profiler data are better geometrically controlled, have higher signal to noise, and spatial resolution than Clementine data. Also, the important space weathering correction currently depends on an algorithm that includes reflectance as an input; and the Clementine data are not normalized for topographic shading so there is significant error. Finally, ground truth both for validation and algorithm refinement is required by study of the CF and near-IR properties of individual sampling sites as done by [18]

References:

[1] Greenhagen et al. (2010) Science 329 (5998), 1507-1509. [2] Glotch et al. (2010), Science 329 (5998), 1510-1513. [3] Salisbury, J.W. and Walter, L. S. (1989) JGR, 94, 9192-9202. [4] Greenhagen et al. LPSC2011, abs. 2679. [5]. Lucey, P. G. (2004), GRL, 31, [6] Donaldson Hanna, K. L., M. B. Wyatt, I. R. Thomas, N. E. Bowles, B. T. Greenhagen, A. Maturilli, J. Helbert, and D. A. Paige (2012), JGR, doi:10.1029/2011JE003862. [7] Nash DB, Salisbury JW, Conel JE, Lucey PG, Christensen PR (1993) JGR 98(E12):23535-23552. [8] Spudis PD, Davis PA (1986) Proc Lunar Planet Sci Conf 17. J Geophys Res 91:E84-E90. [9]Lucey PG, Taylor G.J., Malaret E (1995) Science 268(5214):1150-1153. [10] Korotev, RL, (2000) JGR 105:4317-4345.[11] Ohtake, M. et al. Nature, 461, doi:10.1038/nature08317. [12] Korotev RL (1997) MAPS 32:447-478. [13] Pieters CM (1986) Rev Geophys 24:557-578. [14] Lucey PG, Hawke BR (1987) Proc Lunar Planet Sci Conf 18:578. [15] Ogawa et al. (2011) GRL, VOL. 38, L17202 [16] Prettyman, T.H, J.J. Hagerty, R.C. Elphic, W.C. Feldman, D.J. Lawrence, G.W. McKinney and D.T. Vaniman (2006b), JGR, 111, E12007, doi: 10.1029/2005JE002656. [18] Blewett DT, Lucey PG, Hawke BR, Jolliff BL (1997) J Geophys Res 102:16,319-16,325.

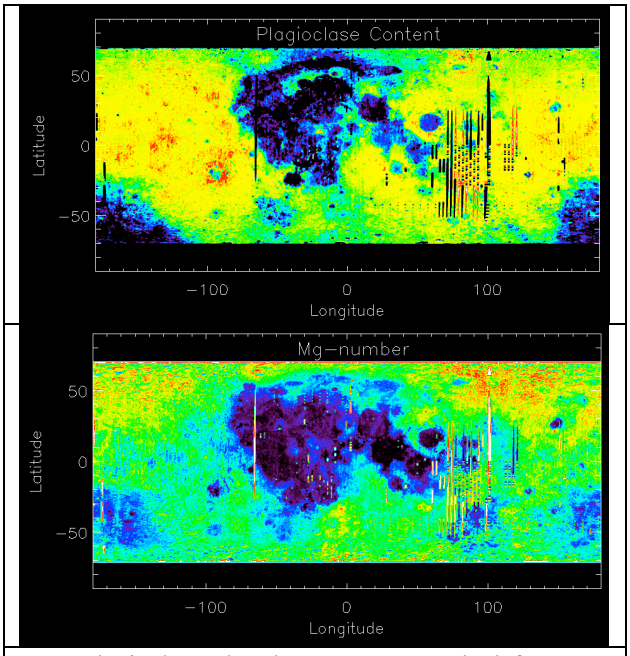

Top: Plagioclase abundance map, stretched from 50-100% (blue to red). Bottom: Mg-number map, stretched from Mg*=50-10 (blue to red).

MAGMATIC VOLATILE RESERVOIRS ON THE MOON AND THE CHEMICAL SIGNATURES OF urKREEP. F. M. McCubbin[1], C. K. Shearer[1], Z. D. Sharp[2]. [1]Institute of Meteoritics, University of New Mexico, Albuquerque, NM 87131. [2]Department of Earth and Planetary Sciences, University of New Mexico, Albuquerque, NM 87131 (fmccubbi@unm.edu)

Introduction: Significant progress has recently been made in determining the nature of lunar indigenous volatiles. Recent SIMS analyses of lunar apatites have revealed that hydroxyl is structurally bound within apatite from a number of different lithologic types [1-5]. Furthermore, F, Cl, H_2O, and S abundances in lunar fire fountain glasses have also been determined [6-7], providing us with the most complete picture of lunar volatiles to date. Lastly, H- and Cl-isotope analyses have been conducted on lunar materials and the results indicate that the Moon is typically enriched in the heavy isotopes relative to Earth [4, 8]. Although significant progress has been made in understanding the abundances of magmatic volatiles in lunar materials, important questions regarding the sources and reservoirs of these volatiles remain. The purpose of the present study is to identify some of these volatile reservoirs and determine their defining characteristics. Furthermore, we will speculate as to the processes that have lead to the formation of these reservoirs and determine how they can be used to understand the thermal and magmatic evolution of the lunar crust and the role of volatiles in the formation of the lunar highlands.

Previous Results: The magmatic volatile abundances of apatite from several lunar lithologic types have been determined, and there are some striking differences in the volatile abundances that correlate to lithologic type. Specifically, rocks from the highlands magnesian-suite, alkali-suite, and KREEP-rich impact melts, all of which are KREEP-rich lithologies, plot together in an OH-poor, relatively Cl-rich portion of the F-OH-Cl ternary [5, Figure 1]. Furthermore, apatite from various mare basalts plot over a range of OH-rich to F-rich compositions that are consistently Cl-poor [5, Figure 1]. Furthermore, the relative abundance of H_2O:F:Cl for the mare basalts match those of the lunar picritic glasses [6-7], indicating all mare source regions are relatively poor in Cl and contain significant H_2O and F [6-7].

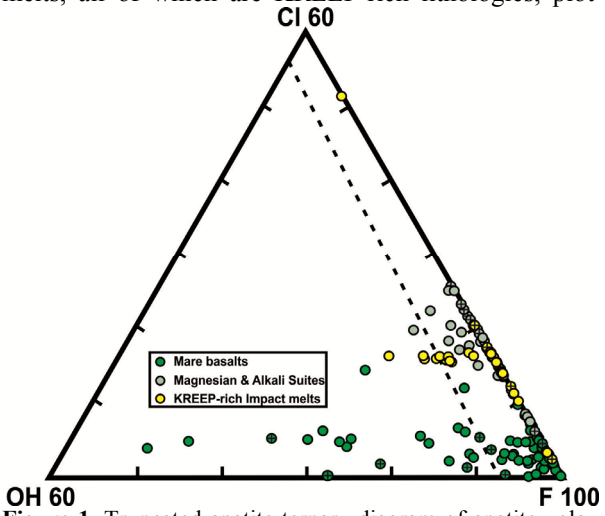

Figure 1. Truncated apatite ternary diagram of apatite volatile contents (F and Cl measured by EPMA, OH calculated by difference and has been generally confirmed by SIMS [1-5]) from several different lithologic types from the Moon.

McCubbin et al. [5] proposed that the relative volatile abundances for the mare source regions were a signature of the lunar mantle. The process proposed to have caused this volatile signature is the storage of F and H in nominally anhydrous minerals (pyroxene, garnet, and olivine) that formed during lunar magma ocean crystallization. Cl would have been largely excluded from these minerals due to its large ionic radius compared to F and OH/H [as shown experimentally by 9-10]. The highland apatites were interpreted to have preserved the relative volatile abundances of urKREEP (i.e., the residual liquid of the lunar magma ocean (LMO)) because they represent a mixture of crustal materials (including urKREEP) and the earliest formed LMO cumulates (which would be some of the most volatile-depleted of the LMO cumulates). Furthermore, the urKREEP volatile signature was taken to represent the relative volatile abundance of the residual liquid to the lunar magma ocean (i.e., the relative volatile abundances of the bulk Moon subsequent to any degassing). Importantly, although there appears to be two distinct volatile reservoirs on the Moon, existing partitioning data for F, Cl, and H_2O between silicate melt and nominally anhydrous minerals requires that the lunar mantle has substantially less volatiles per unit volume than urKREEP (i.e., urKREEP should be the primary volatile reservoir on the Moon).

Previous Cl Isotope Results: The most elevated of the δ^{37}Cl values measured for lunar materials to date are from apatites within KREEP basalt samples (i.e., 21.8-25‰ in apatite from KREEP basalts [8, this study]). Sharp et al. [8] indicated that the elevated δ^{37}Cl values require degassing of metal chlorides. This requires that a magma either has more Cl than H or H and Cl degassing are decoupled. The higher abundance of Cl than H_2O in KREEP-rich magmas is supported by the apatite compositions in KREEP-rich highlands rocks [5, Fig. 1]. Mare basalts, which typically have more H_2O than Cl [5, Fig. 1], also typically have lower δ^{37}Cl values. It is unclear whether or not the δ^{37}Cl values for each sample are ascribed by the source from which they were derived or by degassing processes

from the rock itself. Determining the answer to this question requires additional analyses because thus far, we have compared the apatite compositions from highlands Mg- and alkali-suite rocks to the δ^{37}Cl values from KREEP basalts, which may not be meaningful. The relationship between the highlands KREEP-rich rocks, KREEP basalts, and urKREEP are presently unknown. Consequently, we have analyzed apatites from KREEP basalts by EPMA to better understand this relationship, although additional data on δ^{37}Cl values for highlands rocks is still needed.

KREEP Basalt Apatites: Apatites from KREEP basalt samples 15386, 15382, and Northwest Africa 2977 (olivine gabbro lithology of NWA 773) have been analyzed by EPMA using the same techniques as McCubbin et al. [2, 5]. The apatite data are plotted in Figure 2, and they typically lie between the mare basalt and KREEP-rich highlands rocks portion of the ternary, where the volatile abundances for the two rock suites overlap. On average, the KREEP basalts have much less chlorine than the highlands Mg- and alkali-suite apatites.

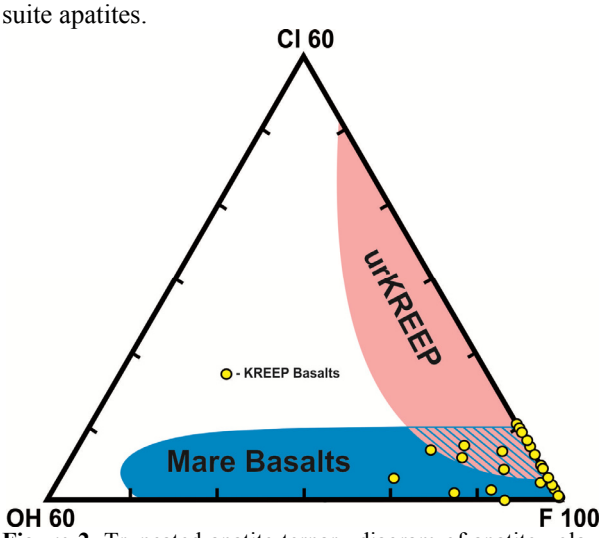

Figure 2. Truncated apatite ternary diagram of apatite volatile contents (F and Cl measured by EPMA, OH calculated by difference and has been generally confirmed by SIMS [1-5]). Fields for mare basalts and urKREEP are labeled shaded in blue and pink respectively. The KREEP basalt data points are in yellow.

Implications for chemical signatures of urKREEP: The KREEP basalt apatites plot within both the mare basalt and urKREEP fields. In addition, the apatites from the KREEP basalts plot in the region of the apatite ternary that is consistent with mixing of urKREEP and mare volatile components. This is not entirely surprising given the mare-like bulk rock compositions of the KREEP basalts. Consequently, the KREEP basalts either formed by partial melting of a mare source region that had a small KREEP component or by assimilation of a KREEP component during ascent and fractional crystallization.

The volatile abundances of the KREEP basalts allow us to test whether or not the elevated δ^{37}Cl values are a signature of urKREEP (i.e., from degassing of urKREEP during LMO crystallization) vs. secondary processes like degassing of the basalt itself. The KREEP basalts have both mare and urKREEP volatile components, so the high δ^{37}Cl values of the KREEP basalts will be low compared to the δ^{37}Cl of highlands Mg-suite and alkali-suite apatites if δ^{37}Cl values are a signature of urKREEP and higher than Mg-suite and alkali-suite apatites if from low-pressure degassing. The later is supported by the plutonic nature of Mg- and alkali-suite rocks (i.e., they formed at higher pressure than most lunar basalts and therefore were less likely to experience extensive degassing). Although chlorine solubility in silicate liquids has not been reported to be pressure dependent, Ustunisik et al. [11] experimentally demonstrated Cl degassing from lunar compositions into a vacuum of higher pressure than the lunar surface, so Cl-degassing of basalts at the lunar surface should be expected. Furthermore, Ustunisik et al. [11] demonstrated the decoupling of Cl and H degassing at these conditions, which is required for the increase in δ^{37}Cl during degassing [8], which could explain some of the slightly elevated values in mare basalts and mare basalt apatites relative to terrestrial values [8].

Implications for H Isotopes: Highlands KREEP-rich samples typically have the lowest δD values measured for lunar materials (i.e., 200-300‰ [4]). If these values are representative of urKREEP than the δD values for the KREEP basalts should be intermediate between the highlands apatite (i.e., 200-300‰ [4]) and typical mare basalt apatite (i.e., 400-1100‰ [4]). To date, no δD values have been determined for KREEP basalt apatites.

Implications for Other Airless Bodies: If the highly fractionated δ^{37}Cl values are indeed a chemical signature of urKREEP that resulted from degassing of the late stage magma ocean liquid, other airless bodies of Mercury size or smaller could have experienced a similar process during a magma ocean. In fact, the existence of a global reservoir with highly fractionated δ^{37}Cl values may be a fingerprint for a magma ocean on an airless body, and it may be a good test for whether or not a magma ocean ever existed on bodies like Mercury, Ceres, 4 Vesta, 2 Pallas, and Hygiea.

References: [1] McCubbin et al. (2010) *Proc. Natl. Acad. Sci.* 27, 11223-11228. [2] McCubbin et al. (2010) *Am Min.* 95 1141-1150. [3] Boyce et al. (2010) *Nature* 466, 466-469. [4] Greenwood et al. (2011) *Nature Geoscience* 4, 79-82. [5] McCubbin et al. (2011) *GCA*. 75, 5073-5093. [6] A. E. Saal et al., Nature 454, 192-195 (2008). [7] E. H. Hauri et al. (2012) *Science* 333, 213-215. [8] Sharp et al. (2010) *Science* 329, 1050-1053. [9] O'Leary et al. (2010) *EPSL* 297, 111-120. [10] Hauri et al., (2006) *EPSL* 248, 715-734. [11] Ustunisik et al., (2011) *Am Min* 96, 1650-1653.

PREDICTING THE SOURCES AND FORMATION MECHANISMS OF EVOLVED LUNAR CRUST BY LINKING K/Ca RATIOS OF LUNAR GRANITES TO ANALOGOUS TERRESTRIAL IGNEOUS ROCKS.

R. D. Mills and J. I. Simon, Center for Isotope Cosmochemistry and Geochronology, Astromaterials Research, NASA Johnson Space Center, Houston, TX, 77058 (rdmills@unc.edu; justin.i.simon@nasa.gov).

Introduction: Although silicic rocks (i.e. granites and rhyolites) comprise a minor component of the sampled portion of the lunar crust, recent remote sensing studies [e.g., 1-4] indicate that several un-sampled regions of the Moon have significantly higher concentrations of silicic material (also high in [K], [U], and [Th]) than sampled regions. Within these areas are morphological features that are best explained by the existence of chemically evolved volcanic rocks. Observations of silicic domes [e.g., 1-5] suggest that sizable networks of silicic melt were present during crust formation. Isotopic data indicate that silicic melts were generated over a prolonged timespan from 4.3 to 3.9 Ga [e.g., 6-8]. The protracted age range and broad distribution of silicic rocks on the Moon indicate that their petrogenesis was an important mechanism for secondary crust formation. Understanding the origin and evolution of such silicic magmas is critical to determining the composition of the lunar crustal highlands and will help to distinguish between opposing ideas for the Moon's bulk composition and differentiation.

The two main hypotheses for generating silicic melts on Earth are fractional crystallization or partial melting. On the Moon silicic melts are thought to have been generated during extreme fractional crystallization involving end-stage silicate liquid immiscibility (SLI) [e.g. 9, 10]. However, SLI cannot account for the production of significant volumes of silicic melt and its wide distribution, as reported by the remote global surveys [1, 2, 3]. In addition, experimental and natural products of SLI show that U and Th, which are abundant in the lunar granites and seen in the remote sensing data of the domes, are preferentially partitioned into the depolymerized ferrobasaltic magma and not the silicic portion [11, 12]. If SLI is not the mechanism that generated silicic magmas on the Moon then alternative processes such as fractional crystallization (only crystal-liquid separation) or partial melting should be considered as viable possibilities to be tested.

Fractional crystallization of a basaltic source without SLI is an inefficient process for generating silicic melts. This is because the distilling process must proceed to completion, which is physically difficult in terms of the degree of crystallization. For example, on the Moon a basaltic magma with K_2O/CaO of ~0.03 must fractionate to ~7 (granite clast from 14321). Figure 1 shows the relationship between crystallization and the predicted fractionation of K and Ca during magma ocean solidification. Results indicate that it is unlikely that fractional crystallization alone can produce K/Ca ratios greater than 0.2. Likewise, segregation and extraction of highly-polymerized viscous melt from a highly crystalline mush is nearly impossible without strong external forces [13] (e.g., gravitational and/or secondary impacts).

Because it is difficult to produce such chemically "evolved" melts solely by fractional crystallization, partial melting of preexisting crust may also have been important and possibly the primary mechanism which produced the silicic magmas on the Moon. Terrestrial studies (e.g., [14]) demonstrate that partial melting of gabbroic rock under mildly hydrated conditions can produce granitic compositions and it has been suggested by [1] that partial melting by basaltic underplating is the mechanism by which silicic melts were produced on the Moon. Isotopic and elemental data can help decipher what source rocks were partially melted and when the melting occurred.

K/Ca isotopic data from a mineral isochron [15] for a granite clast from sample 14321 indicate that the parental material of this silicic magma had a K_2O/CaO ratio of at least 0.8, significantly higher than most known crustal rock types, including KREEP-rich materials [e.g. 16, 17]. This suggests that granite in sample 14321 was produced by partial melting of an already "evolved" rock. Next we use terrestrial chemical data as a proxy for igneous rocks in the lunar crust which allow us to hypothesize what type of rock may have been parental to granite found in Apollo breccia sample 14321.

Terrestrial data: Geochemical data for igneous rocks from the western United States were extracted from the NAVDAT online repository. The ~4000 data with variable L.O.I. represent multiple tectonic settings, including subduction, rifting and anorogenic; however, the ~2200 data from low L.O.I. rocks (likely from relatively dry magmas) define a similar trend on a plot of K_2O/CaO vs SiO_2.

Interpretation: Data from Apollo sample 14321 granite clast [15] indicate that the parental material to the granite had already evolved on a K_2O/CaO trend of approximately 1, consistent with an intermediate/felsic terrestrial magma (Fig. 2). One of the objections to the fractional crystallization model is the lack of intermediate compositions. Taken at face value, the bulk composition implied by the data of [15] could represent an

example of the missing intermediate composition, although it does not provide a unique solution to the problem. More evidence of this type is needed to critical test the mechanism(s) that generated silicic magmas on the Moon.

Next Step: Future investigations will carry out extensive searches for additional evolved igneous rock clasts in Apollo samples and lunar meteorites primarily for K-Ca isotope measurements. As in [15], these data will be used to define the bulk compositions of the source(s) of evolved materials that make up the lunar crust. The search for source(s) will be further refined by comparison of radiogenic isotope compositions (inferred initial $^{40}Ca/^{44}Ca$, $^{87}Sr/^{86}Sr$, and $^{176}Hf/^{177}Hf$ isotopic compositions and isochron ages) in these clasts to the compositions of known lunar rock types.

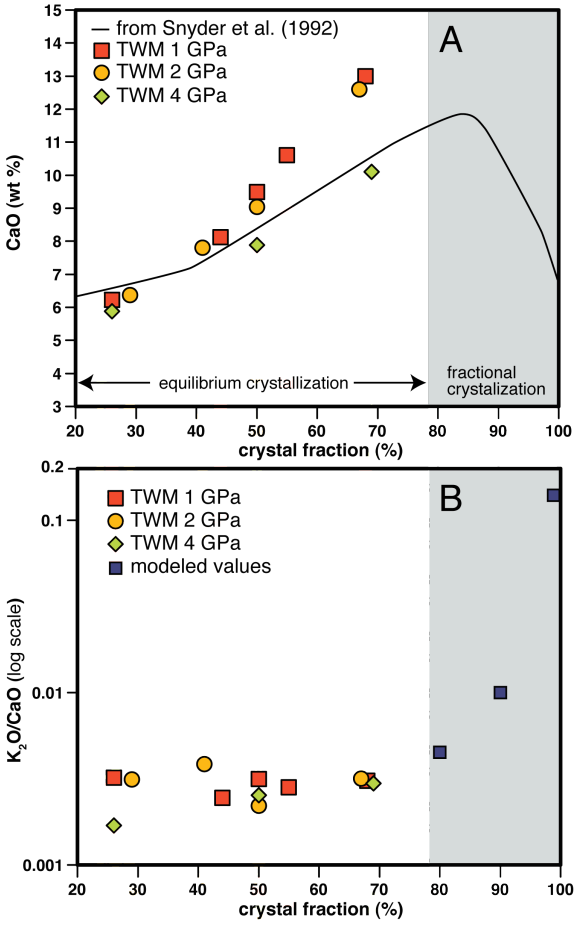

Fig. 1 (A) Plot of CaO vs crystal fraction of the Moon with experimental results [18] from equilibrium crystallization of a Taylor Whole Moon (TWM) composition at 1, 2 and 4 GPa, and modeled results of equilibrium then fractional crystallization [19]. (B) Plot of K_2O/CaO (log-scale) vs crystal fraction of the Moon with data from [18] and modeled values using CaO values from [19] and assuming K behaves completely incompatible.

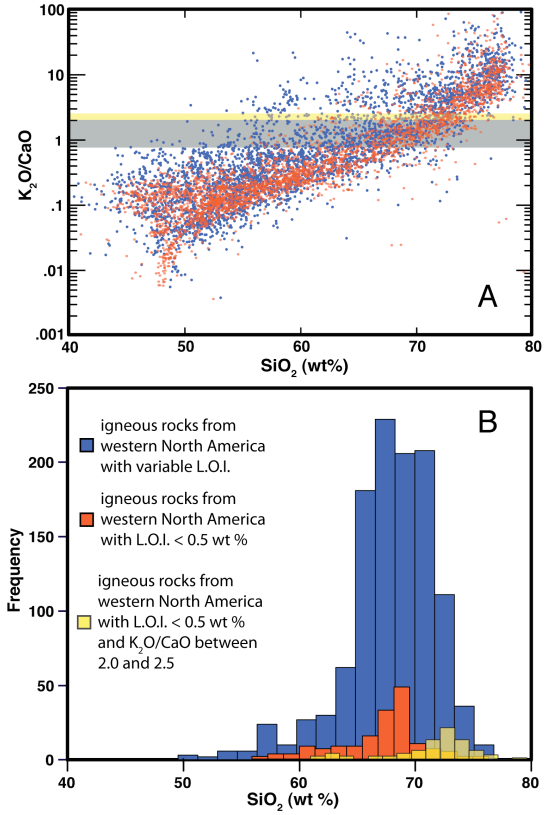

Fig. 2 (A) Plot of K_2O/CaO vs SiO_2 with 4000 igneous rocks from the western US with variable L.O.I. and 2200 igneous rocks from the western US with L.O.I. < 0.5 % (all data extracted from www navdat.org). Gray bar is the calculated K_2O/CaO ratio of the parental material for granite clast from Apollo sample 14321 [15], and yellow bar is the upper estimate using the FAN age from [20] (B) Histogram of SiO_2 for data that fall in the gray bar and yellow bar in A.

References: [1] Hagerty et al. (2006) J. Geophys. Res. 111:E06002. [2] Glotch et al. (2010) Science 305:657-659. [3] Greenhagen et al. (2010) Science 329:1507-1509. [4] Jolliff et al. (2000) J. Geophys. Res. 105:4197-4216. [5] Hawke et al. (2003) J. Geophys. Res. 108:5069. [6] Nyquist and Shih (1992) Geochim. Cosmochim. Acta 56:2213-2234. [7] Meyer et al. (1996) Meteor. Plan. Sci. 31:370-387. [8] Taylor et al. (2009) Earth Plan. Sci. Lett. 279:157-164. [9] Roedder and Weiblen (1972) Proc. Lunar Sci. Conf. 251-279 [10] Rutherford et al. (1974) Proc. Lunar Sci. Conf. 569-583. [11] Neal and Taylor (1989) Proc. Lunar Sci. Conf. 209-218. [12] Shearer et al. (2001) Am. Min. 86:238-246. [13] Marsh (2002) Geochim. Cosmochim. Acta 66:2211-2229. [14] Sisson et al. (2005) Contrib. Mineral Petrol. 148:635-661. [15] Simon et al. (2011) LPSC #2754. [16] Warren (1989) Lunar and Plan. Ins. Tech. Rep. 89:149-153. [17] Ryder (1976) Earth Plan. Sci. Lett 29:255-268. [18] Elardo et al. (2011) Geochim. Cosmochim. Acta 75:3024-3045. [19] Snyder et al. (1992) Geochim. Cosmochim. Acta 56:3809-3823. [20] Borg et al. (2011) Nature 477:70-72.

COMPOSITIONAL VARIATION OF THE LUNAR HIGLAND CRUST. M. Ohtake[1], H. Takeda[2], T. Morota[3], Y. Ishihara[4], T. Mastunaga[4], Y. Yokota[4], S. Yamamoto[4], J. Haruyama[1], Y. Ogawa[5], T. Hiroi[6], Y. Karouji[7] and K. Saiki[8], [1]Planetary Science Department, Japan Aerospace Exploration Agency, 3-1-1 Yoshinodai, Sagamihara, Kanagawa, 229-8510, Japan (ohtake makiko@jaxa.jp), [2]The University of Tokyo, [3]Nagoya University, [4]National Institute for Environmental Studies, [5]The University of Aizu, [6]Brown University, [7]Japan Aerospace Exploration Agency, [8]Osaka University.

Introduction: A global distribution of rocks of very high plagioclase abundance (approaching 100 vol.%; purest anorthosite) has been detected at central peaks, crater walls, and ejecta using an unambiguous plagioclase absorption band recorded by the SELENE Multiband Imager (MI) and Spectral Imager (SP) [1][2]. The estimated plagioclase abundance is significantly higher than previous estimates of 82 to 92 vol.% [3], providing a valuable constraint on models of lunar magma ocean (LMO) evolution.

To understand the compositional variation of these high plagioclase abundance anorthosite rocks (spatial compositional variation on a scale from tens of meters to a global lunar surface with possible vertical compositional trends) is important for addressing the crustal generation mechanism because it is difficult to generate such monomineralic rocks by simple plagioclase flotation from a lunar magma ocean according to the general differentiation mechanism of magma [3][4].

Therefore, this study investigated spatial and vertical compositional (modal abundance) trends of these high plagioclase abundance anorthosite rock over the entire lunar surface within the uppermost mixing layer and the upper and lower crust by using continuous reflectance spectra derived by SP and multiband images derived by MI.

Method: We used MI images (nine bands with wavelength assignments of 415, 750, 900, 950, 1000, 1050, 1250, and 1550 nm and a spatial resolution of 20 m/pixel in the visible and 62 m/pixel in the near-infrared bands) of representative highland material (central peak and basin ring material) to investigate spatial compositional variation on a smaller scale (from tens of meters to several hundreds of kilometers) by observing band depth ratio between 950 nm (pyroxene band) and 1250 nm (plagioclase band).

To investigate global surface compositional variation, we used 26 million SP spectra after data screening to select data with a high signal-to-noise ratio and low correction errors. These spectra were binned into 1-degree intervals, with 30 km resolution at the equator.

We utilize a new algorithm, which uses correlation between mafic mineral (low-Ca pyroxene) abundance and absorption depth around 950 nm where a diagnostic absorption band of pyroxene exists, that determines modal abundance (mafic mineral abundance) to derive a high-spatial-resolution global surface map of mafic mineral abundance. We apply this new algorithm to the global data set obtained by the SP, which has spectral coverage from 500 to 2600 nm in 300 bands and a spatial resolution of 500 x 500 m.

The estimated error of our modal mineralogy estimation has an absolute error of ±1 vol.%. Presence of high-Ca pyroxene may cause small errors in estimating mafic mineral abundance. Therefore, this study discusses only highland areas with low HCP/LCP.

To investigate vertical compositional variations, we used the mafic mineral abundance data described above in and around major highland basins [5][6] to observe correlations between the distance from the basin center, which corresponds to an original depth before excavation, and concentrically averaged mafic mineral abundance of the basin interior and ejecta.

Results: The derived compositional variation up to several kilometers in scale at Jackson central peak and compositional variation up to several hundreds of kilometers at Orientale rings indicates relatively homogeneous composition (mafic abundance ranging from 0 to 3 vol.%) within these most extensive exposures of the upper highland crust, except for areas covered by impact melt, and cannot be expected to retain the original crustal composition [1].

The global surface mafic mineral abundance map indicates its dichotomic distribution having a lower mafic mineral abundance in the farside highlands than in the nearside, which is basically consistent with previous observations [7][8] though our map appears to display more detailed variation both spatially and compositionally and the lowest mafic mineral abundance location does not match exactly with that of the previous datasets.

The compositional variation within and around the basins indicates decreased mafic mineral abundance with original depth (increased mafic mineral abundance with increased distance from the basin center), indicating decreased mafic mineral abundance with depth in the crust in both the upper (< 30km) and lower crusts, possibly up to 60 km deep (Figs. 1 and 2; Freundlich-Sharonov, Kororev, and Dirchlet-Jackson Basins).

Discussion: The observed compositional homogeneity within the crust on a scale of tens of meters to several hundred of kilometers suggests the presence of the PAN (purest anorthosite) rocks within the highland crust as a vast rock body. The previously observed numerous exposures of the PAN outcrops [9][10] suggest abundant presence of the PAN rocks within the highland crust. This information further implies a vast

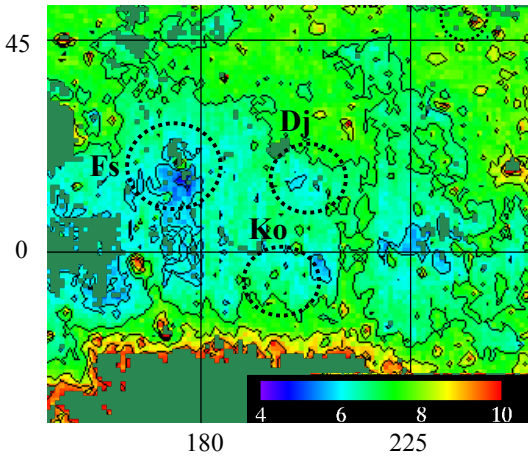

Fig. 1 Mafic mineral abundance map (vol.%) around the analyzed highland basins.

Dotted circles denote three highland basins (Freundlich-Sharonov, Kororev, and Dirichlet-Jackson) analyzed in this. Regions with greater than 11 vol.% of mafic mineral abundance and regions with high HCP/LCP ratios (exceeding 0.2) are indicated in sea green.

mechanism to generate this type of rock in the crust, which cannot be a minor component among the highland material.

The observed decrease of mafic mineral abundance with depth in the highland crust is inconsistent with the previous studies both in terms of the composition of the lower crust (more mafic-rich noritic composition has been suggested [11][12]) and compositional trend within the crust (increase of mafic mineral abundance with depth has been suggested [11][12]).

PAN rocks as widespread magma ocean flotation cumulates are problematic because of the apparent need for a mechanism to generate such cumulates in vast volume, though it may be generated by the most simple flotation mechanism from the magma ocean [13]. The results here indicate that very high plagioclase abundances occur over vast areas, which suggests need of further study of a new lunar magma ocean solidification (post-concentric) model such as [14] to explain our observation.

References: [1] Ohtake, M. et al. (2009) *Nature* 461, 236-240. [2] Matsunaga T. et al. (2008) *Geophys. Res. Let.*, 35, L23201. [3] Warren, P. H. (1990) *Am. Mineral.* 75, 46-58. [4] Longhi, J. (2003) *J. Geophys. Res.* 108, doi:10.1029/2002JE001941. [5] Wilhelms, D. E. (1987) *U.S. Geological Survey (USGS) Professional Paper* 1348. [6] Head, J. W. et al. (2010) *Science* 329, 1504-1507. [7] Jolliff, L. et al. (2000) *J. Geophys. Res.* 105, 4197–4216. [8] Kobayashi, S. et al. (2010) *Lunar Planet. Sci.* 41, #1975. [9] Ohtake, M. et al. (2010) *Lunar Planet. Sci.* 41, #1628. [10]

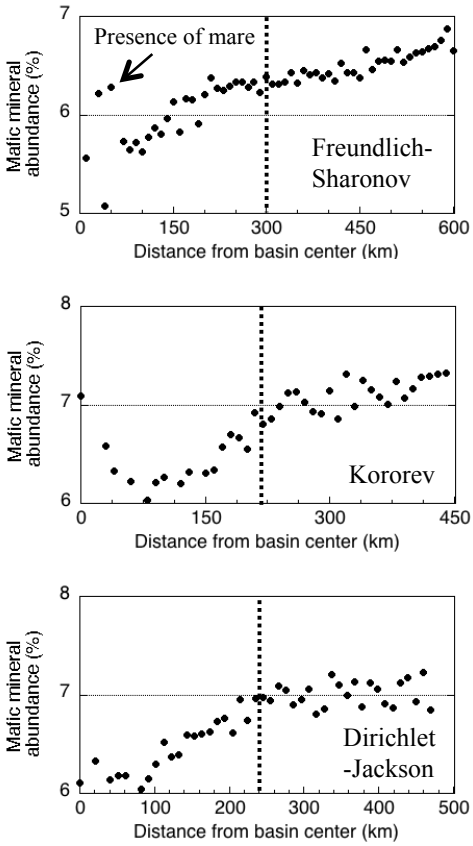

Fig. 2 Variation of mafic mineral abundance within and around highland basins.

Distance from basin center (x-axis) and averaged mafic mineral abundance (y-axis) are plotted. Dotted lines indicate locations of each basin rim. Data of up to one radius from the basin rim are presented here to observe the compositional trend in ejecta. Mafic mineral abundances increase from the center of the basin outward even in the ejecta region. This suggests decreasing mafic mineral abundance with depth, even in the lower crust.

Yamamoto S. et al. (2012) *Lunar Planet. Sci.* 43, #1356. [11] Spudis, P. D., Hawke, B. R. and Lucey, P. (1984) *J. Geophys. Res.* B 89, C197–C210. [12] Tompkins, S. and Pieters, C. M. (1999) *Meteorit. Planet. Sci.* 34, 25–41. [13] Parmentier, E. M. and Liang, Y. (2010) *Lunar Planet. Sci.* 41, #1824. [14] Loper, D. E. and Werner, C. L. (2002) *J. Geophys. Res.* 107, 5046.

CHARACTER AND STRATIGRAPHY OF THE LUNAR HIGHLAND CRUST: THE EVOLVING STORY.
C. M. Pieters[1], D. Dhingra[1], L. Cheek[1], K. Donaldson Hanna[1], D. Moriarty[1]. [1]Geological Sciences, Brown University, Providence, RI 02912 (Carle_Pieters@brown.edu).

Introduction: The lunar highland crust has become the model for evolution of a primary crust, the original crust of a differentiated planetary body [1]. Return of the first lunar samples from a region of mare basalt contained fragments of material hypothesized to be from the nearby lunar highlands, and the composition of these unusual fragments suggested a fractional crystallization sequence for the origin of the ancient lunar crust [2]. The paradigm that developed describes lunar crustal evolution as starting with a magma ocean that through fractional crystallization resulted in first a mafic mantle and later a buoyant plagioclase cumulate crust that separated from the evolving residual melt.

The available lunar samples that have been studied in great detail, however, provide an incomplete picture of the character of the lunar crust. Fortunately, diverse new lunar data acquired remotely from an international array of spacecraft sent to the Moon over the last decade has provided a global perspective and new constraints that expand and modify models for the evolution of the lunar crust. We highlight a few that merit serious discussion (and debate) now and in the years ahead.

Anorthosites. Crystalline anorthosite has unambiguously been identified across the lunar highlands [3. 4]. The purity and scale of exposed anorthosite indicate it forms a massive and global crustal layer just below the megaregolith [5, 6, 7]. This confirms the fundamental magma ocean hypothesis for the Moon.

Olivine. Largely in the form of troctolite, olivine-rich lithologies have been observed in the central peaks of large craters and associated with several large basins [8, 9, 10, 11]. The deep-seated nature of this olivine is recognized, but its origin and relation to the crust and/or mantle is yet unknown.

Mg-Spinel. The newest recognized rock type on the Moon is a pink-spinel anorthosite [11] identified at 5 locations associated with large craters or basins. The spinel is low-Fe and low-Cr, and occurrences contain no detectible mafic minerals (pyroxene, olivine). This Mg-spinel dominated rock type is believed to originate in the lower crust.

Low-Ca pyroxene. The most common mafic mineral observed in the highlands appears to be low-Ca pyroxene. The short wavelength of diagnostic absorptions near 1 and 2 μm imply a relatively Mg-rich composition [e.g., 12]. Furthermore, the farside highlands are found to be more Mg-rich than the nearside [13].

Hydrated Materials. Most feldspathic highlands exhibit small amounts of surficial OH [14, 15]. However, a few areas such as Compton-Belkovich [16] are exceptionally rich in hydrated materials, suggesting additional crustal processes in the highlands such as late-stage volcanism [17].

Hints from the Megaregolith. The megaregolith is an extensive surficial layer of broken and brecciated material a few km deep that is believed to be derived largely from basin deposits [e.g., 18] and mixed by the late heavy bombardment. The prevalence of low-Ca pyroxene in anorthositic breccias throughout the megaregolith appears to require a source area for this mafic component that is neighboring the massive anorthosite from the magma ocean.

Generalized Stratigraphy. Given the plethora of new information rapidly emerging from recent mission data, a plausible crustal stratigraphy is: 2-5 km of megaregolith derived from the upper ~50 km of crust; overlying massive, relatively pure anorthosite 10's of km thick; overlying a mafic-bearing lower crust dominated by low-Ca (Mg-rich) pyroxene; overlying and/or interspersed with a zone containing olivine/troctolite and (less common) Mg-spinel anorthosite.

Open issues: Why is the lunar mantle apparently not readily exposed at large basins? Or, what *is* the composition of the lunar mantle and how does it contrast with the lower crust?

Next Steps. What is the true structure and compositional character of the lunar highland crust and mantle? Possible answers are being and will continue to be tested. As with most important scientific discussions, they are not simple and require information from multiple sources to be integrated - the most fundamental being lunar samples, remote sensing, and geophysics.

Acknowledgements: This work was supported largely through the NASA Lunar Science Institute. We are grateful for access to data from the Chandrayaan-1, Kaguya, and LRO science missions.

References: [1] Taylor, SR (1982) *PEPI* [2] Wood J. A. et al. (1970) *Proc. Apollo 11 Lunar Sci. Conf., 1,* 965 [3] Ohtake M. et al. (2009) *Nature, 461*. [4] Pieters C. M. et al. (2009) *LPS XL*, #2052. [5] Donaldson Hanna K. L. et al. (2012) *LPS XLIII*, #1968. [6] Cheek L. C. and Pieters C. M. (2012) *LPS XLIII*, #2624. [7] Cheek L. C. et al. (2012) *LPS XLIII*, #2731. [8] Pieters, CM, (1982) *Science*, 215. [9] Matsunaga T. et al. (2008) *GRL*, *35* [10] Yamamoto et al. (2010) *Nature Geo*, 3 [11] Pieters, CM et al. (2011) *JGR*, 116, E00G08. [12] Klima et al., (2011) *JGR*, 116, E00G06. [13] Ohtake et al., (2012) *Nature Geo*, April 29 [14] Pieters et al. (2009) Science [15] Clark, RN et al., in preparation, [16] Petro, N. et al. in preparation [17] Jolliff et al. (2011) *Nature Geo* [18] Petro and Pieters (2008) *MaPS* 43, 8. [19] Greenhagen B. T. et al. (2010) *Science, 329*.

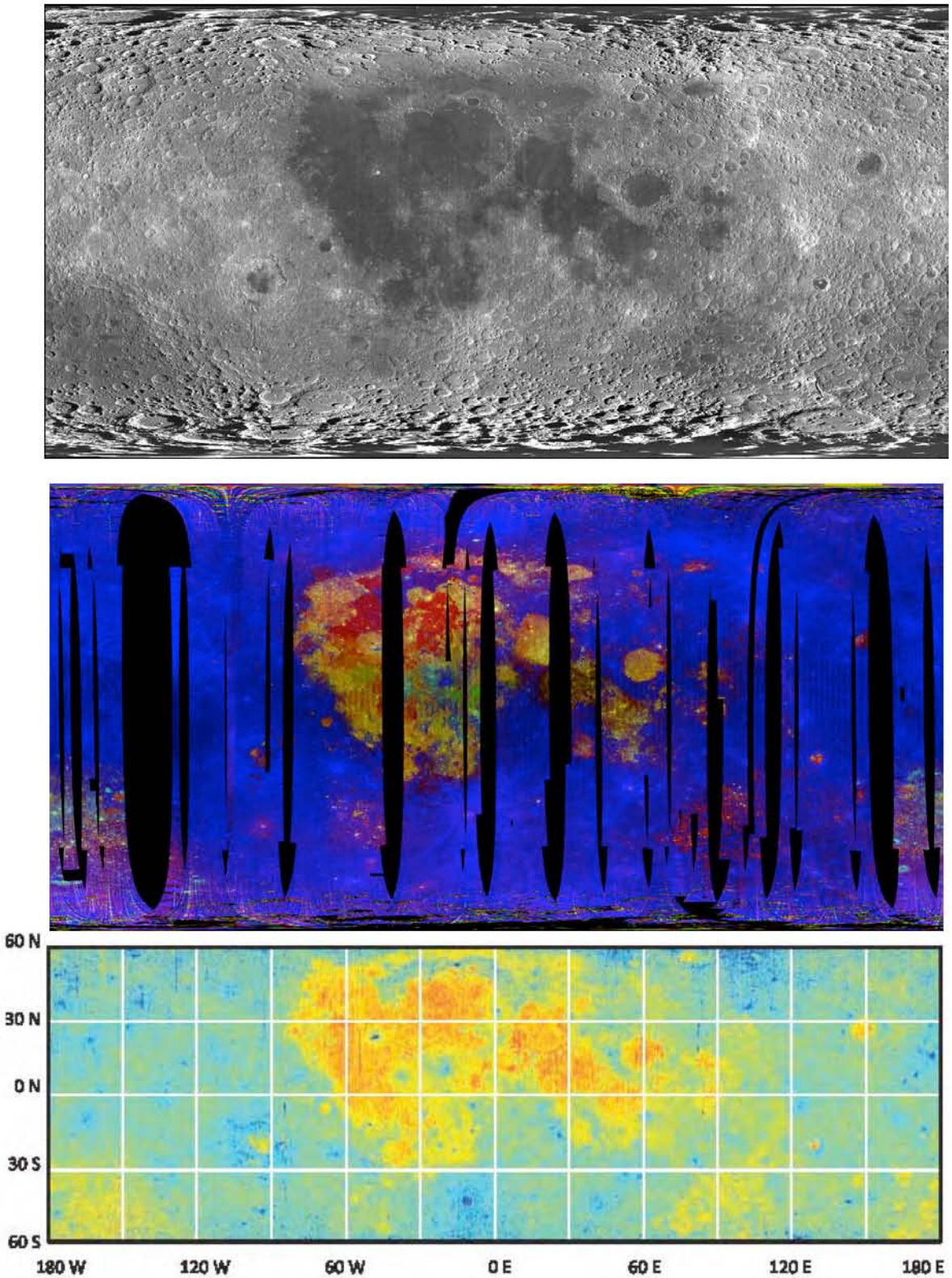

Example high resolution global datasets centered on 0, 0 lat/long that are relevant to compositional analyses of the crust. **Top**: NASA LRO LROC-WAC brightness image. **Middle**: NASA M^3 on Chandrayaan-1, OP2C1 sequence. Red=Integrated 1 μm band strength; Green= Integrated 2 μm band strength; B= Reflectance at 1.489 μm. **Bottom**: NASA LRO DIVINER trends in Christiansen Feature [19]. Red=long wavelength, Blue=short wavelength.

CHEMICAL COMPOSITION OF LUNAR MAGMA OCEAN CONSTRAINED BY THE CONDITIONS OF CRUST FORMATION. R. Sakai[1], H. Nagahara[1], K. Ozawa[1] and S. Tachibana[2], [1]Department of Earth and Planetary Science, The University of Tokyo, 7-3-1 Hongo, Tokyo 113-0033, JAPAN (rsakai@eps.s.u-tokyo.ac.jp), [2]Department of Natural History Sciences, Hokkaido University, N10 W8, Sapporo 060-0810, JAPAN.

Introduction: The Moon has been thought to have molten globally very early in its history and the anorthositic crust was formed by accumulation of anorthite crystallized in the lunar magma ocean (LMO) [1]. Previous studies revealed that the LMO extended to the whole Moon and anorthite began to crystallize from a residual melt after ~80% crystallization of the LMO[2, 3, 4]. The bulk composition of the Moon has been estimated by previous studies on the basis of refractory trace elements in near surface rocks [5-7], composition of the mare basalts [8-10], and geophysical data such as the momentum inertia, the bulk density and the seismic velocity [11, 12]. There are, however, large disparities among the estimates, because of the lack of direct chemical and structural information on the Moon's interior right after the solidification of the magma ocean.

We have investigated the conditions of the effective flotation of anorthite in the LMO to reproduce the observed critical features of the lunar crust [13-16] to constrain the FeO and refractory element contents of the initial LMO. In this study, we refined our model [17] by applying the crystal separation model by [18], which is more realistic than the model by [19], and by adopting an appropriate oxygen fugacity for the lunar interior. Here we report our new and more strongly constrained estimates of the contents of FeO and refractory elements in the initial LMO.

Model: We divide the cooling process of the LMO into three stages: (1) The initial LMO,which is assumed to be 1000 km, (2) differentiation of mafic minerals, where olivine and pyroxene crystallize and settle down to make mantle, and (3) the crust formation stage, where anorthite crystallizes and floats to form the lunar crust. The system consists of Ca-Mg-Al-Si-Fe-O, the MgO/SiO2 and CaO/Al2O3 ratios were fixed at those of the BSE and the solar abundances, respectively, and the abundances of FeO and refractory elements (CaO+Al2O3) were varied as parameters. Titanium was not considered, because it does not affect significantly the LMO evolution. Alkali elements (Na2O and K2O) were not included, because they should be negligibly small to explain the composition of lunar highland plagioclase. The oxygen fugacity of the cooling LMO was kept close to the iron-wüstite buffer to match the estimated oxygen fugacity for the source of mare basalts and igneous glasses [20, 21].

Differentiation processes of mafic minerals were modeled as follows. (1) Crystallization of mafic minerals takes place at the middle depth of the well-mixed turbulent LMO. The phases and compositions of solidified components are calculated with MELTS/ pMELTS [22, 23]. (2) At a certain crystal fraction in the LMO, the mafic minerals are instantaneously settled down to the bottom of the LMO. The critical crystal fraction for mafic mineral separation was varied from 0 to 0.4 as a parameter [24, 25]. After the separation of mafic minerals, phase relations and the depth of the residual LMO were recalculated, and crystallized mafic minerals were separated again at the same critical crystal fraction as the previous step. There procedures were repeated until anorthite appears as a liquidus phase.

We then evaluated the melt composition at the appearance of anorthite if it satisfies the following conditions required for the anorthosite crust formation; (a) the amount of anorthite, which crystallized from the residual melt, is abundant enough to form the crust with the thickness of ~45 km, (b) the pyroxene composition coexisting with anorthite is consistent with that of lunar highland rocks, and (c) anorthite can float in the turbulent LMO.

Results: The crystallization differentiation calculations showed that: (1) anorthite crystallizes except for cases with high enrichment of refractory elements (>2.3x BSE), where spinel crystallizes as a major Al-bearing phase, (2) the degree of crystallization of a LMO reaches ~80 vol% at the time of anorthite appearance after differentiation of mainly olivine and pyroxenes, and (3) the FeO content of the LMO at the appearance of anorthite increases with increasing initial FeO content, but shows little dependence on the initial abuncence of the refractory elements and the critical crystal fraction for sepration.

A mass balance calculation using the CIPW norm showed that the LMO highly enriched both in refractory elements and FeO does not produce the anorthosite crust with the thickness of 45 km from the initial LMO with the depth of ~1000 km.

The Mg# of clinopyroxene coexisting with anorthite at the time of anorthite crystallization was compared with that of pyroxenens in FAN (ferroan anorthosite). The most magnesian cpx in FAN has the Mg# of 75 [15, 16], which gives the upper limit of ~20 wt%

(~3x BSE) for the initial FeO content in the initial LMO.

The compositional range of the LMO required for anorthite flotation was obtained by comparing the critical anorthite size for effective separation for each LMO conposition with the size of anorthite in the Apollo-15 highland rock #15415 (1.8 cm) [26, 27]. It was found that the initial FeO content of the LMO should be larger than ~10 wt%, which is higher than the FeO content of the BSE.

A plausible range of the initial FeO and refractory element contents in the LMO is summarized in Fig. 1. The initial FeO content should be more abundant, and the refractory elements should be also more enriched than those of BSE. The upper limit of the FeO content is constrained more strictly in this study than in our previous study [17] by considering a plausible f_{O2}.

Discussion: The present results show that the BSE-like composition did not form the anorthosite crust observed, because its low FeO content prevented anorthite separateon from a turbulent magma ocean owing to smaller density contrast between the melt and anorthite and a higher melt viscosity.

The present result is roughly consistent with Taylor [7], Jones and Delano [9], Wanke and Dreibus [10], Buck and Toksoz [11], and recent Khan et al. [12]. It is, however, inconsistent with Longhi [8] and Warren [6] who argued for the compositional similarity of the Earth and Moon. The discrepancy might be mainly attributed to the lunar samples they studied, which were derived from particular regions or ages and which might not represent the global and initial features of the Moon.

The higher FeO content estimated for the LMO than the BSE implies that the impactor that hit the proto Earth was enriched in FeO than the BSE or that the oxygen fugacity of the LMO was higher than the BSE. If the terrestrial magma ocean and the proto-lunar disk underwent turbulent mixing to maintain equilibration of oxygen isotopes [28], it may be implausible to assume that the oxygen fugacity of the Earth and Moon were different, suggesting that the higher FeO model for the impactor is favorable.

Although the upper limit of the Al_2O_3 and CaO contents is poorly constrained in the present study, their contents are much higher than the previous estimates by Longhi [8] and Warren [6]. Information of REE pattern in FANs is expected to give a much tigher constraint on the abundance of refractory element in LMO.

We will report a result in our ongoing evaluations: (1) the chemical composition analysis of Yamato-86032 to put a stronger constraint on the Mg# of LMO and/or the grain size of anorthite floated from LMO and (2) an examination of the REE in lunar highland anorthosites to put a stricter constraint on the initial composition and the differentiation process of LMO.

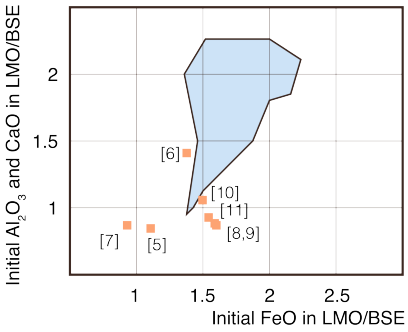

Fig. 1. Plausible ranges of FeO and refractory-element (Al2O3 and CaO) contents in the initial LMO (blue-colored region). The abundances of FeO and refractory elements are normalized to the BSE. The compositions estimated in previous studies (orange squares) are also shown for comparison.

References: [1] Wood J. A. et al., (1970) *Proc. Apollo 11 LSC, 1,* 965–988. [2] Elkins- Tanton L. T. et al., (2011) *EPSL, 304,* 326–336. [3] Snyder G. A., et al., (1992) *GCA, 56,* 3809-3823. [4] Elardo S. M., et al., (2011) *GCA, 75,* 3024-3045. [5] Taylor S. R. et al., (2006) *GCA, 70,* 5904-5918. [6] Warren P. H., (2005) *MAPS, 40,* 477-506. [7] Taylor S. R., (1982) *LPI. Press,* 481pp. [8] Longhi J. (2006) *GCA, 70,* 5919-5934. [9] Jones J. H. and Delano J. W., (1989) *GCA, 53,* 513-527. [10] Wänke H. and Dreibus G. (1986) *LPI. Press,* 649-672. [11] Buck W. R. and Toksöz M. N., (1980) *Proc. LPSC 11th,* 2043–2058. [12] Khan A. et al., (2006) *JGR, 111,* doi: 10.1029 /2005JE002608. [13] Ishihara Y. et al., (2009) *GRL, 36,* L19202. [14] Hikida H. and Wieczorek M. A., (2007) *Icarus, 192,* 150–166. [15] Demidova et al., (2007) *Petrology, 15 (4),* 386-407. [16] Warren P. H. and Kallemeyn G. W., (1991) *Proc. NIPR SAM, 4,* 91-117. [17] Sakai R. et al., (2011) *LPSC, XXXXII,* Abstract #1636. [18] Solomatov V. S. et al., (2003) *EPSL 120,* 387-393. [19] Tonks W. B. and Melosh H. J., (1990) In *Origin of the Earth,* 151-174. [20] Wellman T. R., (1970) *Nature, 225,* 716–717. [21] Sato et al., (1973) *Proc. Fourth LSC, 1,* 1061–1079. [22] Giortho M. S. and Sack R. O. (1995) *CM, 119,* 197-212. [23] Giortho M. S. et al., (2002) *G3 3(5),* doi: 10.1029/2001GC000217. [24] Sato H., (2005) *JMPS, 100,* 133-142. [25] Philpotts A. R. and Carroll M. (1996) *Geology, 24,* 1029-1032. [26] James O. B., (1972) *Science 175,* 432-436. [27] Wilshire H. G. et al., (1972) *GSA Bull. 83,* 1083-1092. [28] Pahlevan K. and Stevenson D. J. (2007) *EPSL, 262,* 438-449.

Post-LMO crustal growth. A comparison of Apollo 17 dunites. C.K. Shearer[1], P.V. Burger[1] and Y. Guan[2]. [1]Institute of Meteoritics, University of New Mexico, Albuquerque, NM 87131 (cshearer@unm.edu), [2]Division of Geological and Planetary Science, California Institute of Technology, Pasadena CA 91125.

Introduction: The plutonic rocks of the magnesian suite (Mg-suite) represent the period of lunar basaltic magmatism and crustal growth (~4.46 to 4.1 Ga) that presumably followed the initial differentiation of the Moon by magma ocean (LMO) formation and crystallization and preceded the eruption on the lunar surface and emplacement into the lunar crust of mare basaltic magmas. The volume and distribution of the Mg-suite and its petrogenetic relationship to latter stages of lunar magmatism (mare basalts) remains obscure. These plutonic rocks exhibit a range of compositions and include dunites and other ultramafic lithologies, troctolites, spinel troctolites, norites, and gabbronorites. Shearer and Papike [1] illustrated the usefulness of using mineral chemistries for unraveling the petrogenetic relationships among Mg-suite lithologies and between Mg-suite and mare magmatism. Here, we compare two types of dunites collected from the Apollo 17 landing site. One suite of dunites (Mg-suite) occurred as clasts in a large boulder, while other dunites occur as xenoliths in high-Ti mare basalts. Do these dunite lithologies represent one or two distinct periods of magmatism (Mg-suite versus mare) or even a lunar mantle lithology? What do the differences between these two dunites reveal about their respective mantle sources?

Analytical Approach: Thin sections of 72415, 72416, 72417, and 72418 were previously examined and analyzed by Shearer and Papike [1]. Thin sections of 74275(96,97) were initially examined and documented using backscattered electron imaging (BSE) on UNM's JEOL JXA-8200 Superprobe electron microprobe (EPMA). Once suitable areas were located, wavelength dispersive (WDS) X-ray maps were collected for Cr, Ca, Mn, P and Ti, while energy dispersive (EDS) maps were collected for Mg and Fe. Maps were collected using a 15 kV accelerating voltage, a 500 nA beam current and a dwell time of 800 ms/pixel. Additionally, quantitative analyses were conducted as traverses, from core to rim, using both UNM's EPMA and secondary ion mass spectrometry (SIMS), via the Camaca NanoSIMS-50L, at Caltech. Spot size was ~1 micron using both techniques. The EPMA run conditions included an accelerating voltage of 15 kV and a beam current of 20 nA. Data was collected for Si, Ca, Mg, Fe, Mn, Ti, Cr, P, Ni and V, and standardization was accomplished using Taylor and Co. mineral standards. Quantitative NanoSIMS analyses were collected on ^{27}Al, ^{28}Si, ^{47}Ti, ^{51}V, ^{59}Co, ^{62}Ni and ^{89}Y, and normalized to the known Si concentration. Unknowns were standardized using in-house UNM pyroxene standards. Future work will confirm the applicability of the standardization and accuracy of results by comparison to quantitative data using UNM's Camaca 4f SIMS instrument.

Apollo 17 Dunites: Samples 72415, 72416, 72417, and 72418 are cataclastic dunites consisting predominantly of olivine (90-95%, Fo90-86) and minor abundances of plagioclase, pyroxene, Cr-spinel, and metal. Ryder [2,3] suggested that this lithology represents the emplacement of Mg-suite magmas into the shallow lunar crust. The dunite has a Rb-Sr age of 4.55±0.1 Ga [4], though it has a complex shock and thermal history and the Pb in the sample is disturbed [5]. The dunite xenoliths in 74275 were first described in detail by Delano and Lindsley [6]. The xenoliths are mm in diameter, consist of multiple individual olivine grains, and have no accessory phases. BSE images and X-ray maps of divalent cations (i.e., Mg) (Figure 1) indicate substantial reequilibration of the xenoliths with the adjacent high-Ti basaltic melt. However, X-ray maps of Ti, P, and Al (Figure 1) illustrate that these elements preserve the initial magmatic zoning of the xenoliths. The 74275 high-Ti basalt also contains olivine xenocrysts and smaller olivine phenocrysts. Based on their composition and zoning, all three types of olivine in 74275 appear to have crystallized within distinctly different thermal-kinetic regimes. Murthy and Coscio [7] dated 74275 at 3.85 ± 0.08 Ga using Rb-Sr.

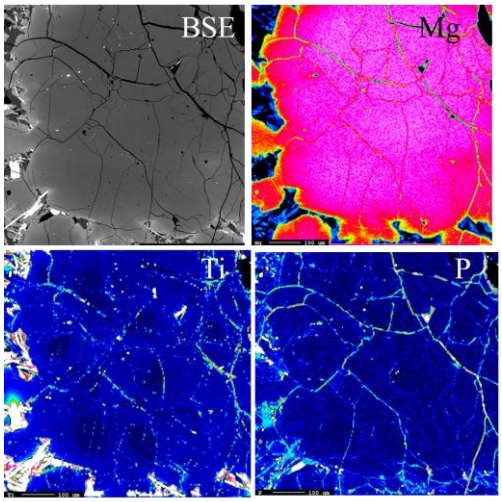

Figure 1. BSE, Mg, Ti, and P x-ray maps of dunite xenolith in 74275

Nyquist et al. [8] obtained an age of 3.81 ± 0.32 Ga. The crystallization age of the dunite xenoliths is unknown.

Comparisons between dunites: Compared to the dunite clast, the dunite xenolith has remnants of igneous zoning preserved (Figure 1). However, Ryder [2,3] observed some variability in Ca that he attributed to igneous processes. The Mg# of the olivine in the xenolith is too high to be in equilibrium with the 74275 melt, and shows evidence of reaction with the melt. Ryder [2] and Shearer and Papike [1] observed that the olivine from the Mg-suite is lower in CaO and Cr_2O_3 than the olivine in mare basalts. Figure 2 illustrates that the CaO in the dunite xenolith overlaps with other olivine in 74275 and is substantially higher than in the dunite clasts. Cr_2O_3 in the xenolith (0.20-0.26 ppm) is lower than in olivine megacrysts (0.25-0.35 wt.%), but is still substantially higher than the olivine in the dunite clasts (0.04-0.06 wt.%). The cores of the individual olivines making up the dunite xenolith have ~0.02 wt.% TiO_2, whereas the rims have ~0.10 wt.% TiO_2. Xenocrysts have ~0.10-0.20 wt.% TiO_2. There appears to be little difference in incompatible trace elements between the two types of dunites. Ni and Co in the olivine in the xenoliths are similar to Mg-suite olivine, and dramatically different from low- Ti mare basalts (Figure 3). Ni and Co concentrations in olivine from the dunite xenolith, however, overlap with measured values for olivine in the high-Ti basalts [1].

Conclusions: Although the dunite xenoliths in the high-Ti basalt have reacted with the surrounding melt, most of the data suggests that this dunite was derived from accumulation of olivine during the crystallization of a mare magma. The lack of accessory minerals is

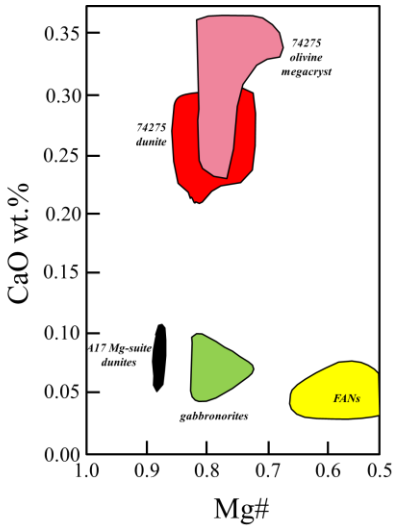

Figure 2. Mg# versus CaO for olivines. Diagram modified after Ryder (1984, 1992).

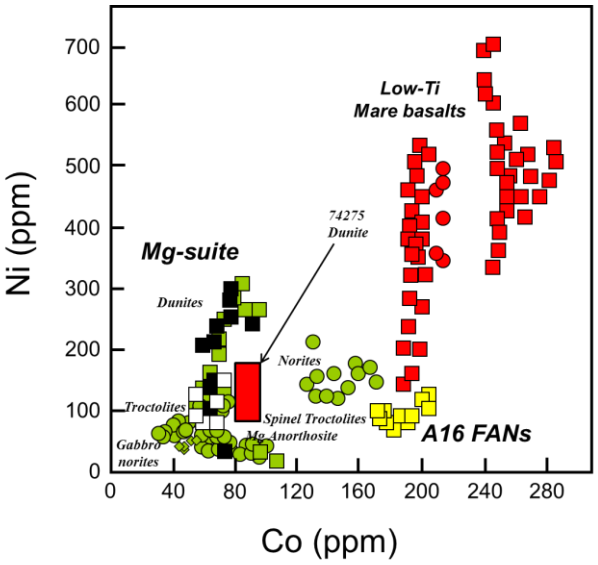

Figure 3. Ni vs. Co in lunar olivines

consistent with the mare basalt fractional crystallization paths determined by Longhi [9] The three populations of olivine in 74275 crystallized from different basalts; going from phenocrysts to xenocrysts to dunite xenolith, one observes an increase in Mg# along with a decrease in TiO_2. This suggests that the different olivine populations crystallized in distinct crustal environments. The dunite xenoliths are not petrologically related to the clasts of dunites that have been associated with Mg-suite magmatism. Comparisons of these two dunites highlight differences between these two episodes of lunar magmatism. Although Ryder [2,3] attributed differences in Ca in the olivine to the depth of emplacement in the lunar crust, it is more likely that these differences reflect diverse melt chemistry. Differences in both Ti and Cr in the dunites are a produce of location in the LMO cumulate pile (early versus late). Finally, compatible elements such as Ni and Co are similar in these two dunite lithologies. This may simply be a coincidence tied to the behavior and nature of Ni and Co in early- versus late- LMO cumulates [1,10] or it may be due to the involvement of late-stage cumulates in the petrogenesis of the parental magmas to both types of dunites.

References: [1] Shearer and Papike (2005) *Geochimica et Cosmochimica Acta*, 69, 3445-3461. [2] Ryder (1984) Lunar Planet. Sci. XV, 709-710. Lunar Planetary Institute, Houston [3] Ryder (1992) 22nd Lunar Planet. Sci. Conf. 373-380. Lunar Planetary Institute, Houston. [4] Papanastassiou and Wasserburg (1975) Proc. 6th Lunar Sci. Conf. 1467-1489. [5] Tera et al. (1974) Earth Planet. Sci. Lett. 22, 1-21. [6] Delano and Lindsley (1982)Lunar Planet. Sci. XIII, 160-161. Lunar Planetary Institute, Houston [7] Murthy and Coscio (1977) Lunar Sci. VIII, 706-708. Lunar Planetary Institute, Houston. [8] Nyquist et al. (1976) Proc. 7th Lunar Sci. Conf. 1507-1528. [9] Longhi et al. (2010) *Geochimica et Cosmochimica Acta*, 56, 2235-2251. [10] Longhi et al. (2010) *Geochimica et Cosmochimica Acta*, 74, 784-798.

COMPOSITIONAL DIVERSITY INSIDE LOWELL CRATER, ORIENTALE BASIN: EVIDENCES FOR EXTENSIVE SPINEL RICH DEPOSITS. N. Srivastava[1] and R. P. Gupta[2], [1]PLANEX, Physical Research Laboratory, Ahmedabad, India – 380009, email-sneeraj@prl.res.in, [2]Earth Sciences, IIT Roorkee, Roorkee, Uttarakhand, India – 247667, rpgupta.iitr@gmail.com.

Introduction: Spinel dominant rock exposures devoid of mafic minerals such as olivine and pyroxenes, have been recently found in certain areas both on the far-side and on the near-side of the Moon using data from NASA's Moon Mineral Mapper (M^3) onboard Chandrayaan-1, India's first mission to the Moon [1, 2]. These include, far-side exposures along the ring of Moscoviense basin, where they were first reported [3] and several near-side exposures such as the extensive occurrences in Sinu Aestuum, in the Theophilus crater, Copernicus crater floor and few exposures in the Tycho crater [4-9]. The mode of formation of this newly discovered rock type on Moon is not clearly understood in the current perspective about the evolution of Moon. Except for Tycho crater, all the above mentioned exposures are found in similar geologic settings i.e., along the rings of major basins. Hence it is envisaged that most of these rock exposures constitute previously deep-seated rocks which have been exhumed on to the surface due to impacts. Finding similar exposures at other locations on the Moon is essential to test this hypothesis and to constrain the extent of these rocks in the lunar crust and to understand the petrographic conditions for its formation [3,5] Here, we report regional spinel rich exposures in various geologic settings inside and around the Lowell crater using M^3 data.

Lowell crater (12.9°S 103.1°W, diameter: ~ 66 km) is located in the NW quadrant of the Orientale basin just beyond the western limb of the Moon (Figure 1). It is younger Copernican in age [10], and occurs in the Montes Rook formation between the Outer Rook Ring (ORR) and the Cordillera ring of Orientale basin. It has prominent central peak, sharp rim, terraced wall and numerous surface mounds on its floor. A partially collapsed small (~ 10 km diameter) rayed impact crater lies along the fringe of the eastern rim. A low albedo fresh resurfaced unit covering ~ 60 sq. km, extends ~ 17 km inwards from this crater [11].

Data used: Global mode Level 2 M^3 hyper-spectral data M3G20090213T115953_V01 _RFL.IMG provided through public access web portal http://ode.rsl.wustl.edu/moon/indexproductsearch.aspx have been used in the study. The data comprises of 83 near-contiguous bands spanning 540 – 2980 nm. The spatial resolution is 140 meters and the spectral resolution varies between 20 – 40 nm . The bands are photometrically and thermally corrected.

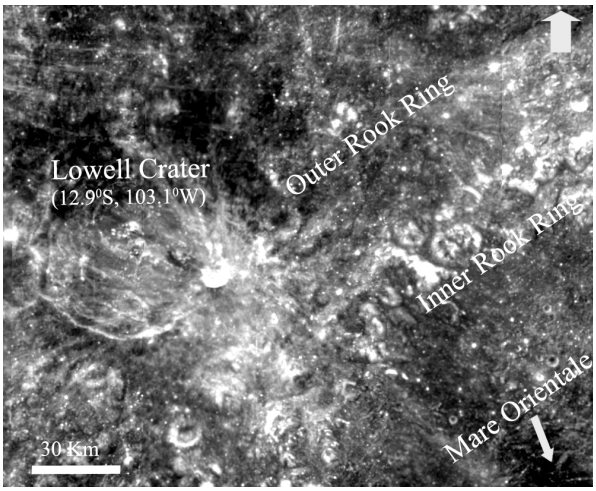

Figure 1: Clementine albedo image showing the regional geologic setting of Lowell crater.

Methodology: The composition of the exposures in the region have been identified on the basis of characteristic spectral reflectance curves of the dominant mineral present in them. Spinel rich lithology with absence/minor mafic silicates such as olivines and pyroxenes are identified on the basis of a prominent broad absorption feature centred at ~2 μ but with no/weak absorption feature at ~1 μ [3]. In contrast, the pyroxenes show broad absorption features centred at ~1 μ and 2 μ, olivine shows a single composite absorption centred ~ at 1.1 μ, crystalline plagioclase exhibits a minor broad absorption band centered at ~ 1.25 μ and shocked plagioclase shows a featureless, monotonically increasing spectra. High Ca Pyroxenes can be distinguished from low Ca-pyroxenes on the basis of absorption at slightly longer wavelengths i.e. between 0.95 – 1 μ for one micron band and ~ 2.2 μ for the two micron band. In case of low Ca pyroxene the one micron band occurs between 0.9 - 0.95 and the two micron band occur at ~ 2 micron.

Dominant mineralogy in the various geologic settings: Figure 2 a-c shows M^3 750 nm image of the study area depicting the sites (1-7) for which spectral reflectance curves have been derived and their corresponding spectra (S1 – S7). An account of the compositional diversity in various distinct geologc units is as follows:

Central Peak of Lowell crater. Discrete exposures of spinel dominant lithology (e.g. S1) are present on the central peak of Lowell crater. The other accompa-

nying rock-type in the adjacent areas on the peak is pyroxene, especially high Ca-pyroxene (e.g. S2) consistent with [12].

Prominent resurfacing on the eastern side. The unit with peculiar features of a recently built volcanic terrian i.e. fresh viscous flows, pits, cone with melt pond at the summit etc. shows pervasive high-Ca pyroxene signature (e.g. S3) indicative of either a recently built volcanic unit [11] or impact melts and debris flow from the small crater on the Lowell crater wall. Here, only few areas show spinel dominant signature alongwith a weak 1 micron feature indicating presence of minor quantities of high-Ca Pyroxene also.

Mounds on the Lowell crater floor. Signatures of spinel dominant lithology have also been found on numerous surface mounds on the Lowell crater floor. Though, in most of these exposures the accompanying lithology is pyroxene dominant, one of the surface mound near the central peak shows co-existing signature of crystalline plagioclase and spinel in some areas (e.g. S4), transitioning into spinel rich rocks.

Lowell crater wall and Ejecta . The Lowell crater wall is dominantly composed of noritic rocks (e.g. S5) in association with spinel rich exposures in certain areas (e.g. S6). The ejecta is a mixture of spinel and pyroxene.

Peaks and plateaus North of Lowell crater. These portions of Montes Rook formation, representing the sample target rocks for Lowell impact event show persistent signature of spinel dominant lithology (e.g. S7).

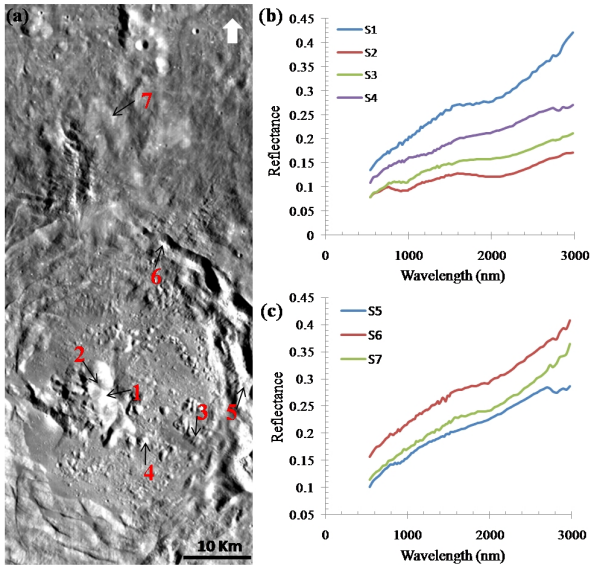

Figure 2: a) M3 750 nm image of a portion of Lowell crater showing locations (marked as 1-7) for which spectral reflectance curves have been derived; b) Average (4 pixel) reflectance spectra for sites 1-4; c) Average (4 pixel) reflectance spectra for sites 5-7 with offset induced for clarity.

Discussions: The pervasive signatures of spinel rich lithology in almost all the geologic settings studied here indicate that laterally and vertically extensive spinel dominant rocks are present in this area. The Montes Rook formation are understood to be composed of ejecta from deeper portion of lunar crust formed during the Orientale impact event. Therefore, possibly the spinel rich rocks would have been derived from deeper portions of the crust similar to most of the other earlier findings. Since the central peaks would have sampled the rocks from maximum depth, the present day lower limit to this stretch could be as deep as 6.6 km from the surface considering depth/ diameter = 0.1 for Lowell crater.

Conclusions: Extensive exposures of spinel dominant lithology without noticeable mafic silicates such as olivines and pyroxenes have been found in Lowell crater and in other portions of Montes Rook formation. The other accompanying mafic rock in the adjacent areas is mainly pyroxene. These findings indicate presence of possibly spinel rich layer at depth in the primordial crust, consistent with [13]. Still, the option of spinel-anorthosite production due to basaltic melt - anorthositic wall rock reaction at depth >10 km as proposed by [14] cannot be ruled out here due to co-existing crystalline plagioclase and spinel signature observed in one of the surface mounds on the crater floor. Further, possibility of intrusives in the lower crust prior to the Orientale impact event also make the scenario feasible. Finding similar exposures at other locations in the Orientale basin would be crucial for further understanding in this regard.

References: [1] Goswami J. N. and Annadurai M. (2009) *Curr. Sci., 96, 4,* 486-491. [2] Pieters C.M. et al. (2009) *Curr. Sci., 96, 4,* 500-505. [3] Pieters C.M. et al. (2011) *JGR, 116,* E00G08, doi: 10.1029 /2010 JE003727. [4] Sunshine J.M. et al. (2010), *LPS XXXXI,* Abstract # 1508 [5] Dhingra D. et al. (2011) *LPS XXXXII,* Abstract # 2388. [6] Dhingra D. et al. (2011) *GRL, 38,* L11201, doi: 10. 1029/2011G L047314. [7] Lal D. et al. (2011) *LPS XXXXII,* Abstract # 1339. [8] Dhingra D. and Pieters C.M. (2011) *LEAG,* Abstract # 2024 [9] Kaur P. et al. (2012) *LPS XXXXIII,* Abstract # 1434. [10] McEwen, A.S., et al. (1993), *JGR, 116, E9,* 17,207-17,231. [11] Srivastava N. et al. (2011), *Conf. on Planetary Sci. and Exp.*, PRL, Ahmedabad, India, Abstract, 97 – 98. [12] Tompkins S. and Pieters C.M. (1999*MAPS*, 34 (1), 25-41. [13] Prissel T.C. et al. (2012) *LPS XXXXIII,* Abstract # 2743. [14] Pieters C.M. et al. (2011) *LPS XXXXII,* Abstract # 2173.

MINI-MAGMA OCEAN PETROLOGY: DIFFERENTIATION OF MASSIVE IMPACT MELT SHEETS ON THE MOON. W. M. Vaughan[1], J. W. Head[1], P. C. Hess[1], L. Wilson[2], G. A. Neumann[3], D. E. Smith[4], and M. T. Zuber[4]. [1]Department of Geological Sciences, Brown University, Providence, RI 02912, USA, Will_Vaughan@brown.edu. [2]Lancaster Environment Centre, Lancaster University, Lancaster, LA1 4YQ, UK. [3]Solar System Exploration Division, NASA Goddard Space Flight Center, Greenbelt, MD 20771. [4]Department of Earth, Atmospheric, and Planetary Sciences, MIT, Cambridge, MA 02139.

Introduction: Impact melt emplacement and evolution in lunar multi-ring basins is poorly understood since impact melt deposits in basins are generally buried by mare basalt fill and obscured by subsequent impact cratering. The relatively young Orientale basin [1-3], which is only partially flooded with mare basalt [4-5], opens a rare window into basin-scale impact melts.

We describe the geology of impact melt-related facies in Orientale and suggest that the central depression of Orientale may represent a solidified impact melt lake that vertically subsided shortly after basin formation due to solidification and cooling [6]. We use Lunar Orbiter Laser Altimeter (LOLA) data to measure the depth (~1.75 km) and diameter (~350 km) of this central depression. If all the observed subsidence of the central depression is due to solidification and cooling, the melt lake should be ~12.5-16 km deep, far more voluminous (~10^6 km^3) than the largest known differentiated igneous intrusions on Earth [7-8]. We investigate the possibility that the Orientale melt lake has differentiated and model 1) the bulk composition of the melt lake, 2) the operation of melt mixing in the melt lake, and 3) the chemical evolution of the resulting liquids on the An-Fo-Qz ternary in order to predict the lithologies that might be present in the solidified Orientale melt lake. Finally, we consider the possible significance of these lithologies.

Geology of melt-related facies in Orientale: The topography of the Orientale basin is shown in Figure 1. The Inner Rook Ring, at a radius of 480 km from the basin's center, and the Outer Rook Ring, at a radius of 620 km, are interpreted respectively as the peak ring [9] and an approximation of the rim crest of the transient cavity prior to cavity collapse [1, 10]. Models of impact melt production suggest that most melt is formed in a hemispherical or spherical melt cavity interior to the peak ring [11]. Assuming that only a small proportion of melt is completely ejected by the collapse of the melt cavity during crater modification [12], most impact melt should remain interior to the Outer Rook Ring [12-13].

In fact, the Maunder Formation, which lies inside the Outer Rook Ring, comprises two facies which have been interpreted as impact-melt related [1-2, 14-15]. A smooth inner plains facies, exposed through thin mare fill [5, 16] and interpreted as a pure impact melt sheet [1-3], occupies the central depression of the Orientale basin. Near the edges of the central depression, wrinkles, fractures, and polygonal cracks are apparent in the smooth facies and overlying mare. About 175 km from the center of the Orientale basin, the topography abruptly rises ~1.75 km

Depth of the Orientale melt lake: What caused the substantial (~1.75 km) vertical subsidence of the Orientale basin's central depression? One possibility is that the vertical subsidence of the smooth facies is related to thermal stresses resulting from impact-generated heat and uplift of crustal isotherms [17]. This model predicts gentle radial vertical subsidence. However, new, high-resolution LOLA altimetry [18] shows that the vertical subsidence of the central depression is abrupt: along the west edge of the depression, the topography drops ~2 km over a radial distance of ~20 km. The model of [17] cannot fully explain this abrupt vertical subsidence. The fractures of the smooth inner plains facies bear resemblance to the deformed surfaces of terrestrial lava lakes [19]; if the smooth facies is an impact melt sheet, these fractures could result from lateral shrinkage upon solidification and cooling. The vertical subsidence of the central depression could similarly result from solidification and cooling of the impact melt sheet [6]. This constrains the depth of the impact melt sheet: a body of hot magma emplaced on the lunar surface should undergo ~11-14% vertical subsidence [6] upon solidification and cooling. ~1.75 km average vertical subsidence is observed (Fig. 1), implying the melt sheet is up to ~12.5-16 km deep.

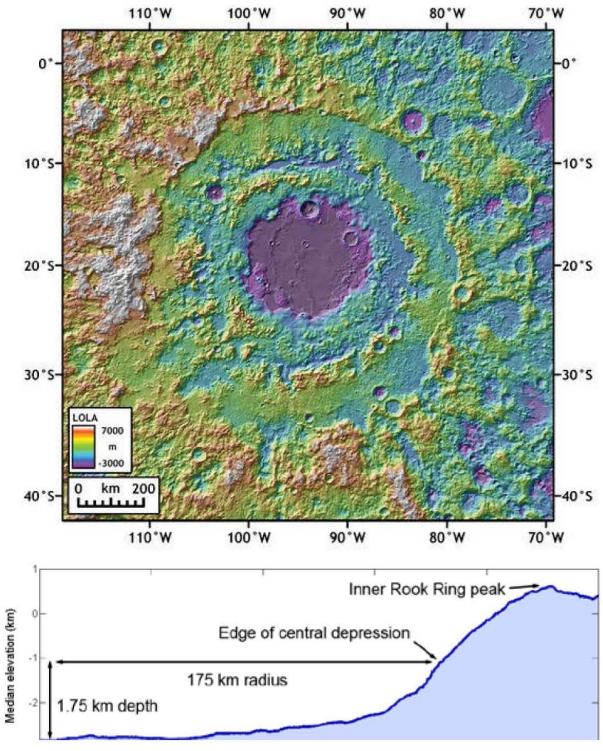

Differentiation of the Orientale melt lake: The Orientale melt sheet (which, volumetrically, may be better described as a lake) is ~350 km in diameter and may be up to ~12.5-16 km deep, implying a volume of ~10^6 km^3, far greater than the largest differentiated igneous intrusions known on Earth [7-8]. Could the Orientale melt sheet have differentiated? Previous work [20] has argued that impact melt sheets do not differentiate since 1) few or no differentiated impact melt sheets are known on Earth, 2) impact "melt" sheets are better described as magmas carrying cold clasts, assimilation of which rapidly depresses liquid temperature. However, mounting evidence suggests that several large terrestrial impact melt sheets have differentiated (namely, the Sudbury Igneous Complex [21-22], Manicouagan [23], and Norokweng [24]). Also, the volume of shock melt produced by an Orientale-size impact is so enormous [11] that huge clast-free volumes seem likely to exist. We therefore develop a simple model to predict the lithologies that might crystallize from the Orientale melt lake and other solidified multi-ring basin impact lakes based on 1) the bulk composition of the melt lake, 2) the operation of melt mixing in the melt lake, and 3) the chemical evolution of the resulting liquids on the An-Fo-Qz ternary.

Bulk composition of the melt lake. We model the lunar crust as a planar layer of anorthosite ~26.9 km thick overlying an anorthositic norite layer extending to a depth of 52.0 km based on the dual-layered crustal thickness model presented in [25]. The anorthosite layer has a density of 2.82 g/cm^3 and a composition of 86 wt. % anorthite, 10.5 wt. % enstatite, and 3.5 wt. % forsterite; the anorthositic norite layer has a density of 3.04 g/cm^3 and a composition of 60 wt. % anorthite, 30 wt. % enstatite, and 10 wt. % forsterite. These compositions are highly approximate; the modal anorthosite is based on [25] and the modal mafic minerals are calculated based on a 3:1 enstatite:forsterite proportion by weight.

The melt cavity has a complex geometry [11] which we approximate as a hemisphere with its largest cross section coincident with the top of the anorthosite crustal layer. M^3 [16] and Kaguya [26] spectra of the Orientale region detect no evidence for the presence of subcrustal mafic mantle material in Orientale basin deposits, so we assume that the Orientale impact did not sample the upper mantle. Therefore, we choose the radius of our modeled melt cavity to be 50 km, slightly less than the thickness of the far side crust [25]. The mass of each layer melted was calculated as the product of the volume of the melt cavity hemisphere intersecting the anorthosite and anorthositic norite layers and the density of these layers.

Melt mixing. Impact melt is vigorously mixed and may therefore be homogenous; i.e., the composition of any small volume of melt will be identical to the bulk composition of the melt lake. However, even a well-mixed melt lake may not be homogenous [22]: impact-melted liquids with very different viscosities may be effectively immiscible on short timescales and stratify according to density contrasts. In the Orientale melt lake, viscous anorthosite liquid and fluid mafic liquid could be effectively immiscible and separate by density to produce anorthosite liquid overlying dense mafic, pyroxenitic liquid.

Igneous differentiation. We treat igneous differentiation of the homogenous melt lake on the well-known An-Fo-Qz ternary phase diagram at 1 atm (since lunar crustal pressures are low). Impact melt has an initial temperature well above the liquidus at 1400 °C. Upon crystallization, the processes of crystal settling and convection operate to fractionate and mix crystals and liquid. We consider homogenous and density-stratified liquids operated upon by fractional crystallization and equilibrium crystallization to bound the resulting lithologies (Fig. 2).

Implications. Three puzzles in lunar petrology are young anorthosites [27], the provenance of Mg-suite rocks [28], and the provenance of Mg-spinel lithologies [29]. Young anorthosites could have crystallized from melt sheets. Mg-suite norites and troctolites could form in melt sheets, although their distinctive geochemical signature [28] would be hard to explain. Mg-spinel lithologies could form from mixing of anorthosite and olivine-rich mantle liquids. We continue to investigate remotely-sensed data and the lunar sample suite in order to identify possible impact melt differentiates.

Figure 2. Model differentiated melt lake lithologies.

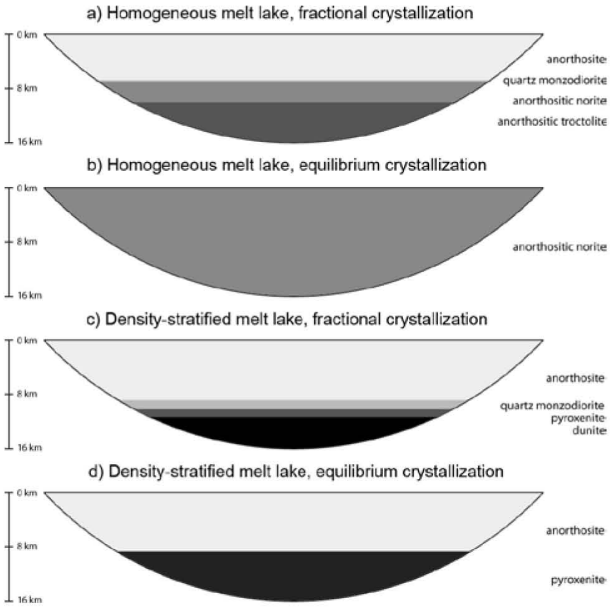

References: [1] Head J. W. (1974) *The Moon, 11,* 327-356. [2] Howard K. A. et al. (1974) *Rev. of Geophys., 12,* 309-327. [3] McCauley J. F. (1977) *PEPI*, *15*, 220-250. [4] Greeley R. et al. (1993) *JGR, 98,* 10873-10882. [5] Whitten S. J. et al. (2010) *LPS,* 41. [6] Head J. W. and Wilson L. (2011) *LPS, 42*. [7] Nielsen T. F. D. (2004) *J. Pet., 45,* 507-530. [8] Bonini W. E. (1982) *Mag. Proc. of Early Plan. Crusts*, 53-55. [9] Baker D. M. H. et al. (2011) *Icarus, 214,* 377-393. [10] Head J. W. (2010) *GRL, 37.* [11] Cintala M. J. and Grieve R. A. F. (1998) *MAPS, 33*, 889-912. [12] Hawke B. R. and Head J. W. (1976) *Imp. and Expl. Cratering,* 815-841. [13] Osinski G. R. et al. (2011) *EPSL*, *310*, 167-181. [14] Spudis P. D. (1993) *The geology of multi-ring impact basins,* Cambridge. [15] Head J. W. and Wilson L. (1992) *GCA, 55,* 2155-2175. [16] Head J. W. et al. (2010) *LPS, 41.* [17] Bratt S. R. et al. (1985) *JGR, 90*, 12415-12433. [18] Smith D. E. et al. (2010) *GRL, 37*. [19] Barberi F. and Varet J. (1970) *Bull. Volc., 34,* 848-917. [20] Warren P. H. et al. (1996) *GSA Special Papers, 307*, 105-124. [21] Therriault A. M et al. (2002) *Econ. Geo.*, *97,* 1521-1540. [22] Zieg M. J. and Marsh B. D. (2005) *GSA Bull., 117,* 1427-1450. [23] Spray J. G. and Thompson L. M. (2008) *MAPS, 43,* 2049-2057. [24] Hart R. J et al. (2002) *EPSL, 198,* 49-62. [25] Wieczorek M. A. et al. (2006) *RIMG, 60,* 221-364. [26] Yamamoto S. et al. (2010) *Nature Geo., 3,* 533-536. [27] Borg L. E. et al. (2011) *Nature Geo.*, *477,* 70-72. [28] Hess P. C. (1994) *JGR*, *99,* 19083-19093. [29] Pieters C. M. et al. (2011) *JGR, 116.*

LET'S GET REAL: NOT EVERY LUNAR ROCK SAMPLE IS BIG ENOUGH TO BE REPRESENTATIVE FOR EVERY PURPOSE. Paul H. Warren, Institute of Geophysics, Department of Earth and Space Science, University of California, Los Angeles, CA 90095-1567, USA; pwarren@ucla.edu.

Lunar samples have never been widely available. The Apollo program provided 382 kg, of which ~285 kg is in the form of (>1 cm) rocks. Although lunar meteorites have since added about 56 kg, well over 90% of this mass is held by private collectors. The severely limited supply of accessible "new" lunar highland material naturally leads to a temptation to overinterpret small clasts as if they are the sampling equals, or near-equals, of the larger Apollo highland samples.

This general phenomenon is nothing new. Way back in 1970, Wood et al. [1] won acclaim (the most widely-cited lunar petology paper of all time?) with a model linked, in part, to overinterpretion of tiny highland rocklets. In justification of their seminal proposal of the lunar magma ocean (LMO) hypothesis, Wood et al. claimed to discern "true cumulate textures" in tiny Apollo-11 anorthosite fragments, none bigger than 5 mm and mostly <2 mm. Their prime example (their Plate 5) has a texture that today would be interpreted as very obviously poikilitic impact melt breccia. Whether or not magma "ocean" is apt terminology, Wood et al. [1] were probably correct in their then-radical suggestion that a very large portion of the Moon underwent primordial melting, and ensuing cumulus plag flotation formed a highly annorthositic crust. But we should not conclude from this one fortunate case that loose interpretation of tiny samples is a good idea.

Distinguishing between impact-mixtures (including impact-melt products) and compositionally pristine, endogenously igneous rocks will always be a key problem in lunar highland petrology. If this distinction is inadequately respected, mixture-samples will dampen apparent compositional diversity, and intermediate compositions may appear common when they are actually, among pristine rocks, rare or virtually nonexistent. Completely erroneous conclusions may ensue.

The two main criteria useful for distinguishing pristine rocks [2] are texture and siderophile element contents. Siderophile analyses are seldom feasible for small samples (although if metal is present, simple EPMA might be revealing, depending upon whether the metal's Co/Ni ratio is far from chondritic [3]). The main textural criterion is grain size. The suggestion of 3 mm as a threshold grain size [2] was never meant to be absolute. Leeway toward finer grain size is justified if a rock has siderophile evidence of pristinity, or if its composition, especially its major-element composition (e.g., felsite [4]), is so unusual as to be highly improbable as an impact-mixture. Otherwise, however, among samples in the range of norite-troctolite-anorthosite, any sample lacking grains at least nearly 3 mm across should be regarded as suspect; and the further below 3 mm, the higher the suspicion.

This 3 mm criterion has been implicitly criticized as too restrictive by countless subsequent authors, most recently [5]. When we originally proposed 3 mm [2], we anticipated the existence of rocks such as 14286 [6,7]. The texture of 14286 should give pause to anyone who thinks lunar impact melts (small enough to be deeply excavated by subsequent impact-gardening) never produced equant, intrusive-seeming textures with grains of order 1 mm. The rock consists mainly of FeNi metal, with a high W content implying that it equilibrated in a volume of Apollo-14-regional (KREEPy) impact melt [7]; probably near the bottom.

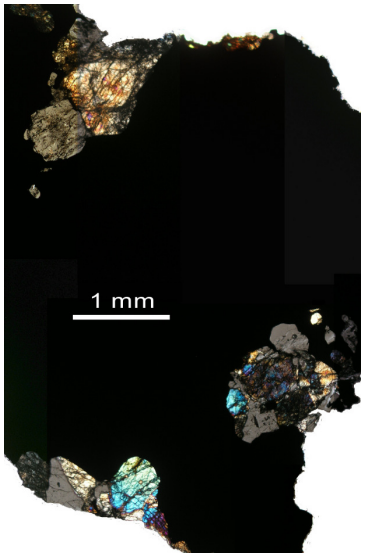

Fig. 1. Thin section view (transmitted light, partly crossed nicols) of impact-melt rock 14286,11. The rock's opaque core is mainly FeNi-metal, with minor schreibersite and FeS. *Equant*, relatively coarse silicates of very obvious *impact melt* origin occupy several lobes within the rock's periphery.

This is the only known instance of a lunar rock with fortuitous attachment of impact-melt silicates onto a mass of metal large enough (4 g) that it presumably sank deep within the impact melt. There is no reason to suppose that the parent impact was outstandingly large. The largest basins probably produced melt pools in which metals sank to such depths (many km) that they were never, or practically never, excavated [cf. 8]. A larger impact melt volume would presumably have cooled more slowly and engendered yet coarser and more equant silicates. Despite the very small number of grains present, truncation of some of them by the edge of the section, and confinement of all within (probably pre-existing) lobes on the fringe of the metal, the largest pyroxene (tan-red in upper left in Fig. 1) is 1.2 mm across (or 1.0 mm without its fractured perimeter).

Plag/maskelynite grains (grey) extend up to 1.0 mm. The lesson seems clear: Absent siderophile evidence (or an odd composition such as felsite), grain size ought to be very obviously coarser than that of 14286 before any lunar highland sample may be regarded with even slight confidence as pristine.

Recently, Gross et al. [5] claimed an ability to "sink the magma ocean" on the basis of a suite of lunar-meteorite anorthositic clasts, of which the largest is only 3.5 mm (*sic*) in maximum dimension; most of their clasts are much smaller than that. At such a sampling scale, it is patently impossible to establish that the grain size even approaches 3 mm. Gross et al. made no mention of what grounds they might have for regarding these clasts as pristine. Nevertheless, Gross et al. [5] claimed that when mineral-composition data from these clasts are compared with the ranges previously established for the two main types of pristine rocks [e.g., 2], ferroan anorthosites and Mg-suite cumulates, the new samples show intermediate compositions and thus eliminate a compositional hiatus between those two rock types; with profound implications for the magma ocean hypthothesis [e.g., 9].

It would make about as much sense to regard anorthositic impact spheroids [10] as pristine pyroclastic materials extending the range of the superficially similar mare-pyroclastic spheroids. The compositions (and mineral compositions) of impactites form by a fundamentally different process, which typically begins with mixing-homogenization of the various materials caught up in the zone of proximity to the impact. The bigger and more mass-consequential the impact, the hotter and more thorough will be the initial mixing, and the more diverse will be the provenance of the mixed materials. There is even a very real potential for the largest impact melts to undergo differentiation [11]. *That random clasts from the impact-battered lunar highlands are dominated by impactite-mixtures with intermediate compositions should surprise no one.* Many variations of the same problem, conflating semi-random highland clasts with pristine rocks, might be cited, but usually [e.g., 12] the interpretation is merely vague and does not claim to turn pristine-rock petrology on its head.

A related issue concerns claims for novel rock types, most notably magnesian anorthosite, on the basis of tiny thin-section clasts. It is impossible to prove that such rocks do not exist on the Moon, but the samples adduced to date have been unimpressive. Takeda et al. [13] proposed the magnesian anorthosite rock type on the basis of a 3.0×1.3 mm clast, with largest plag size of 1.6 mm and mafic silicates 0.7×0.4 mm. Even accepting that this clast is pristine (for which there is practically zero evidence; no metal was found for testing Co/Ni, and the olivine is *not* impressively uniform:

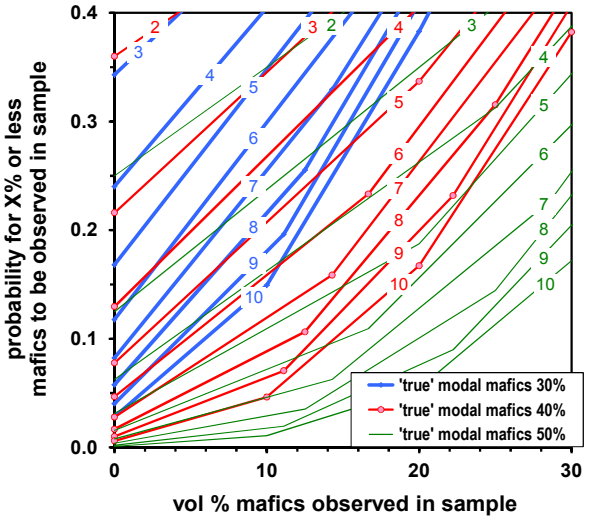

Fig. 2. Application of binomial statistics to the issue of reliability of a mode for limited-size sampling of a coarse-grained rock (or clast). Numbers on curves refer to total number of grains sampled – referring to the *original,* coarse igneous grains, assumed to be ~ uniform in size.

$Fo_{75\text{-}79}$), there is little reason to be confident that the "anorthosite" mode is significant. In the lunar highland context, "anorthosite" implies >90% plag [14]; or at any rate, a high enough plag content to be buoyant within a crystallizing layered intrusion (or magma ocean). A mode with 30 vol% mafic silicates would be regarded as a typical member of the Mg-suite [9].

A pristine rock's grains may be fractured and scattered (at mm-cm scale) remnants of coarser original grains. Ignoring possible diversity in the sizes of the grains, some idea of the number of (original) grains that must be included for sample to be reliably anorthosite (<10% mafics) may be gleaned from binomial probability theory (Fig. 2). For example, an observation of <10% mafics is not reliably (2-σ) distinct from a 40% "true" mode without at least 10 separate grains; resolution from a 30% "true" mode would require at least 10 separate original grains *just for 80% probability*. It should *not* surprise that occasionally 3-mm sized clasts combine "anorthosite" modes with high *mg*.

References: [1] Wood J. A. et al. (1970) *Proc Apollo 11 LSC,* 965. [2] Warren P. H. and Wasson J. T. (1977) *PLSC* **8***,* 2215. [3] Ryder G. et al. (1980) *PLPSC* **11**, 471. [4] Jolliff B. L. et al. (1999) *Am. Min.* **84**, 821. [5] Gross J. et al. (2012) *LPS* **43**, #2306. [6] Warren P. H. et al. (1991) *LPS* **22**, 1469. [7] Albrecht A. et al. (1995) *LPS* **26**, 13. [8] Schlichting H. et al. (2012) *Ap. J.*, in press. [9] Warren P. H. (1990) *Am. Min.* **75**, 46. [10] Korotev R. L. et al. (2010) *GCA* **74**, 7362. [11] Darling J. R. and Moser D. E. (2012) *LPS* **43**, #2164. [12] Yamaguchi A. et al. (2010) *GCA* **74**, 4507. [13] Takeda H. et al. (2006) *EPSL* **247**, 171. [14] Stöffler et al. (1980) *Proc. Conf. Lunar Highland Crust*, 51.

ARISTARCHUS OLIVINE IN CONTEXT WITH CIRCUM-IMBRIUM OLIVINE DEPOSITS. S. M. Wiseman[1], K. L. Donaldson Hanna[1], J. F. Mustard[1], P. J. Isaacson[2], C. M. Pieters[1], B. L. Jolliff[3], [1]Brown University (sandra_wiseman@brown.edu), [2]University of Hawaii at Manoa, [3]Washington University in St. Louis.

Introduction: The Copernican-aged Aristarchus impact crater occurs on the SE margin of the Aristarchus plateau, which is located to the west of the Imbrium basin (Fig 1). The plateau may have been uplifted as a consequence of the Imbrium event [e.g., 1,2,3]. Aristarchus crater occurs near the contact between plateau materials and western Procellarum basalts, which embay the plateau (Fig 1). The impact event postdates Vallis Shroteri and impact implaced materials overlie pyroclastic deposits [e.g., 4] on the plateau. Materials with variable compositions are exposed in and around the crater [e.g., 4,5,6]. Of particular interest is the origin of olivine-bearing deposits that occur as ejecta overlying the SE portion of the crater rim [7].

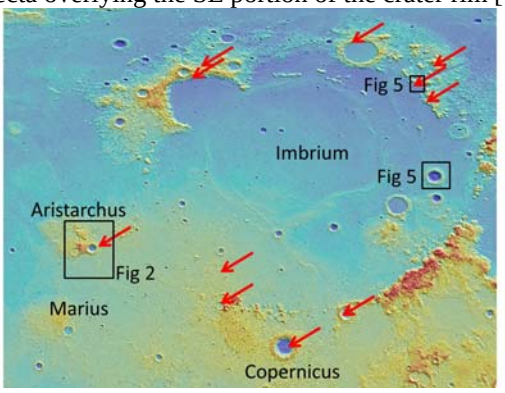

Figure 1. WAC color coded topography overlain on shaded relief. Red arrows indicate olivine exposures [8].

M^3 and Diviner Data: The Chandrayaan-1 Moon Mineralogy Mapper (M^3) is a visible to near infrared (VNIR) (0.43-3.0µm) imaging spectrometer [9]. Data acquired at a global mapping resolution of 140 m/pixel with 85 channels were used. M^3 data were calibrated and photometrically corrected (PDS level 2).

The Lunar Reconnaissance Orbiter Diviner Lunar Radiometer Experiment acquires data from 0.3 to 200µm in 9 channels [10]. Channels centered at 7.8, 8.2, and 8.6µm allow estimation of the Christiansen Feature (CF), an emissivity maximum at mid-infrared wavelenths that is diagnostic of composition [11].

Aristarchus Crater: Some material exposed by the Aristarchus impact has a high albedo (Fig 2). These bright exposures have been interpreted to contain anorthosite [4,5]. Investigations by [12] found crystalline plagioclase features in the central peak, though this feature near 1.25µm is not readily apparent at the spatial resolution of M^3. Bright material exposed in SW ejecta deposits was inferred to be silicic due to short CF positions identified in Diviner data [13].

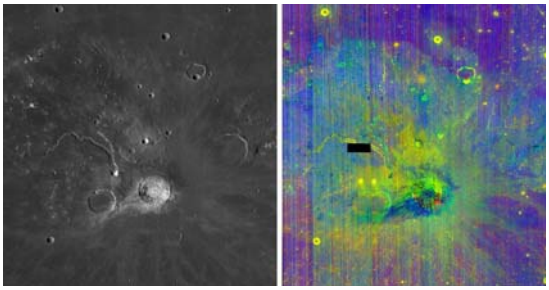

Figure 2. (left) Subset of WAC global mosaic showing Aristarchus crater. (right) M^3 spectral parameter composite with R=1005nm band depth, G=2000nm integrated band depth, B=950/750nm. Red indicates olivine-bearing units.

NW portions of the rim and ejecta expose plateau materials and are spectrally dominated by pyroxene in the VNIR and exhibit both 1 and 2µm absorptions (Fig 3a,b). The olivine-bearing material exposed in the SE ejecta (Fig 3a, red arrow) is spectrally dominated by olivine, although a subtle absorption at 2µm could be caused by pyroxene and/or spinel [7] (Fig 3c).

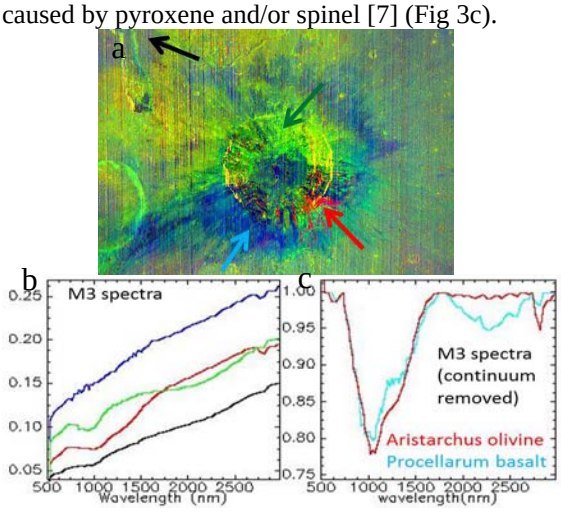

Figure 3. (a) Zoom in of Aristarchus crater (Fig 2). (b) Spectra extracted from locations with arrows. (c) continuum removed spectra. Red spectrum is shown in part b and cyan spectrum was extracted from olivine-bearing western Procellarum basalt (purple unit in Fig 2).

Although the olivine-bearing material is dissimilar from other materials exposed in the crater, olivine-bearing western Procellarum basalts [e.g.,14] are exposed to the north of the plateau and olivine-bearing flows originating from the Marius Hills [e.g., 15] occur to the south. However, the western Procellarum and Marius Hills units exhibit distinct pyroxene related absorptions in addition to olivine features (Fig 3c). The olivine-bearing material exposed in the SE Aris-

tarchus ejecta is spectrally distinct from olivine-bearing western Procellarum and Marius Hills basalts.

Although VNIR spectra of the olivine-bearing ejecta deposits are dominated by olivine, it is important to note that Fe-poor phases that may be mixed with the olivine are spectrally neutral and difficult to detect in the VNIR. Based on the geologic context, it is likely that the olivine-bearing ejecta is mixed with spectrally neutral material similar to the blue exposures in Fig 3a. Diviner spectra are consistent with a mixture of olivine and other phases (Fig 4).

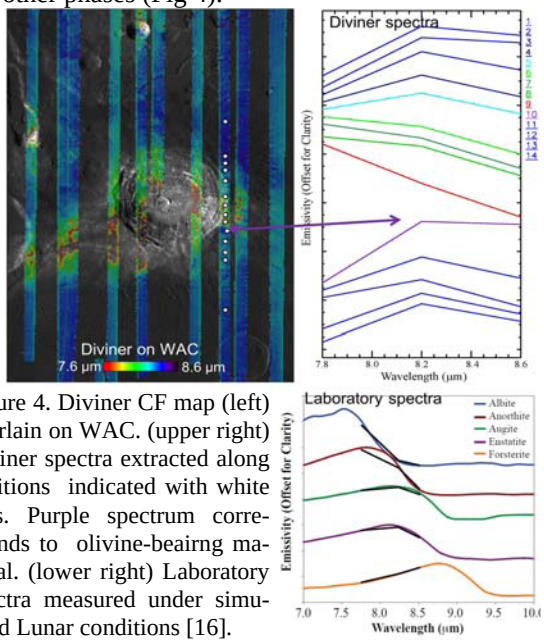

Figure 4. Diviner CF map (left) overlain on WAC. (upper right) Diviner spectra extracted along positions indicated with white dots. Purple spectrum corresponds to olivine-beairng material. (lower right) Laboratory spectra measured under simulated Lunar conditions [16].

Origin of Olivine: Potential sources of the olivine-bearing material excavated by the impact include western Procellarum or Marius Hills basalts. Both the Procellarum basalts [e.g., 14] and some units associated with the Marius Hills [15] are olivine-bearing. However, these materials also have significant pyroxene spectral contributions which are not observed in the Aristarchus ejecta. As the olivine is associated with impact melt and ejecta, impact processes may have played a role. Examination of NAC image M102464936R shows that the olivine signature is preferentially associated with blocky material.

The olivine-bearing deposits could be derived from a shallow pluton that is not represented by other surface exposures (perhaps related to the formation of the plateau and/or pyroclastic deposits) or re-excavated material originally deposited by the Imbrium forming event. Several olivine-bearing deposits have been detected in the vicinity of Imbrium [8]. Such deposits may have been excavated from the lower crust/ upper mantle [17]. Alternatively, these olivine-bearing deposits could be excavated troctolites that formed as a result of intrusions near the base of the crust [18].

There are several olivine bearing deposits in the vicinity of Imbrium [8]. We investigated these deposits and looked for additional deposits using M^3 data. Some of these deposits (e.g., Fig 5) are spectrally dominated by olivine, although the spectra are not as spectrally pure as the Aristarchus olivine-bearing spectra. These deposits are smaller and thus more likely to be spatially mixed with other material. One such deposit is exposed in a crater and another deposit occurs in blocky material that is likely Imbrium ejecta (Fig 5).

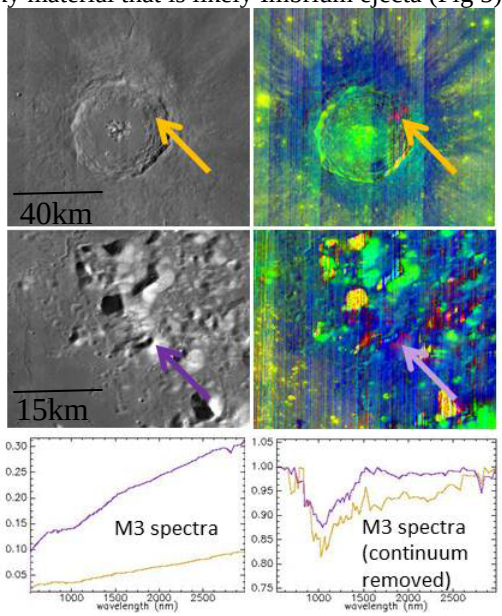

Figure 5. M^3 image subsets, locations shown in Fig 1. Parameter map is same as in Fig 2. Red indicates olivine.

Discussion and Future Work: Given that spectrally similar deposits to those of the olivine-bearing Aristarchus ejecta are found in other exposures in the vicinity of Imbrium, the deposit in Aristarchus may represent re-exposed Imbrium ejecta or other impact transported deposits [19]. Future work will focus on spectral modeling of M^3 and Diviner spectra to determine the abundance and Mg# of the olivine exposed in Aristarchus and the vicinity of Imbrium.

References: [1] H. J. Moore (1965) *U.S. Geol. Survey, Geol. Invest. Map*, I-465, [2] J. E. Guest (1973) *Geol. Soc. Am. Bull*., 84, [3] S. H. Zisk et al (1977) *Moon*, 17, [4] McEwen et al (1994) *Science*, 266, [5] Lucey et al (1986) *JGR*, 91, [6] Le Mouelic et al (1999) *G*RL, 26, [7] Mustard et al (2011) *JGR*, 116, [8] Yamamoto et al (2010) *Nat. Geosci*., 3, [9] Pieters et al., (2011) *JGR* 116, [10] D. A. Paige et al. (2009) *Space Sci. Rev.*, 150, [11] J. E. Conel (1969) *JGR* 74, [12] Ohtake et al (2009) *Nature*, 461, [13] Glotch et al (2010) *Science*, 329, [14] Staid et al (2011), *JGR*, 116, [15] Besse et al (2011) *JGR*, 116, [16] Donaldson Hanna et al (2011), *JGR*, 117,[17] Stewart (2011) *LPSC 42*, 1633, [18] Lucey (2010), *Nat. Geo*, 3. [19] Powell et al (2010), *LPSC 43*, 1689.

SPHERULES AND GLASSES IN LUNAITE SHIŞR 161 RECORD REWORKED REGOLITH AND A MAGNESIAN COMPONENT OF THE FELDSPATHIC HIGHLANDS TERRANE. Axel Wittmann[1], Randy L. Korotev[1], Bradley L. Jolliff[1], and Anthony J. Irving[2]. [1]Department of Earth & Planetary Sciences, Washington University Saint Louis, MO; [2]Department of Earth & Space Sciences, University of Washington, Seattle, WA.

Introduction: Petrologic models for the feldspathic highlands terrane invoke a global magma ocean with plagioclase accumulation in the crust [e.g., 1] variably modified early-on by intrusive activity [e.g., 2]. Some 4.4 Ga later, this surface is saturated with impact craters, their ejecta blankets, and regolith. Shişr 161, a 57.2 g lunaite, is a feldspathic, fragmental regolith breccia [3] and, thus, a recent sample from this surface. It's bulk rock composition indicates high MgO (8.17 wt%) relative to FeO (5.93 wt%) together with a low incompatible element content (TiO_2 0.34 wt%, Th 0.16 ppm) [4]. We explore its petrogenesis from bulk chemistry and petrography with a focus on melt spherules and glass shards.

Samples and Methods: Petrographic observations were made on a 5.5 cm^2 thin section area of Shişr 161. Compositions of 13 spherules and 12 glass shards were determined by electron microprobe analysis. Bulk chemical compositions of the spherules were approximated by modal recombination after the relative proportions of components were determined by image anlysis, using NIH's ImageJ software.

Results: In thin section, Shişr 161 is composed of a fine, clastic matrix that embeds lithic clasts. Clasts <0.5 mm make up 25 % of the thin section area (n=69): 18 % poikilitic melts, 26 % aphanitic melts, 31 % granulites, 13 % polymict breccias, ferroan anorthosites (FAn), plagioclase, Fe-rich Cpx, and 12 % basalt; agglutinates were not observed. The 12 glasses occupy ~0.05 % and the 12 spherules ~0.06 % of the thin section area.

Petrography: The 12 glasses are 0.1 to 0.4 mm long shards; 8 of these are holohyaline without inclusions. Two contain tiny blebs of (Fe,Ni)S. One has variably assimilated debris along its rim; another displays domains with acicular plagioclase crystals, and one is clast-rich with variably assimilated plagioclase, olivine, pyroxene, chromite, and minor, ~1 µm-size blebs of (Fe,Ni)S. Most glass particles are fused to dense portions of the matrix, suggesting reworking and emplacement as parts of polymict breccia clasts.

The 13 spherules are 50 to 480 µm in size and their degree of crystallization ranges from cryptocrystalline (3) to aphanites with tiny crystallites of plagioclase and/or pyroxene (2) to progressively coarser crystallized aphanites with plagioclase laths >5 µm (4); the most coarsely crystallized one has an ophitic texture of plagioclase, pyroxene and olivine with interstitial mesostasis that is enriched in Si, K, P, and Ti. Three spherules bear evidence for thermal metamorphism. One of them equilibrated with the surrounding matrix, presumably as part of a breccia-in-breccia clast; two metamorphosed spherules are components of breccia clasts. One of these belongs to an aphanitic, dark clast that contains abundant, partly assimilated plagioclase fragments in a mafic matrix that crystallized plagioclase laths. The other metamorphosed spherule is part of a more strongly crystalline clast composed of angular plagioclase crystals in a poikilitic olivine-pyroxene matrix (Fig. 1A). This spherule crystallized ~10 µm plagioclase laths that are enclosed in pyroxene. One cryptocrystalline spherule composed of fused droplets, is a component of a polymict breccia clast.

Geochemistry: All glasses and all but two spherules exhibit atomic Mg/Al <1.5, and all glasses and 11 of 13 spherules have atomic Mg/Ca <1, which suggests an impact origin for all glasses and most spherules [5]. The 3 spherules that do not follow this trend belong to a group of 7 spherules containing FeNiS and/or FeNi inclusions, which are likely impactor components. One of them is a possible GASP (*gas-associated spheroidal precipitate* [6]; 0.17 wt% Al_2O_3,

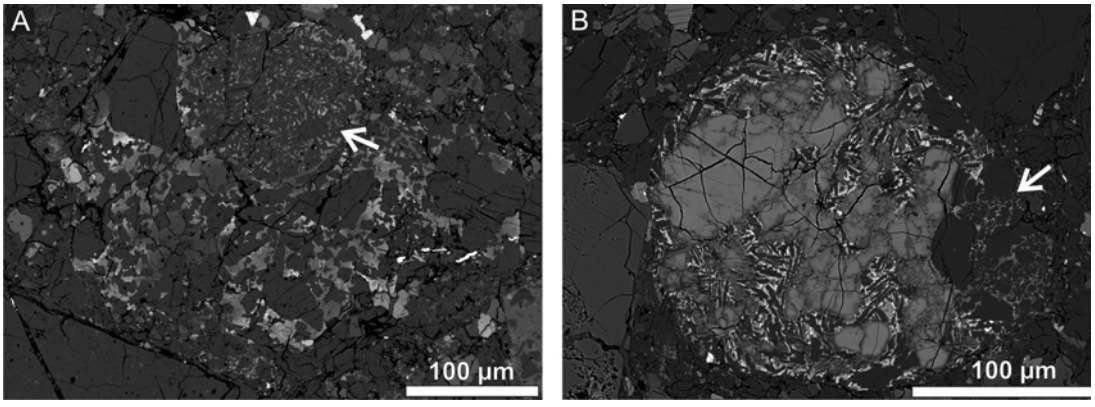

Fig 1. Shişr 161 back-scattered electron images. A – Metamorphosed spherule (arrow) in poikilitic clast. B – Olivine-rich spherule with accreted feldspathic melt (arrow).

64.4 wt% SiO_2, 28.7 wt% FeO), and another one accreted feldspathic melt (Fig. 1B). These characteristics suggest probable impact origins for all these glasses and spherules.

TiO_2 contents reach up to 4.3 wt% but are <0.5 wt% in 20 of the 25 particles analyzed. P_2O_5 concentrations are <0.1 wt% in 23 of the 25 particles and K_2O contents are mostly <0.1 wt%. One glass particle and one spherule are exceptions; they contain 0.8 and 1.1 wt% K_2O, and correlated high TiO_2 and P_2O_5 abundances, likely indicating KREEP components.

Compared with the normative anorthositic norite bulk composition of Shişr 161, normative mineralogies for the glasses and spherules reflect mainly plagioclase-rich precursor lithologies such as anorthosites (2), noritic anorthosites (8), troctolitic anorthosites (4), anorthositic norites (5) and anorthositic troctolites (1). However, two spherules indicate troctolitic normative compositions, a mafic glass, and one spherule have noritic normative compositions, and a possible GASP-particle has a pyroxenitic normative composition.

Comparison of the bulk chemical composition of Shişr 161 [4] with the 5-degree Lunar Prospector gamma-ray spectrometer data [7] points to three broad areas, where the average regional composition is similar: a) southern farside highlands, NW of Tsiolkovskiy crater; b) highlands between Smythii-Marginis, Mendeleev and Tsiolkovskiy; and c) highlands SE of Fecunditatis, between Furnerius and Australe.

Discussion: Although spherules are generally thought to represent distal ejecta, terrestrial examples of fallback debris near the center of the 10 km Ø Bosumtwi [8] and the 18 km Ø El'gygytgyn craters [9] show that such particles may form late fallback material on top of crater-fill impactites (*"microtektite-like spherules"*). In a lunar crater, spherule bearing fallback debris may, thus, blanket the surface of melt splashes and melt sheets, providing thin insulation layers that become thermally metamorphosed. Other interpretations of crystallized lunar spherules invoke prolonged residences in ejecta plumes of large craters [10,11]. Petrographic evidence (Fig. 1A), indicates post-depositional thermal metamorphism affected at least a subset of the crystallized spherules in Shişr 161. The large fraction of impact melts and granulites in Shişr 161 adds weight to the formation scenario as reworked fallback material of a large impact crater.

The compositional variability of spherules and impact glasses in Shişr 161 reflect heterogeneities in their precursors. These include rare KREEP and FeO-rich components, and dominant anorthositic-, FAn- and magnesian-like components. The resulting bulk composition of Shişr 161 suggests a mixture between anorthositic, mare, KREEP-bearing, and magnesian components (Fig. 2). Magnesian granulites and a hypothetical peridotitc component were recently advocated as components for similar feldspathic meteorites [13]. Troctolite clasts in Dhofar 305, 306, 307, olivine pyroxenite clasts in Dhofar 305, dunite clasts in Dhofar 307 [14] and spinel pyroxenites and dunites in Dhofar 310 [15] may represent other endogeneous ultramafic components of the lower highlands crust that contributed to the magnesian character of Shişr 161. Conceivably, admixture of ultramafic impactor material could also account for a magnesian component.

Conclusions: Variably crystallized spherules in lunaite Shişr 161 could record formation as metamorphosed fallback ejecta in a highlands impact crater. Compositions of glasses and spherules suggest larger variability among their precursor rocks than expected from the bulk rock composition [4]. They comprise minor KREEP and mare basalt, dominant anorthitic and poorly defined magnesian lithologies.

References: [1] Wood J. A. et al. (1970) *Proc. Apollo 11 Lunar Sci. Conf.*, 965-988. [2] Shearer C. K. et al. (2006) *RiMG 60,* 365-518. [3] Foreman A. B. et al. *LPSC XL*, abstr. # 2304. [4] Korotev R. L. (submitted) *MAPS.* [5] Joy K. H. et al. (2011) *GCA 75*, 2420-2452. [6] Warren P. H. (2008) *GCA 72*, 3562-3585. [7] Prettyman T. H. et al. (2006) *JGR 111*, E12007. [8] Koeberl C. et al. (2007) *MAPS 42*, 709-729. [9] Wittmann A. et al. (submitted) *MAPS.* [10] Ivanov A. V. et al. (1976) *Proc. Lunar Sci. Conf. 7th*, 743-757. [11] Symes J. K. et al. (1998) *MAPS 33*, 13-29. [12] Korotev R. L. et al. (2003) *GCA 67*, 4895-4923. [13] Treiman A. H. et al. (2010) *MAPS 45*, 163-180. [14] Demidova S. I. et al. (2003) *LPSC XXXIV*, abstract #1285. [15] Demidova S. I. et al. (2003) *66th Ann. Met. Soc. Meeting*, abstr. #5046.

Acknowledgment: A. Foreman and R. Zeigler for initial contributions to the study of Shişr 161. This work was supported by NASA grants NNX10AI44G, and NNX11AB26G.

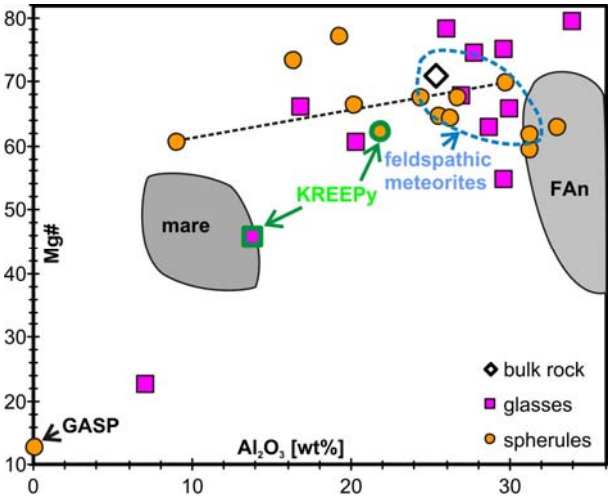

Fig. 2 Variation of Mg# [mole% Mg/(Mg+Fe)] with Al_2O_3 in Shişr 161 bulk rock, glasses and spherules; diagram after [12]. Dotted line connects feldspathic and mafic portions of spherule in Fig. 1B.

ARISTARCHUS CRATER AS A PROBE OF THE LUNAR CRUSTS MOST FRACTIONATED ROCK TYPES. Michael Zanetti and Bradley L. Jolliff, Department of Earth & Planetary Sciences and the McDonnell Center for the Space Sciences, Washington University, Saint Louis, MO. michael.zanetti@wustl.edu

Introduction: Aristarchus Crater (~42 km diameter), located in the northwestern portion of Oceanus Procellarum on the southeastern boundary of the Aristarchus Plateau, has long been recognized for the unusual and diverse suite of materials it excavated [1-10]. Remote sensing data sets have provided increasingly more detailed and sharper focus on the characteristics of these materials. Most recently, LRO has obtained compositional data (Diviner, [11]) and high-resolution images (LROC-NAC [12]) that allow the correlation of compositionally distinctive signatures to specific morphological and lithologic units. From the integration of these data sets, we infer that the Aristarchus target section features a petrogenetically diverse suite of rocks including materials of the Aristarchus Plateau, young and relatively Th-rich basalts of Oceanus Procellarum, a differentiated, KREEP-rich igneous intrusive body, and diverse ejecta deposits from the Imbrium basin including olivine-rich materials [13] and KREEP-rich impact-melt deposits. Here we focus on the mapped distribution of these deposits, in particular, the compositionally evolved crustal materials.

Clementine data: The 1994 Clementine mission obtained multispectral data from which coupled mineralogy and compositional information were derived [5,6,7,14]. Plagioclase identifications and low FeO concentrations in the central peaks, derived from the UVVIS data indicated that the deepest materials excavated could be anorthositic [5,6,9,14]. According to these data, the crater interior and the brightest ejecta deposits have FeO concentrations of ~5-11 wt%.

Lunar Prospector: The 1998 Lunar Prospector Gamma-Ray Spectrometer (LP-GRS) results showed that Aristarchus Crater lies at the center of one of the strongest Th hot spots on the Moon [8,15,16]. Modeled values, taking into account the broad spatial response function, could be as high as 15 ppm [8]. Crater and proximal ejecta deposits, however, are lithologically mixed materials so some of the endmember rock components could have significantly higher concentrations. Using mixing trends, [17,18] argued that at least some of the materials excavated by Aristarchus are extraordinarily rich in Th, perhaps even more so than can be explained by a KREEP-rich substrate such as KREEP basalt (~13 ppm) or high-K Fra Mauro impact-melt breccia (~18 ppm). Lunar samples with the "right" Th and FeO values to satisfy mixing trends include Th-rich impact-melt breccia (Apollo 12, ~30 ppm Th [19], and potential differentiates of KREEP magmatism such as quartz-monzogabbro and granite.

Kaguya (Multiband Imager, Spectral Profiler) and Chandrayaan-1 (Moon Mineralogy Mapper): Multispectral and hyperspectral data for Aristarchus Crater have yielded higher quality spectral identifications of mineralogy, including both spectral and spatial resolution. The 2007 Kaguya (SELENE) mission multiband imager data indicate that Aristarchus central peak material may contain very pure crystalline anorthosite (PAN rocks with >98 vol %), and is the only location of these rocks within the Procellarum KREEP Terrane [20]. The interpretation of these rocks is based on the presence of a prominent 1.25 micron absorption band indicating a Fe-bearing crystalline plagioclase. The M3 hyperspectral imager on 2008's Chandrayaan-1 mission, in contrast, revealed spectra of the central peak which are reported as very bright but lack any distinctive mafic or plagioclase absorption features, indicating that the central peak are dominated by low-Fe feldspathic materials [10]. Also identified in the ejecta of Aristarchus by both instruments are olivine dominated materials in the south and southeast portions crater walls and ejecta blanket [10,13,21], which can now be directly correlated photogeologically with specific surface features [e.g. 10,22].

LRO: The Diviner lunar radiometer includes three narrow spectral bands centered at 7.8, 8.25, and 8.55 μm that cover the Christiansen Feature (CF), which is sensitive to silicate mineralogy and the bulk SiO_2 content (essentially the degree of polymerization) [11]. On the basis of these data, ejecta on the southwestern rim of Aristarchus appear to be silicic, i.e., consistent with the presence of abundant quartz (or cristobalite or tridymite) and alkali feldspar, i.e., granite or alkali feldspar [11] (arrow in Fig. 1d). Narrow angle camera (NAC) images, with resolution of ~ 0.5 m/pixel, cover approximately 85% of the crater interior and the proximal ejecta blanket with variable illumination geometry. Detailed geomorphologic mapping of the crater is currently underway [22].

Discussion: Aristarchus Crater has an extensive bright ray system that extends several hundred km from the crater rim and these materials, along with rocks in the crater itself, constitute an unusual set of associations. In addition to basaltic components, the crater excavated very high albedo crater material and ejecta. High albedo materials are especially concentrated south and southwest of the crater rim (Fig. 1a), and olivine-rich rocks are concentrated in ejecta along a narrower radial deposit east – southeast of the crater [10]. This diversity of lithologic materials associated with the crater and located in the target area reflect the diversity of the target rock formations that exist in the

upper few km in this region, and the specific target rocks may be highly localized. Furthermore, some of the components are not easily relatable to specific morphologic units [10,22] and cannot be explained by any simple petrogenetic scenario. For example, compositionally evolved KREEP-rich rocks and olivine-rich rocks [13] are not expected together, and we infer that these may simply reflect juxtaposition of Imbrium ejecta deposits with evolved intrusive rocks of the PKT. Possible origins of the olivine-rich material are discussed by [13]. The high albedo materials, including those within the crater and the SW ejecta unit are most likely low-FeO, alkali-rich differentiates of a KREEP-rich, near-surface intrusive body and not primary anorthosite of the Moon's early primary crust.

Given the extensive volcanic activity that occurred in this region of the Moon, basaltic underplating, as suggested by Hagerty et al. [23], of KREEP rich rocks, may have caused partial melting and intrusion of silicic magma (with a small degree of melting) or melting and injection of an evolved KREEP-rich magma such as quartz monzogabbro to a shallow level in the Aristarchus target section. Aristarchus occurs close to two other localities where evolved, silicic volcanics are indicated by compositional and morphological data, the Mairan and Gruithuisen Domes [8,11,23], which may indicate that this was a special or even unique petrologic province on the Moon.

Acknowledgements: We gratefully acknowledge the LRO Project and the LROC Team for their work in collecting the data and for support of this research.

References: [1] Guest (1973) GSA Bulletin 84. [2] Zisk et al. (1977) Moon 17. [3] Etchegaray-Ramirez et al. (1983). JGR 88 supplement p A529-A543 [4] Guest & Spudis (1985) Geol. Magazine 144. [5] Lucey et al. (1986) JGR 91. [6] McEwen et al. (1994) Science 266. [7] Le Mouélic et al. (1999) GRL 26. [8] Hagerty et al. (2009) JGR 114. [9] Chevrel et al. (2009) Icarus 199. [10] Mustard et al. (2011) JGR 116. [11] Glotch et al. (2010) Science 329. [12] Robinson et al. (2010) Space Science Reviews, 150. [13] Wiseman et al. (2012) LPSC 43, Abs #2515. [14] Pinet et al. (1999) LPSC 30, Abs 1555. [15] Lawrence, D. et al. (2003) JGR 108. [16] Lawrence, D. et al. (2007) GRL 34. [17] Jolliff (2004) LPSC 35, Abs #2032. [18] Zhang and Jolliff (2008) LPS 39, #2534. [19] Korotev et al. (2011). Geo Chem Acta 76, 6 [20] Ohtake et al (2009) Nature, 461. [21] Yamamoto et al., (2010) Nat Geo, 3. [22] Zanetti et al. (2011) LPSC 42, Abs #2330. [23] Hagerty et al., 2006 JGR 111. [24] Scholten F. et al. (2012) JGR 117, E00H17.

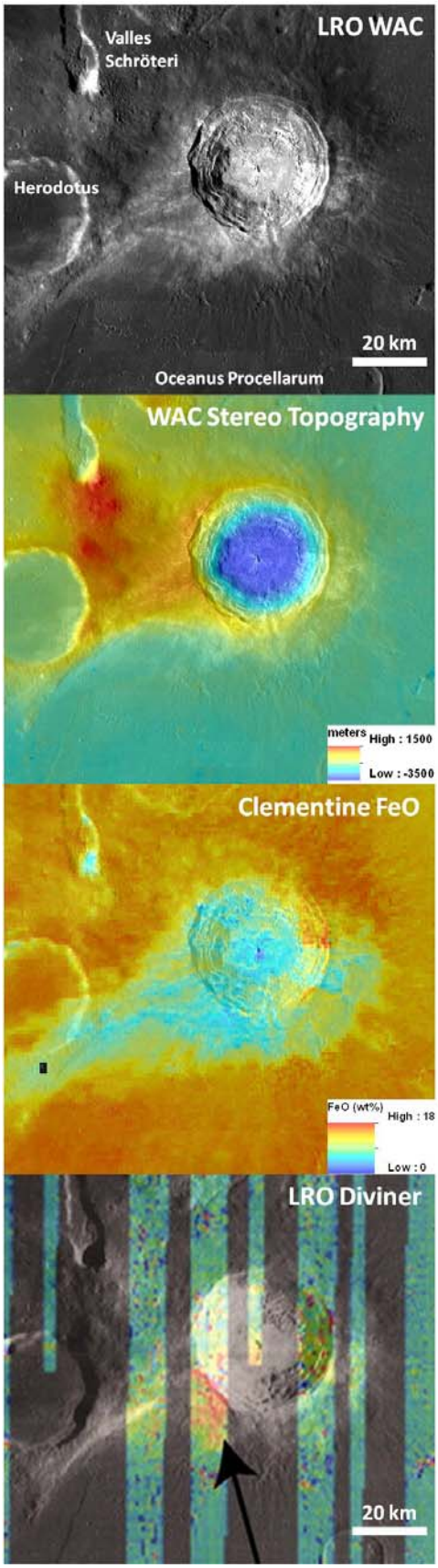

Figure 1: Aristarchus Crater situated on the SE edge of the Aristarchus Plateau. A) LRO WAC image, 100 mpp mosaic, B) WAC derived stereo topography, GLD100 [24], C) Clementine UV-VIS-derived FeO, D) LRO Diviner data (modified from [11]).

FELDSPATHIC LUNAR METEORITE GRAVES NUNATAKS 06157, A MAGNESIAN PIECE OF THE LUNAR HIGHLANDS CRUST. R. A. Zeigler[1], R. L. Korotev[2] and B. L. Jolliff. [1]NASA Johnson Space Center, KT, 2101 NASA Pkwy, Houston, TX 77058 (ryan.a.zeigler@nasa.gov). [2]Washington University in St. Louis, CB 1169, 1 Brookings Dr., St. Louis, MO 63130.

Introduction: To date, 49 feldspathic lunar meteorites (FLMs) have been recovered, likely representing a minimum of 35 different sample locations in the lunar highlands. The compositional variability among FLMs far exceeds the variability observed among highland samples in the Apollo and Luna sample suites [1]. Here we will discuss in detail one of the compositional end members of the FLM suite, Graves Nunataks (GRA) 06157, which was collected by the 2006-2007 ANSMET field team [2]. At 0.79 g, GRA 06157 is the smallest lunar meteorite so far recovered. Despite its small size, its highly feldspathic and highly magnesian composition are intriguing (Fig. 1). Although preliminary bulk compositions have been reported, thus far no petrographic descriptions are in the literature [3]. Here we expand upon the bulk compositional data, including major-element compositions, and provide a detailed petrographic description of GRA 06157.

Methods: Trace-element compositions were determined by INAA (instrumental neutron activation analysis) on 57 mg of GRA 06157. Major-element compositions were determined by electron probe microanalysis (EPMA) of fused beads (FB) prepared from the INAA samples [4]. Petrography was determined using backscattered electron (BSE) images, elemental x-ray maps, and quantitative EMPA on polished thin section GRA 06157,8 (~10 mm^2; Fig. 2).

Petrography: GRA 06157 is a glassy-matrix regolith breccia containing abundant lithic and mineral clasts and a few small impact spherules (Fig. 2 blue). All of the lithic clasts identified are granulite clasts. The mineral clast population is dominated by plagioclase, pyroxene, and olivine, with trace amounts of FeTiCr oxides, FeNi metal, and FeS. The meteorite has a discontinuous vesicular fusion crust on three sides.

The most abundant type of lithic clast is highly feldspathic granulite (>90% plagioclase) consisting of large plagioclase grains, up to 1 mm in their longest dimension, that contain tiny rounded inclusions of pyroxene, almost always less than 2 μm wide. All granulite clasts have highly calcic plagioclase (An_{94-97}). Rarely there are strings of larger pyroxene grains (up to ~20 μm wide) present along the borders of some plagioclase grains (Fig. 2 green). Augite is the dominant pyroxene ($En_{44}Wo_{42}Fs_{14}$; Fig. 3), with rare occurrences of hypersthene ($En_{64}Wo_3Fs_{33}$); there is no compositional difference between the different size pyroxenes. Minor olivine grains also occur, with a relatively wide range in compositions (Fo_{60-78}). There are also troctolitic granulite clasts, including the largest lithic clast in the section (~1.5 x 1.5 mm; Fig. 2 magenta). They contain up to 50% magnesian olivine (Fo_{85-90}), <5% magnesian augite ($En_{53}Wo_{37}Fs_9$), <5% near end member magnesian spinel (mg' = 83; 1.7 wt% Cr_2O_3), and trace amounts of bronzite ($En_{77}Wo_2Fs_{20}$). A few small (~150 μm) mafic granulite clasts (plagioclase is <20% by mode) are compositionally similar to the more feldspathic granulite clasts (Fig. 2 orange), albeit with more ferroan pyroxene compositions ($En_{39}Wo_{42}Fs_{19}$; $En_{55}Wo_2Fs_{43}$).

A single large (200 x 150 μm) basaltic spherule is present. It is partially devitrified with magnesian olivine (Fo_{78}) quenching out of the glass (Fig. 2 cyan). It has a bulk composition very similar to Apollo 15 yellow pyroclastic glass [5]. Plagioclase mineral clast compositions have a restricted range (An_{94-98}). In contrast, olivine mineral clasts span nearly the entire compositional range (Fo_{7-93}); most clasts are at the Mg-rich end of the range, however. Most pyroxene mineral clasts are exsolved, with augite ($Wo_{41-43}Fs_{18-40}$) and orthopyroxene ($Wo_{1\ 5-3}Fs_{34-72}$) lamellae ranging from sub-micron all the way up to nearly 100 μm thickness (5-10 mm is typical; Fig. 2 red, yellow).

Geochemistry: GRA 06157 is one of the most feldspathic meteorites (3.5 wt% FeO). With an mg' of 77 (molar Mg/[Mg+Fe]*100), it is distinct in being more magnesian than any other lunar meteorite from Antarctica and any other fragmental or regolith breccia lunar meteorite of which we are aware (Fig. 1). Additionally, GRA 06157 has low concentrations of incompatible elements (e.g., 0.23 ppm Th). Despite being a regolith breccia, GRA 06157 has low concentrations of siderophile elements compared to most regolith breccias [4].

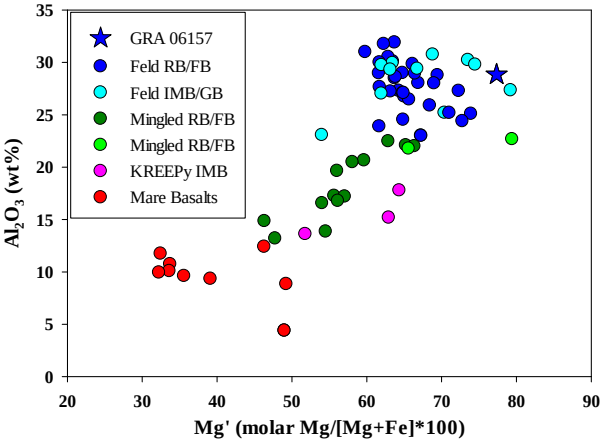

Figure 1: Al_2O_3 vs. mg' for 72 of 78 known lunar meteorites. Data from FB- EPMA at Washington University.

Discussion: On the basis of significant differences in mg', siderophile-element concentrations, and clast populations, GRA 06157 is not paired with any other FLM. The high Mg' of GRA 06157 is due to the overall magnesian nature of its clasts, in particular the presence of the highly magnesian spinel-bearing troctolitic granulite clasts and forsterite mineral clasts. The presence of spherules makes GRA 06157, by definition, a regolith breccia (this is also supported by the presence of a vesicular fusion crust). The paucity of impact spherules or glass clasts of any kind, coupled with low siderophile concentrations suggests it represents an immature regolith. Low concentrations of incompatible elements commonly associated with KREEP suggests that its provenance was distant from the Procellarum KREEP Terrane. Finally, the presense of a likely pyroclastic spherule indicates there is at least a minor basaltic component in GRA 06157. The absence of lithic basalt clasts, the coarse-grained nature of the pyroxene exsolution, and the overall magnesian nature of the sample suggest that the basaltic component is minor.

Acknowledgements: We thank ANSMET for collecting the meteorite and JSC for allocating it to us. This work was supported by NASA grants NNX10AI44G and NNX11-AB26G. **References:** [1] Korotev et al. (2012) *P2CLHC,* this volume. [2] McBride K et al. (2007) *Ant. Met. News.*, **30**(2). [3] Korotev RL et al. (2008) *LPSC* **39**, #1209. [4] Korotev RL et al. (2009) *MAPS* **44**, 1287–1322. [5] Shearer CK and Papike JJ (1993) *GCA* **57**, 4785–4812.

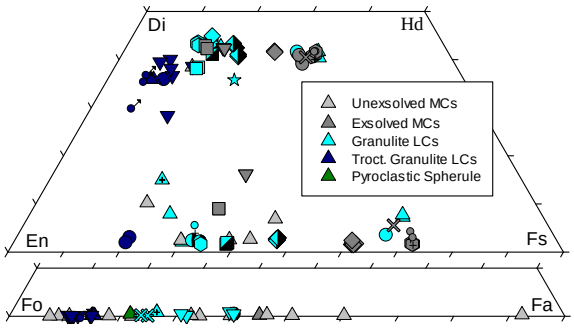

Figure 3: Pyroxene and olivine compositions in GRA 06157 mineral clasts (MC, grey) and lithic clasts (LC, blue,cyan). Different symbols in the same color represent different clasts.

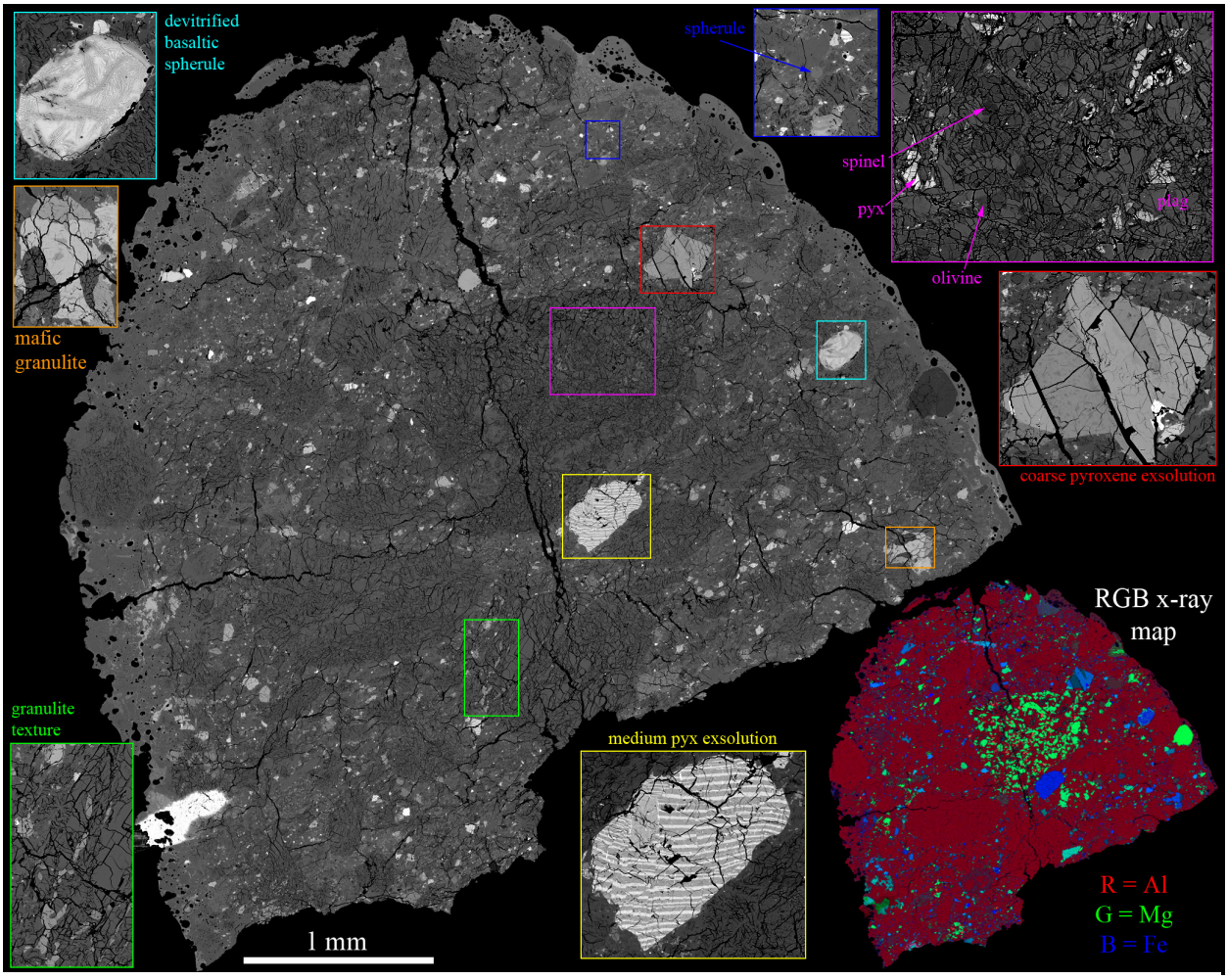

Figure 2: BSE images (grey scale) and an RGB elemental x-ray map of lunar meteorite GRA 06157. The scale bar applies only to the main image.

PRELIMINARY RESULTS ON THE STRUCTURE OF LUNAR HIGHLAND CRUST FROM GRAIL GRAVITY AND LOLA ALTIMETRY. Maria T. Zuber[1], David E. Smith[1], Sami W. Asmar[2], Alexander S. Konopliv[2], Frank G. Lemoine[3], H. Jay Melosh[4], Gregory A. Neumann[3], Roger J. Phillips[5], Sean C. Solomon[6], Michael M. Watkins[2], Mark A. Wieczorek[7], James G. Williams[2], James W. Head III[8], Erwan Mazarico[1], Mark H. Torrence[9], [1]Department of Earth, Atmospheric and Planetary Sciences, Massachusetts Institute of Technology, Cambridge, MA 02129-4307, USA (mtz@mit.edu); [2]Jet Propulsion Laboratory, Pasadena, CA 91109-8099, USA; [3]NASA Goddard Space Flight Center, Greenbelt, MD 20771, USA; [4]Department of Earth and Atmospheric Sciences, Purdue University, West Lafayette, IN 47907, USA; [5]Planetary Science Directorate, Southwest Research Institute, Boulder, CO 80302, USA; [6]Department of Terrestrial Magnetism, Carnegie Institution of Washington, Washington, DC 20015, USA; [7]Institut de Physique du Globe de Paris, 94100 Saint Maur des Fossés, France; [8]Department of Geological Sciences, Brown University, Providence, RI 02912, USA; [9]SGT, Inc., Greenbelt, MD 20770, USA.

Introduction: The lunar crust is the product of early melting and preserves the surficial and shallow subsurface record of the Moon's post-accretional evolution. Deciphering this record requires an understanding of crustal composition, volume, structure and physical state [*e.g.,* 1]. Substantial advances in our geophysical understanding of the lunar crust are now possible due to recent and ongoing acquisition of high-resolution topography and gravity data sets from the Lunar Orbiter Laser Altimeter (LOLA) [2] and Gravity Recovery and Interior Laboratory (GRAIL) mission [3].

LOLA Altimetry: LOLA [2], a payload instrument on NASA's Lunar Reconnaissance Orbiter mission [4], has been operating nearly continuously in lunar orbit since 13 July 2009. LOLA is a multi-beam laser altimeter that operates at a wavelength of 1064.4 nm with a 28-Hz pulse repetition rate. The instrument's configuration and sampling strategy produce five parallel profiles along LRO's sub-spacecraft ground track. Surface spots are 5 m in diameter, profiles are 10-12 m apart, and observations along each profile are separated by ~56 m, determined by the laser pulse repetition rate and spacecraft velocity. At this point in the LRO extended mission, LOLA has collected over 5×10^9 valid measurements of elevation with a ranging precision of 10 cm and radial accuracy of <1 m. The along-track resolution is ~20 m, and average cross-track resolution is <1 km at the equator and decreases poleward.

A recent LOLA topographic model is shown in Fig. 1. LOLA altimetry has been used to assemble a precise global model of lunar topography. The global grid currently in the NASA Planetary Data System (PDS) is LDEM_512, with a pixel size in latitude of 59.225 m. A spherical harmonic expansion of the gridded data to degree and order 720 (spatial block size 7.5 km) has permitted refinement of fundamental parameters of the lunar shape [5], as well as studies of global bombardment [6] and local studies of landform evolution [7].

GRAIL Gravity: GRAIL [3] is the lunar analog of the very successful GRACE [8] twin-spacecraft terrestrial gravity recovery mission that continues to map Earth's gravity field since its launch in 2007. GRAIL was implemented with a science payload derived from GRACE and a spacecraft adapted from the Lockheed Martin Experimental Small Satellite-11 (XSS-11) mission, launched in 2005.

GRAIL has two primary objectives: to determine the structure of the lunar interior, from crust to core; and to advance understanding of the thermal evolution of the Moon. In addition, as a secondary objective, GRAIL observations will be used to extend knowledge gained on the internal structure and thermal evolution of the Moon to other terrestrial planets.

From the mapping orbit, GRAIL acquires high-precision range-rate measurements of the distance change between the two spacecraft using a Lunar Gravity Ranging System (LGRS) [9], built by the Jet Propulsion Laboratory. The LGRS consists of dual Ka-band (32 GHz) transmitters and microwave antennae that measure the inter-satellite distance change, and S-band (2 GHz) Time Transfer Systems that are used to correlate time between the spacecraft. Ultra-Stable Oscillators (USOs), built by The Johns Hopkins University Applied Physics Laboratory, drive both the Ka-band and S-band systems. Also referenced to the same USO is an X-band (8 GHz) beacon from each spacecraft to ground stations, independent of the telecommunications system, for precise Doppler and monitoring the payload's performance. The spacecraft-to-spacecraft range-rate data provide a direct measure of lunar gravity that leads to a high-spatial-resolution, high-accuracy global gravity field.

GRAIL began collecting data on 1 March 2012 and has completed two of three month-long mapping cycles in the primary mission. In these first two mapping cycles more than 99.99% of the acquired observations were successfully received by the Deep Space Network [10]. Preliminary gravity models reveal low noise levels to the shortest wavelengths resolved thus far, indi-

cating that additional signal exists at even shorter wavelengths than the nominal planned field (degree and order 180) in at least some regions of the Moon. There is a high correlation of gravity with topography to much higher high degrees and orders than with any previous gravity model [*e.g.,* 11- 13].

Shallow Interior Structure of the Moon: Understanding the role of the highland crust in the thermal evolution of the Moon [*cf.* 14, 15] requires global models of crustal thickness as well as the effective elastic thickness of the lithosphere, both of which are derived from a combination of global, high-resolution gravity and topography data. The volume of the crust provides an important constraint on the extent of melting of the magma ocean, and its distribution forms the basis for models of crustal evolution. Variations in crustal thickness may reflect spatial variations in melting and/or re-distribution by impact at a range of scales. The effective elastic thickness yields the thermal structure in the shallow Moon at the time of surface or subsurface loading. Such analysis is particularly valuable in reconstructing the thermal state of the Moon during and subsequent to the late heavy bombardment of the lunar crust. Estimation of physical properties such as density [16], porosity [17] and the extent of crustal brecciation [18] and intrusive magmatism [19] is also possible and underway.

Topography and gravity maps in the vicinity of Tycho crater, shown in Fig. 2, underscore the promise of advancing understanding of lunar crustal structure.

References: [1] Wieczorek M. A. et al. (2006), in *New Views of the Moon,* eds. B. J. Jolliff & M. A. Wieczorek, *Rev. Min. Geochem., 60,* 221-364. [2] Smith D. E. et al. (2010) *Space Sci. Rev., 150,* doi:10.1007/s11214-009-9512-y. [3] Zuber M. T. et al. (2012) *Space Sci. Rev.,* submitted. [4] Chin G. et al. (2007) *Space Sci. Rev., 129,* doi:10.1007/s11214-007-9153-y. [5] Smith D. E. et al. (2010) *Geophys. Res. Lett., 37,* doi:10.1029/2010GL043751. [6] Head J. W. et al. (2010) *Science, 329,* doi:10.1126/science.1195050. [7] Zuber, M. T. et al. (2012) *Nature,* in press. [8] Tapley B. D. et al. (2004) *Science, 305,* 503-505. [9] Klipstein W. M. et al. (2012) *Space Sci. Rev.,* submitted. [10] Beerer J. G. and Havens, G. G. (2012), in *12th Int. Conf. on Space Operations,* submitted. [11] Konopliv A. S. et al. (2001) *Icarus, 150,* 1-18. [12] Namiki N. et al. (2009) *Science, 323,* doi:10.1126/science.1168029. [13] Mazarico E. et al. (2010) *J. Geophys. Res., 115,* doi:10.1126/science.1168029. [14] Solomon S. C. et al. (1981), in *Basaltic Volcanism on the Terrestrial Planets,* eds. T. R. McGetchin, R. O. Pepin & R. J. Phillips, Pergamon Press, N.Y., pp. 1129-1233. [15] Zuber M. T. et al. (1994) *Science, 266,* 1839-1843. [16] Wieczorek M. A. and Phillips R. J. (1997) *J. Geophys. Res., 102,* 10,933-10,943. [17] Huang Q. et al. (2012) *EOS Trans. Am. Geophys. Un.*, P44B-97. [18] Dvorak J. and Phillips R. J. (1977) *Geophys Res. Lett., 4,* 380-382. [19] Phillips R. J. and Dvorak J. (1981) in *Multi-ring Basins, Proc. Lunar Planet. Sci. Conf. 12*, ed. P.H. Schultz, & R.B. Merrill, pp. 91-104, Lunar Planet. Inst., Houston

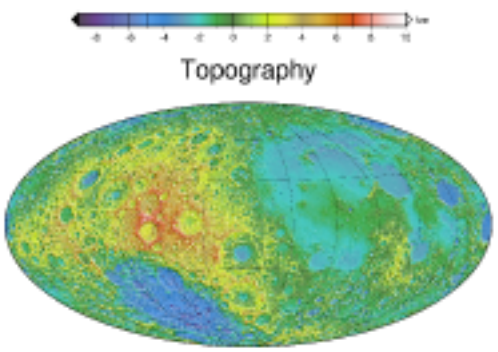

Figure 1. Hammer equal-area projection of LOLA topography [5]. The central longitude is 270°E; nearside is on the right and the farside is on the left.

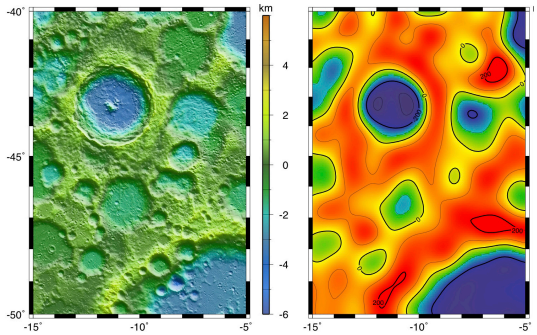

Figure 2. LOLA topography (left) and preliminary GRAIL gravity field (right) for the 86-km-diameter Tycho crater. In both panels Tycho is the prominent structure at upper left. In the GRAIL map reds correspond to mass excesses and blues to mass deficits. Here LOLA topography has a spatial resolution of 0.24 km and GRAIL gravity has a spatial resolution of 18 km.